1-1-2017

Six Degrees of Freedom: Kinematics of the Healthy Ankle Syndesmosis Joint

Veronica A. Hogg-Cornejo
University of Denver

Six Degrees of Freedom: Kinematics of the Healthy Ankle Syndesmosis Joint

Abstract

Syndesmotic injury, more commonly known as a "high ankle sprain", accounts for over 12% of all ankle sprain incidents in the US; of which, over 25% occur during a sporting activity. Typically, harm to the syndesmosis occurs in sports such as football, soccer, lacrosse, and hockey where it is common for an athlete to experience rapid and extreme dorsiflexion-external rotations of the foot. Severe syndesmotic sprains have been noted by clinicians as the most difficult ankle injury to accurately diagnose and treat, require the most recuperation time, and often results in life-long dysfunction. Even more problematic, 40% of patients suffering from a high ankle sprain also report joint instability 6 months after the initial injury. The distal tibiofibular syndesmosis joint consists of a fibrous interosseous membrane and four stabilizing ligaments, allowing for only slight movements of the fibula about the tibia. These distal bone surfaces closely articulate with the talus to form a stable mortise joint, giving the ankle joint complex its hinge-like range of motion (ROM). In the case of severe ankle sprains, excessive external rotation, dorsiflexion, and eversion of the foot can cause tearing of these stabilizing ligaments, distraction of the bones, or even fracture. A rigid screw fixation method is the standard practice for repair in these severe cases, although new dynamic fixation techniques using sutures and buttons instead of a screw are thought to allow for a more natural motion of the joint during healing and better post-operative results. However, most research of the ankle joint complex has primarily been dedicated to the talocrural joint formed between the talus and tibia, where the fibula is treated as single segment with the tibia. Very little research has been dedicated towards understanding the unique role the fibula plays in dynamic weight-bearing tasks to overall ankle joint strength, stability, and mobility. This gap in knowledge of fibular articulation and load bearing, lends to the difficulty and inaccuracy in properly reducing the bones during syndesmotic fixation. There also lacks a clear and consistent method for syndesmotic fixation with minimal validation that dynamic fixation heeds superior post-operative results. Gaining insight on healthy syndesmosis joint motion could provide baseline measures for more realistic loading conditions of cadaveric testing various fixation devices, serve as design parameters for new device design, set a gold standard for normal range of motion (ROM) in rehabilitation, and ultimately improve diagnostic and treatment modalities for syndesmotic injury.

The goals of the project were to establish a standard for the six degree of freedom (DOF) kinematics in the syndesmosis and talocrural joints in healthy active adults, as well as define the normal ROM. This was done using a high speed stereo radiography (HSSR) system to capture dual plane in-vivo motion of the bones with sub-millimeter and sub-degree accuracy. Changes in bone positioning during static and dynamic weight bearing activities were compared to a non-weight bearing neutral pose of the foot. The second scope of this work defines average values of medial and lateral clear space widening between the bones. Both are current clinical measures used to gauge the degree of ankle injury and instability present. Knowing the kinematics of the bones primarily responsible for stability of the ankle joint complex, along with their expected distraction between each other could help bridge the gap in the diagnosis and treatment of severe high ankle sprains, as well as reduce the risk of incorrect healing and chronic ankle instability.

Document Type

Thesis

Degree Name

M.S.

Department
Mechanical Engineering

First Advisor
Bradley S. Davidson, Ph.D.

Second Advisor
James Fogleman

Third Advisor
Paul Rullkoetter

Keywords
Fluoroscopy, Kinematics, Syndesmosis

Subject Categories
Biomedical Engineering and Bioengineering

Six Degrees of Freedom Kinematics of the Healthy Ankle Syndesmosis Joint

---

A Thesis

Presented to

The Faculty of the Daniel Felix Ritchie School of Engineering and Computer Science

University of Denver

In Partial Fulfillment

of the Requirements for the Degree

Master of Science

---

by

Veronica A. Hogg-Cornejo

June 2017

Advisor: Bradley S. Davidson

Author: Veronica A. Hogg-Cornejo
Title: Six Degrees of Freedom Kinematics of the Healthy Ankle Syndesmosis
Advisor: Bradley S. Davidson
Degree Date: May 2017

ABSTRACT

Syndesmotic injury, more commonly known as a “high ankle sprain”, accounts for over 12% of all ankle sprain incidents in the US; of which, over 25% occur during a sporting activity. Typically, harm to the syndesmosis occurs in sports such as football, soccer, lacrosse, and hockey where it is common for an athlete to experience rapid and extreme dorsiflexion-external rotations of the foot. Severe syndesmotic sprains have been noted by clinicians as the most difficult ankle injury to accurately diagnose and treat, require the most recuperation time, and often results in life-long dysfunction. Even more problematic, 40% of patients suffering from a high ankle sprain also report joint instability 6 months after the initial injury. The distal tibiofibular syndesmosis joint consists of a fibrous interosseous membrane and four stabilizing ligaments, allowing for only slight movements of the fibula about the tibia. These distal bone surfaces closely articulate with the talus to form a stable mortise joint, giving the ankle joint complex its hinge-like range of motion (ROM). In the case of severe ankle sprains, excessive external rotation, dorsiflexion, and eversion of the foot can cause tearing of these stabilizing ligaments, distraction of the bones, or even fracture. A rigid screw fixation method is the standard practice for repair in these severe cases, although new dynamic fixation techniques using sutures and buttons instead of a screw are thought to allow for a more

natural motion of the joint during healing and better post-operative results. However, most research of the ankle joint complex has primarily been dedicated to the talocrural joint formed between the talus and tibia, where the fibula is treated as single segment with the tibia. Very little research has been dedicated towards understanding the unique role the fibula plays in dynamic weight-bearing tasks to overall ankle joint strength, stability, and mobility. This gap in knowledge of fibular articulation and load bearing, lends to the difficulty and inaccuracy in properly reducing the bones during syndesmotic fixation. There also lacks a clear and consistent method for syndesmotic fixation with minimal validation that dynamic fixation heeds superior post-operative results. Gaining insight on healthy syndesmosis joint motion could provide baseline measures for more realistic loading conditions of cadaveric testing various fixation devices, serve as design parameters for new device design, set a gold standard for normal range of motion (ROM) in rehabilitation, and ultimately improve diagnostic and treatment modalities for syndesmotic injury.

The goals of the project were to establish a standard for the six degree of freedom (DOF) kinematics in the syndesmosis and talocrural joints in healthy active adults, as well as define the normal ROM. This was done using a high speed stereo radiography (HSSR) system to capture dual plane in-vivo motion of the bones with sub-millimeter and sub-degree accuracy. Changes in bone positioning during static and dynamic weight bearing activities were compared to a non-weight bearing neutral pose of the foot. The second scope of this work defines average values of medial and lateral clear space widening between the bones. Both are current clinical measures used to gauge the degree of ankle injury and instability present. Knowing the kinematics of the bones primarily responsible for stability of the ankle joint complex, along with their expected distraction between each other could help bridge the gap in the diagnosis and treatment of severe high ankle sprains, as well as reduce the risk of incorrect healing and chronic ankle instability.

ACKNOWLEDGEMENTS

This work was made possible by the invaluable help and support of several people. First, I would like to thank Dr. Kevin Shelburne and Dr. Paul Rullkoetter for entrusting me to take on a project that was a new area of research for the Human Dynamics Lab, as well as providing invaluable insight on research methods, presenting skills, and professional networking. I would also like to thank my advisor, Dr. Bradley Davidson, for recognizing and encouraging my passion for biomechanics. Without his guidance and motivation, I would not have made it to the University of Denver to pursue my dream.

If it weren't for the incredible help from Dr. Casey Myers, Dr. Erin Mannen, and all of my fellow lab mates, I would not have been able to successfully troubleshoot problems, stay optimistic and focused on my research, or have enjoyed my time as much throughout the graduate program.

I am very appreciative to DePuy Synthes for providing funding for this project, and to Dr. Kenneth Hunt for taking on a special interest in this research. The clinical expertise and mentorship given by Dr. Hunt was absolutely valuable to my deeper understanding of the project and strong clinical impact my data could provide.

Lastly, I would like to give my deepest gratitude to my family and friends for loving me unconditionally and making me feel like I could accomplish absolutely anything.

TABLE OF CONTENTS

LIST OF TABLES

LIST OF FIGURES

CHAPTER 1. INTRODUCTION

An estimated 2.15 per 1000 persons experiences an ankle injury each year, resulting in over 2 million sprains in the United States alone (Waterman et al., 2010). In an aged-matched comparison, males 15-24 years old showed higher risk of ankle injury when compared to their female counterparts, and women 30 years or older were most at risk (Waterman et al., 2010). Injury to the syndesmosis joint specifically has been diagnosed in up to 15% of all ankle sprain cases, but in the world of athletics, "high ankle sprains" are the most prevalent injury to occur accounting for up to 30% of all athletic injuries (Waterman et al., 2011). Collegiate football players are 14 times more susceptible to severe syndesmotic ankle injury than any other athlete involved in a contact sport (Hunt et al., 2016). Although the incidence of syndesmotic injury to the general population is not overwhelming, it's alarmingly common occurrence among young athletes is cause for concern. Of the ankle injuries due to sporting activity, more than half resulted in severe fracture of the bones or rupture of the surrounding ankle ligaments (Jensen et al., 1998). Waterman et al. (2011) stated that syndesmotic and medial ankle sprains require the most recuperation time and result in life-long dysfunction, while Hermans et al. (2010) said that 40% of people suffering from severe high ankle sprains report joint instability 6 months after the initial injury. However, there exists a general lack of understanding for the unique role that the fibula plays in dynamic weight-bearing tasks to overall syndesmosis joint strength, stability, and mobility. This gap in knowledge of fibular articulation and load bearing, lends to the difficulty and inaccuracy of properly repairing the joint during surgical fixation.

A comprehensive understanding of the mechanics and mobility of the syndesmosis joint could drastically reduce the risk of misdiagnosing injury, undergoing unnecessary surgeries, prolonging time missed from competing or suffering from life-long complications and discomfort for athletes and young active adults.

The overarching goal of the work was to develop a baseline understanding of healthy syndesmosis articulation to improve current treatment modalities for patients suffering from severe high ankle sprains and chronic instability. There are two primary objectives that define the scope of this work:

Objective 1: Identify the six DOF kinematics of the syndesmosis and talocrural joints in order to define healthy range of motion (ROM) of the ankle joint.

Objective 2: Define normal limits of medial and lateral clear space widening between the bones to describe healthy bone distraction within the ankle joint complex.

The following chapters illustrate the organization of this document: Chapter 2 provides an overview of the published literature describing the kinematics, mechanisms of injury, modalities for repair, and the clinical impact of syndesmotic joint health and ankle stability. Chapter 3 presents the six DOF kinematics and ROM of the distal tibiofibular and talocrural joints to illustrate healthy joint motion. Chapter 4 presents gap distances between the talus and medial malleolus of the tibia, as well as distances between the fibula and lateral tibia to define normal limits of clear space widening in the ankle. Chapter 5 summarizes the results of this thesis and additional suggestions for future work.

CHAPTER 2. THE SYNDESMOSIS & ANKLE JOINT COMPLEX

2.1. Introduction

This literature review will describe the anatomy and kinematics of the syndesmosis joint, mechanisms of injury, modalities for repair, and its clinical significance to overall ankle stability. There is a general lack of information currently available on tibiofibular mechanics during dynamic weight-bearing activities, particularly in activities similar to those experienced in sports which are the main cause of syndesmotic injury. Since past research of the foot has primarily focused on the talocrural and subtalar joints, the unique role that the fibula plays in the integrity of the ankle is poorly understood. Knowing how the fibula contributes to mobility, stability, and load transmission in concert with the tibia and talus could shed a light on better management of syndesmotic injuries.

2.2. Anatomy

The ankle syndesmosis is located on the distal lower limb between the tibia and fibula (Figure 2.1). This joint consists of a fibrous interosseous membrane between the bones along with four stabilizing ligaments: the anterior tibiofibular ligament (AITFL), posterior tibiofibular ligament (PITFL), transverse tibiofibular ligament (TTFL), and interosseous ligament (IOL). These structures maintain the integrity of the gap distance between the tibia and fibula bones and allow only slight movements between the two bones. In a cadaveric study, Williams et al. (2014) quantified the characteristics of each syndesmotic ligament showing that: the superficial bands of the AITFL averaged 7.8 mm in length spanning from the tibial plafond to the anteromedial malleolus of the fibula, and that the PITFL originates on the medial edge of the fibular peroneal groove spanning approximately 11.6 mm to the posterolateral tubercle of the tibia. Both of these ligaments are known for their trapezoidal shape and provide a majority of the strength needed in the syndesmosis. The IOL originates at the distal end of the interosseous membrane just above the talocrural joint line and has a length ranging from 6.3-7.2 mm (Williams et al., 2014). The fibers of the IOL traverse distolaterally between the medial fibula and lateral tibia acting to restrict superior translation of the talus into the distal syndesmosis. The deep fibers of the TTFL lie inferior to the PITFL and insert on the distal posterior ridge of the fibular malleolus. This ligament acts to restrain posterior translation of the talus. The deltoid ligament, although not considered a part of the syndesmosis joint architecture, prevents excessive lateral excursion of the talus and contributes significantly to the structural support of the ankle joint. The stability of the ankle joint is highly dependent on not only these surrounding tissues, but also the distinct osseous relationship between the distal bones (Hunt et al., 2015b).

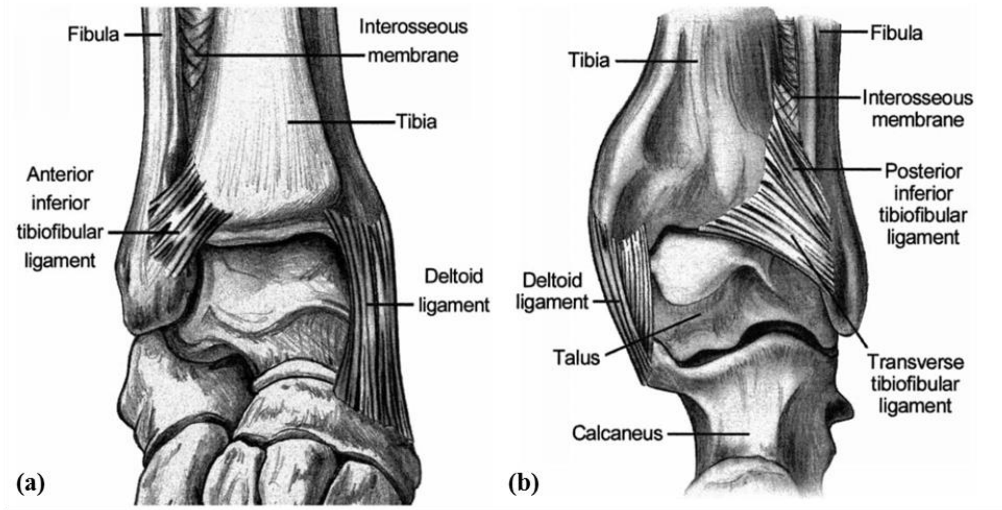

Figure 2.1. Anatomy of the distal tibiofibular syndesmosis joint: (a) anterior and (b) posterior views (Norkus and Floyd, 2001).

The unique anatomical geometry of the distal tibia and fibula are such that the bones align perfectly with one another creating a secure fit and limited range of motion within the joint (Figure 2.2). The convex medial surface of the distal fibula sits within the concave lateral surface of the tibia between its anteriorlateral (Chaput's tubercle) and posterolateral (Volkmann's tubercle) aspects. The incisura fibularis of the tibia forms the apex of this pocket and has varying depths between 1-7.5 mm (Rammelt et al., 2008). The shallowness of the incisura has been thought to influence the risk of repeated severe syndesmotic injuries, where a flatter incisure has a potentially higher predisposition of fibular dislocation outside of the tibial pocket causing ankle sprains (Sora et al., 2004). Women have been shown to have flatter incisura than men (Yildirim et al., 2003). The synovial recess of the distal joint encompasses multiple articulating surfaces between the tibia and fibula. These areas of bone that come into direct contact are covered in hyaline cartilage approximately 0.5-1.0 mm thick (Hermans et al., 2010). The facets of cartilage are found on the most anterior ridge of the tibia and fibula, but are not always necessarily present in the foot anatomy (Bartonicek, 2003). Surgeons use these easily identifiable landmarks of the bones to aid in their proper alignment while placing fixation devices. Thus, having a clear understanding of the bone geometries and their influence on the articulation of the joint is crucial for accurate repair of syndesmotic injuries. As stated by Williams et al. (2014), familiarity of the boney prominences can "optimize current surgical fixation techniques, improve anatomic restoration, and reduce the risk of iatrogenic injury from malreduction or misplaced implants."

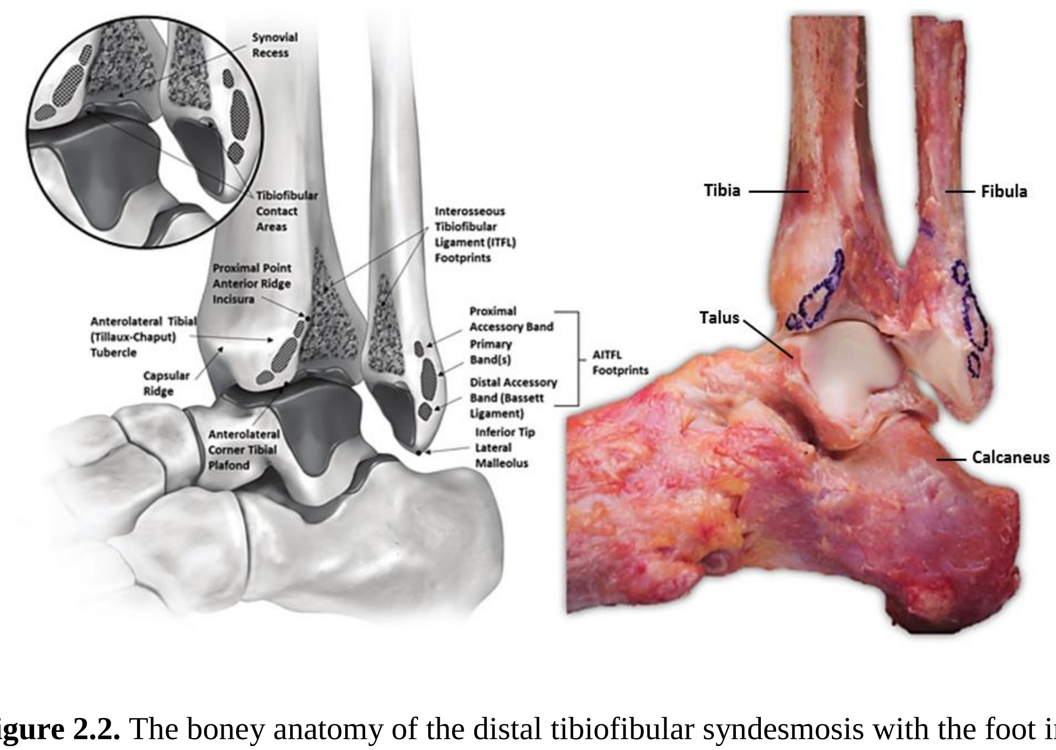

Figure 2.2. The boney anatomy of the distal tibiofibular syndesmosis with the foot in a neutral position. An anterolateral view of osseous contact areas and ligament footprints (Williams et al., 2014).

2.3. Injury

In contact sports such as football, soccer, basketball, or lacrosse, rapid and high-impact motions place large shear stresses on the ankle joint, causing the mortise to widen and become at risk for tearing ligaments, distraction of the bones or even fracture. Typically, damage to the syndesmosis occurs with excessive supination-eversion, external rotation, and dorsiflexion of the foot (Bauer et al., 1985; Michelsen et al., 1996). In this case, when the foot is flexed and subjected to an external torque, the wider anterior portion of the talus pushes the fibula laterally, externally rotating it, and separating from the tibia. The AITFL is the first ligament to rupture due to this excessive fibular rotation. Commonly, an athlete will plant their foot in a slightly externally rotated position to perform a cutting motion, then after colliding with another player, fall forward to dorsiflex and further externally rotate the foot, leading to injury of the syndesmosis joint (Nussbaum et al., 2001). Skiers and hockey players run the risk of syndesmotic rupture from catching a toe edge and powerfully jerking their foot outward in external rotation. Other mechanisms of injury include any sort of extreme weight-bearing motion such as plantarflexion, inversion, or twisting that places the ligaments of the ankle under maximum tension (Thormeyer et al., 2012). To further understand the mechanisms of syndesmotic injury, researchers have aimed to describe the mechanical properties of the stabilizing ligaments and biomechanics of the ankle joint.

Several cadaveric studies have been performed in an attempt to identify ligament behavior during different loading conditions and their correlation to injury. In a study performed by Xenos et al. (1995), it was found that increased diastasis and rotation of the fibula was directly related to the degree of ligamentous injury present. After complete rupture of the AITFL, IOL, and PITFL, a 7.3 mm and 10.2 degree change from an unloaded to loaded state was observed (Xenos et al., 1995). This work also highlighted a slight widening of the ankle mortise and posterior excursion of the fibula. Similarly, Hunt et al. (2015) observed a posterior shift of the fibula, but no widening of the syndesmosis after loading a cadaveric limb under 700N compression and 20 Nm torque while sequentially dissecting the ligaments simulating increasing severities of ankle injury. In a quantitative analysis of each ligament’s contribution to overall ankle stability, Ogilvie-Harris et al. (1994) determined that the AITFL provides most resistance to lateral joint diastasis (35%), then the PITFL (33%), followed by the IOL (22%) when subjected to cyclic lateral loading conditions. Clanton et al. (2017) performed a study in which sequential sectioning of the individual syndesmotic ligaments showed the AITFL providing the highest resistance to external rotation and posterior translation of the fibula, while the PITFL predominantly resisted internal rotation. It was also noted that resistance to external rotation drastically decreased after each additional ligament was cut (Clanton et al., 2017). Hunt et al.'s (2015) work simulating progressive injury also illustrated a significant increase in tibiotalar contact pressure that could help explain the lingering discomfort and change in ankle biomechanics associated with moderate to severe injuries.

Ankle injuries are graded into three types (A, B, and C) according to the Danis-Weber classification system or into class I, II, III as damage and instability increases. Weber types B and C (or class II and III) describe the degree of syndesmotic injury to the joint in which 14-47% of all injuries classified as Weber C include ankle fracture (Hughes et al., 1979). In addition to a fibular break, Weber C injuries consist of complete rupture of the syndesmosis, widening of the intermalleolar space with a lateral shift of the talus due to tearing of the deltoid ligament, fracture of the medial malleolus, and inherent instability at the joint (Peter et al., 1994). When displacement of the lateral malleolus is greater than 5mm or there exists a tibiofibular clear space of 6mm or greater, open reduction and internal fixation (ORIF) is required (Metzler and Johnson, 2013).

When diagnosing syndesmotic injury, clinicians may ask patients to perform maneuvers such as a toe-rise, walking, or a single-leg hop to assess functional disability. Provocative tests such as the squeeze, external rotation, Cotton, fibular translation, or cross-leg are also commonly used to evaluate pain and the integrity of the syndesmosis (Hunt et al., 2015). A positive indication of syndesmotic rupture during a squeeze test, for example, is distal pain of the limb as the tibia is compressed with the fibula at mid-calf level. The external rotation test has been reported to be the most reliable clinical measure, having the lowest rate of false positives and inter-tester variability. A positive test for this is indicated by localized syndesmotic and medial pain when the foot is forced into a dorsiflexed position and externally rotated. Localized swelling on the anterior syndesmosis is another notable measure of injury.

In an attempt to standardized a procedure to classify the severity of syndesmotic injury, Nussbaum et al. (2001) stated that the length of tenderness present along the interosseous membrane was significantly correlated to the number of days missed from competition for their cohort of 60 collegiate athletes with acute ankle sprains. The management protocol described by this work consists of three phases of treatment which ends once the athlete can successfully complete 15 single-leg hops and passes functional testing. Functional disability, defined as the inability to perform 10 single-leg hops without gross pain also helps identify potential damage to the primary stabilizing AITFL (Nussbaum et al., 2001). According to Nussbaum et al. (2001), the four criteria to be used for accurately diagnosing syndesmotic damage includes: the length of interosseous membrane tenderness, functional disability, the external rotation test, and palpable tenderness of the AITFL. Although useful for classifying minor high ankle sprains, the need for a consistent diagnostic and rehabilitation protocol for more severe class II and class III cases continues to be a pressing issue. Moderate class II sprains prove to be the most difficult to identify and properly gauge the necessity for surgical stabilization. As stated by Williams et al. (2014), none of the tests previously mentioned clearly indicate the need for surgical fixation, which only becomes apparent in the case of class III injuries where frank diastasis of the bones is easily diagnosed via x-ray, magnetic resonance imaging (MRI), or computed tomography (CT). Radiographic measurements of a tibiofibular (syndesmosis) clear space >6mm or a medial clear space >4mm are indicative of severe ankle injury and need for surgical fixation (Hunt et al., 2015) (Figure 2.3). The medial clear space is defined as the distance between the medial talar dome and lateral face of the medial malleolus. Stress films indicating diastasis of greater than 2mm when compared to the un-injured limb provide additional clues for inherent severe syndesmotic instability requiring internal fixation (Rammelt et al., 2008).

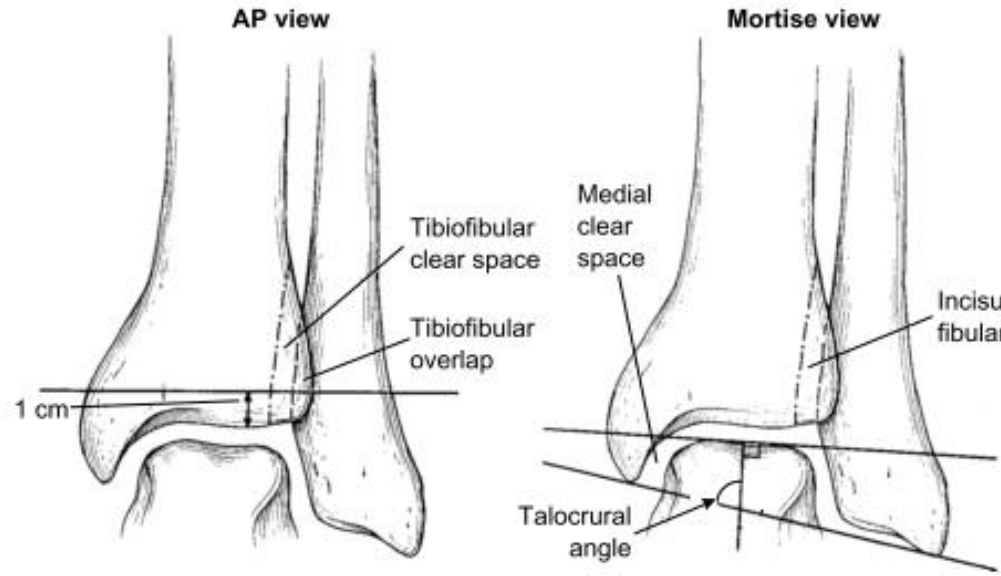

Figure 2.3. Radiographic measurements of tibiofibular and medial clear space (Wuest, 1997).

2.4. Repair

Implantation of rigid screws is the standard method for surgical fixation, although new dynamic fixation techniques are thought to allow for more natural and beneficial motion of the syndesmosis during healing.

2.4.1. Screw Fixation

Depending on the degree of injury and syndesmotic instability**,** surgical reattachment of the ligaments or realignment of the bones using implantable fixation devices may be necessary. Open reduction internal screw fixation is the most common method for repairing the distal tibiofibular syndesmosis (Figure 2.4). Even so, every repair is variable in terms of the number and size of screws to use, location and orientation of their placement, amount of bone cortices to include, and post-operative care (Hunt et al., 2015). Screws are aligned parallel to the line of the mortise joint, 2-5 cm proximal to that line, and oriented anteriorly (Hunt et al., 2015). Cortical screw sizes used for repair are either 3.5mm or 4.5mm in diameter (Figure 2.5). Some argue that patients of a larger stature should be fitted with 4.5mm screws to reduce the risk breaking and provide more fixation strength, but there has been no evidence showing a biomechanical advantage of the larger screw size over the smaller (Thompson and Gesink, 2000). Hansen et al. (2006) suggested that 4.5mm screws provide greater protection against shear stress than 3.5mm screws. Screw size and the number of cortices incorporated during fixation were also found to have little influence on the mechanical strength or stability of the distal joint when subjected to loading (Markolf et al., 2013). Huber et al. (2012) also found this limited effect, but additionally concluded that the use of two quadricortical screws provided stronger fixation than a single quadri- or tricortical screw. Since this method inhibits normal physiological range in motion of the ankle, removal of the screws prior to weight-bearing or gait activities is recommended. Additive risks, such as infection, broken hardware, or joint diastasis, are inherent with routine screw removal, and have been reported to be up to 22.4% (Schepers et al., 2011). However, there are new dynamic fixation devices emerging that are thought to allow more natural motion in the joint during healing and eliminate the risks associated with additional surgeries for syndesmotic screw removal.

Figure 2.4. Proper alignment of cortical screws (Thormeyer et al., 2012).

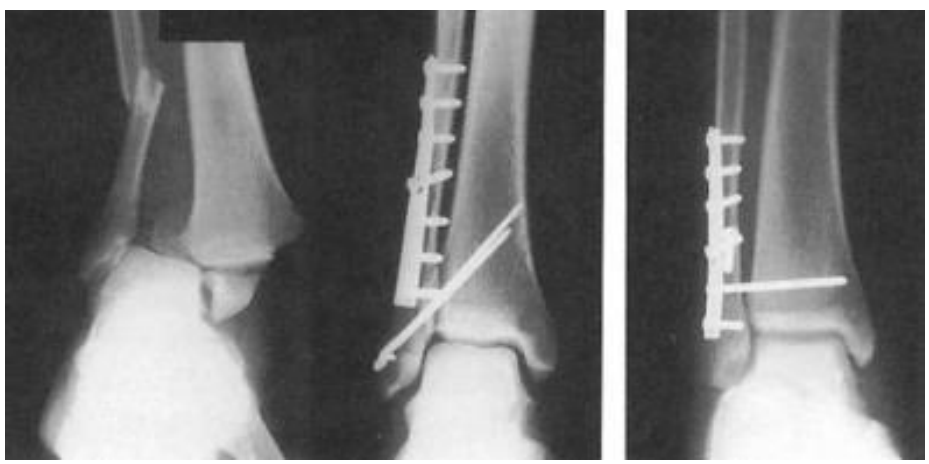

Figure 2.5. Varying approaches of internal screw fixation of the distal tibiofibular syndesmosis (Peter et al., 1994).

2.4.2. *Dynamic Fixation*

Due to the normal physiological motion of the syndesmosis joint, leaving rigid screws in place permanently can increase post-operative risks such as loosening or fracture of the hardware, stiffness of the ankle, and long-term discomfort. New alternative fixation devices using a suture-button system, have recently been designed and adopted to allow for more natural movement of the joint, while still resisting harmful distraction between the bones and eliminating the need for post-operative removal (Hunt et al., 2015) (Figure 2.6). This is believed to provide clinical benefits over the rigid fixation, but there is no universal consensus on which approach is superior.

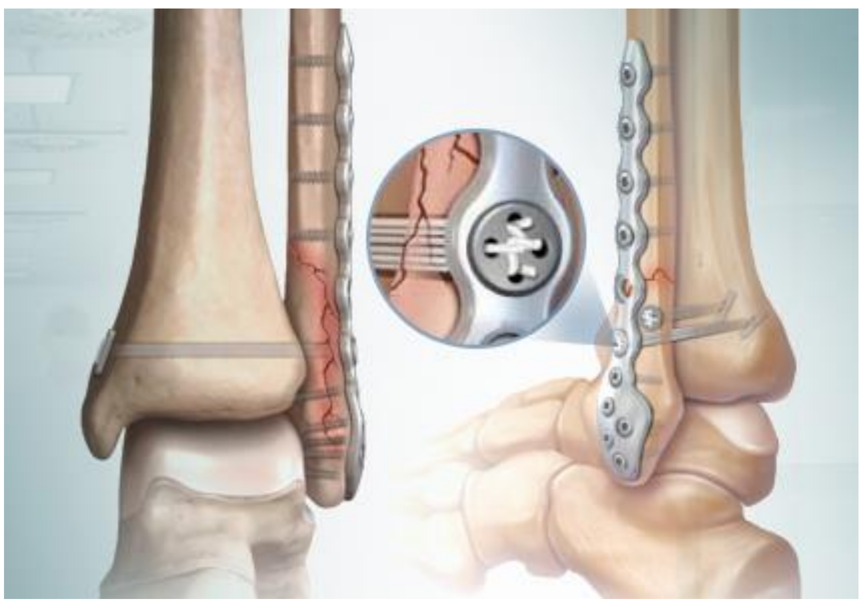

Figure 2.6. Arthrex Knotless Tightrope dynamic fixation device (Arthrex Inc., Naples, FL).

The Arthrex Tightrope system (Figure 2.6) stabilizes the distal tibia and fibula with a strong #5 UHMWPE suture tensioned between two metallic buttons, to closely mimic the natural articulation of the joint. The buttons are secured atop the outer tibial cortex and a fibular plate. The tautness of the suture between the buttons mimics a tightrope wire and replicates the mechanical stability that would naturally be provided by the surrounding syndesmotic ligaments (Thornes et al., 2005). This dynamic device has been shown to produce equivalent strength in resisting joint diastasis when compared to screw implantation. In a cadaveric study performed by Thornes et al. (2003), there were no significant differences in mean failure rates between screw or suture-button devices when the foot was subjected to an externally rotating torque. It was also concluded that suture-buttons performed more consistently under the loading conditions, indicating reliability in cortical anchoring of the buttons. Others claimed that dynamic fixation is easier to implement, thus improving the accuracy of bone reduction and reducing the risk of malalignment (Naqvi et al., 2009). The simple and less invasive approach for implanting suture-button devices promotes earlier weight-bearing and a faster recovery time when compared to screw fixation. It has been shown that suture-button patients require an average of 2.8 months to return to normal work activities, while those with screw implants took 4.6 months to fully recover (Thornes et al., 2005). New knotless designs may also reduce the risk of skin and wound complications that have been associated with subcutaneous knots or screw implants (Hunt et al., 2015). Adequate information regarding the optimal placement and orientation of the dynamic device is still needed.

Alternative repair methods such as using both a screw and suture-button have been suggested (Figure 2.7). In this case, a rigid screw is initially implanted to stabilize the joint along with a proximal suture-button. After proper bone reduction has taken place, the screw is removed and replaced with a second suture-button. Although there lacks sufficient data describing the effectiveness of this approach, Hunt et al. (2015) recommended this technique for athletes weighing more than 250lbs requiring an early return to their high-impact sport.

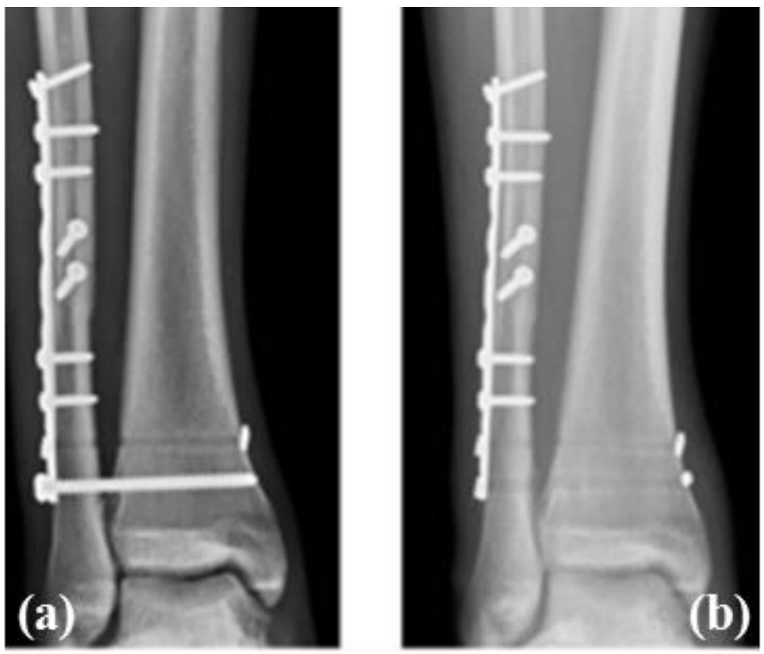

Figure 2.7. Collegiate football player treated with (a) screw and suture-button, then later (b) replaced the screw with a second suture-button (Hunt et al., 2015).

Accurately and properly fixing the bones during syndesmotic repair can be difficult. Malreduction and poor alignment of the tibia or fibula can lead to improper healing and long-term dysfunction including tibiofibular diastasis, instability, and osteoarthritis (Mukhopadhyay et al., 2011). Current implantable devices aim to restrict the motions known to cause syndesmotic injury, primarily lateral dislocation and rotation of the fibula relative to the tibia. Limiting distraction of the fibula, as well as not over compressing the joint poses some difficulties for surgeons when implanting screws. Clinicians also aim to maintain the foot in a neutral position during fixation such that the fibula rests in its natural anatomical alignment within the incisura fibularis of the tibia. Immobilization and non-weight bearing of the foot are required for up to 6 weeks post-repair. Rehabilitation should focus on gradual weight bearing, strengthening, as well as restoring maximum ROM and stability of the ankle. Press et al. (2009) also recommended proprioceptive tests, balance exercises, and practicing specific sport-related maneuvers as important components to rehabilitation and injury management.

2.5. Biomechanics of the Ankle Joint Complex (AJC)

There is limited research highlighting the unique role that the fibula plays in the mechanics of the ankle during rapid high-loading maneuvers. Knowing how the ligamentous and osseous structures of the fibula work in concert with the tibia and talus in ankle biomechanics could shed a light on better management of syndesmotic injuries in athletics.

Motivation for better understanding ankle stability first ignited when Ramsey and Hamilton (1976) published results indicating that just 1-mm of lateral talus translation reduced tibiotalar contact area by an astounding 42%. Additionally, it was noted that as the talus moved incrementally farther the tibiotalar contact area continued to decrease. Areas of bone in direct contact become exposed to higher stresses and contact pressure. Reducing the total base of support in the ankle reduces overall stability. These findings were indicative of how even the slightest bone displacement could have a powerful influence on ankle kinematics, joint kinetics, and whole-body balance. This research also brought clinical awareness to Weber B (class II) injuries involving an intact deltoid ligament. As long as the deltoid ligament continues to provide stability at the joint and prevent the talus from migrating, surgical intervention with this type of injury may be unnecessary. These conclusions encouraged a wave of investigations into ankle injuries, calling into question when invasive surgery becomes a necessity for proper recovery or when it needlessly extends recovery time for patients who may heal with simple bracing.

Building upon Ramsey and Hamilton's work on talar contact pressure and excursion due to injury, several other studies have been performed to better understand the effects of syndesmotic injuries and repairs on talar articulation, ankle biomechanics, and overall joint health. Michelsen et al., (1996) performed a cadaveric study to first identify healthy intact ankle range of motion (ROM) for the talus, then illustrate the changes in talar articulation after injury of the deltoid ligament. Mean values of 1.9 ± 4.12 degrees and 7.2 ± 3.88 degrees internal and external rotation were defined for the talus when the foot was passively moved from maximum dorsiflexion through maximum plantarflexion (Michelsen et al., 1996). Once the deltoid ligament was compromised, the talus dislocated significantly during plantarflexion and showed significantly increased ER. Further injury by fibular osteotomy and repair with a talocalcaneal screw illustrated no other significant effects on ankle kinematics. There were also no significant changes noted in varus (inversion) or valgus (eversion) angulation with any combination of ligament resection or fibular osteotomy. This work further supported the belief that the primary source of ankle stability came from an intact deltoid ligament in which the talus is unable to displace and rotate excessively (Michelsen et al., 1996). Additionally, the data suggested that lateral reconstruction of the fibula in a complete ankle injury partially restored the mechanical integrity of the joint; indicating that class II injuries involving an intact deltoid ligament are still stable and justifies non-operative treatment of fibular malleolus fractures. Since the talus directly articulates with the distal tibia and fibula, understanding the biomechanics of the syndesmosis joint could better explain overall ankle motion**.**

The ligamentous tissues surrounding the syndesmosis are the primary sources of structural support for the joint. Previous literature has identified the mechanical role of the ligaments when intact. In a neutral static stance, the ankle experiences minimal shear stresses that are typically caused by quick twisting of the body. Therefore, the ligaments stabilizing the syndesmosis are minimally tensioned in this static pose. During dynamic weight-bearing tasks, the ankle is subjected to forces up to 6 times body weight and these ligamentous tissues provide the structural support and elasticity needed to withstand such conditions (Thormeyer et al., 2012). For example, the AITFL experiences maximum tension during plantarflexion whereas the PITFL is maximally tensioned during dorsiflexion, both maintaining the integrity of the mortise joint formed between the tibia, fibula, and talus (Rammelt et al., 2008). The IOL provides most of the mechanical elasticity to the distal joint by buffering and distributing the forces experienced during high impact landings.

There have been several studies conducted to identify the structural function of the fibula during weight bearing, as well as the resulting changes in load acceptance and joint articulation due to injury. Beumer et al. (2003) found no universal kinematic pattern of the fibula with respect to the tibia when comparing non-weight bearing to weight bearing neutral poses, as well as little and variable superior/inferior dislocations. In a biomechanical analysis to define the normal range of motion of the intact syndesmosis when subjected to a 750N axial load and 15 degrees of external rotation, Clanton et al. (2017) revealed that the fibula externally rotates 2.8 degrees and posteriorly translates 2.6mm. When the torque was reversed to cause internal rotation of the foot, the fibula internally rotated 1.5 degrees and shifted anteriorly 0.7mm. Similarly, Beumer et al. (2003) found that external rotation of the ankle caused posterior fibular translation of 1-3.1mm and external rotation of 2-5 degrees. In a maximal dorsiflexed position, distraction from the tibia ranges from 1-1.5mm and fibular external rotation approximates 2 degrees (Close, 1956; Peter et al., 1994). During a full gait cycle, the distal fibula has been shown to translate inferiorly 2.4mm and anteroposteriorly 0.2-0.4mm (Rammelt et al., 2008). In a different study, the fibula was found to account for approximately 6.4-7.12% of the load transmitted while in the neutral position and reached maximal load bearing in a fully dorsiflexed and everted position (Goh et al., 1992). Resection of the fibula followed by rigid screw fixation decreased load transmission to just 1.71-5.14%, highlighting one of the major shortcomings of this surgical technique. Ogilvie-Harris et al. (1994) reported a peak lateral displacement of 2mm for an intact syndesmosis under a cyclic 87N lateral force was applied. Complete tearing of the syndesmosis indicated diastasis of up to 7.3mm (Xenos et al., 1995). Although small, these dynamic motions of the fibula relative to the tibia are what give the syndesmosis joint the elasticity and structural integrity it needs to support ankle motion and torque production. Some claim that the unique muscle characteristics and anatomical variability among people leads to a wide range in fibular articulation during weight bearing, which has made defining a common kinematic pattern for the micro motions of the syndesmosis joint very difficult (Beumer et al., 2003). Unfortunately, measurement of in-vivo ankle joint motion has proven to be tough and imprecise with traditional motion capture and radiography methods because articulation is typically very small and dynamic. These challenges have explained the slow progression of research in the field, although new imaging technology has recently encouraged a wave of accurate in-vivo bone tracking measures.

The use of fluoroscopy to track bone motion gave way into in-vivo analysis of the 6 DOF kinematics of the healthy ankle joint complex (AJC). De Asla et al. (2006) used dual plane fluoroscopy and MRI to image 5 healthy ankles in 4 non-weight bearing poses reflecting maximum passive range of motion in the sagittal and frontal planes. Additionally, De Asla et al. (2006) captured 3 weight bearing poses meant to simulate heel-strike, mid-stance, and toe-off phases of gait. The data illustrated the individual contribution of the subtalar and talocrural joints to in-vivo ankle motion, suggesting that the talocrural joint is primarily responsible for plantar/dorsiflexion while the subtalar joint provides in/eversion and internal/external rotational motions. Other studies using dual plane fluoroscopy have focused on measuring the individual joint kinematics of the tibiotalar (talocrural) and subtalar joints during dynamic tasks such as slow or fast walking, and balanced single-leg calf raise. Roach et al. (2016) established that the talocrural joint was mostly responsible for allowing dorsiflexion and plantarflexion (DF/PF) of the hindfoot, whereas the subtalar joint primarily contributed to inversion/eversion (IV/EV) and internal/external rotations (IR/ER). Slow walking illustrated significantly greater anterior/posterior (A/P) excursions of the subtalar joint than the talocrural joint, while heel-rise showed significant differences in DF/PF and IV/EV ranges of motion between the joints (Roach et al., 2016). Again, notable variation in joint angles and ROM across subjects was observed and hypothesized to be the result of subject-specific bone geometry and muscle activation. Despite the growing use of in-vivo ankle research using dual-plane fluoroscopy, most studies have solely focused on the subtalar and talocrural joints (Figure 2.7). Additionally, the weight-bearing tasks captured in these previous studies do not entirely represent of the rapid and high-impact activities performed by athletes, nor the extreme motions known to cause syndesmotic injury. The sub-millimeter and sub-degree accuracy of dual-plane fluoroscopy provides a means to accurate measure dynamic micro motions of the syndesmosis joint while performing forceful and quick movements.

To date, very limited data have been published using bi-plane fluoroscopy to measure three-dimensional motion of the distal tibiofibular syndesmosis. Wang et al., (2015) used dual fluoroscopy to quantify normal range of motion of the joint during the stance phase of slow walking. The study demonstrated that IR/ER and S/I degrees of freedom showed the most ROM. There was 1.69 degrees of dorsiflexion, 3.61 degrees eversion, and 3.95 degrees external rotation about the tibia from heel strike to mid-stance, whereas 1.04 degrees of plantarflexion, 4.95 degrees inversion, and 5.13 degrees internal rotation occurred from mid-stance to heel-off (Wang et al., 2015). Measurement during stance phase also demonstrated 2.63mm medial/lateral, 3.86 mm anterior/posterior, and 4.12 mm superior/inferior translations. As demonstrated by the study, fluoroscopy offers accurate and effective means for non-invasive measurement of the tibiofibular articulation during dynamic weight bearing activities. Application of this technology to capture fast and demanding motions, such as those seen in sports, would provide a more physiological representation of syndesmotic kinematics leading to potential injury.

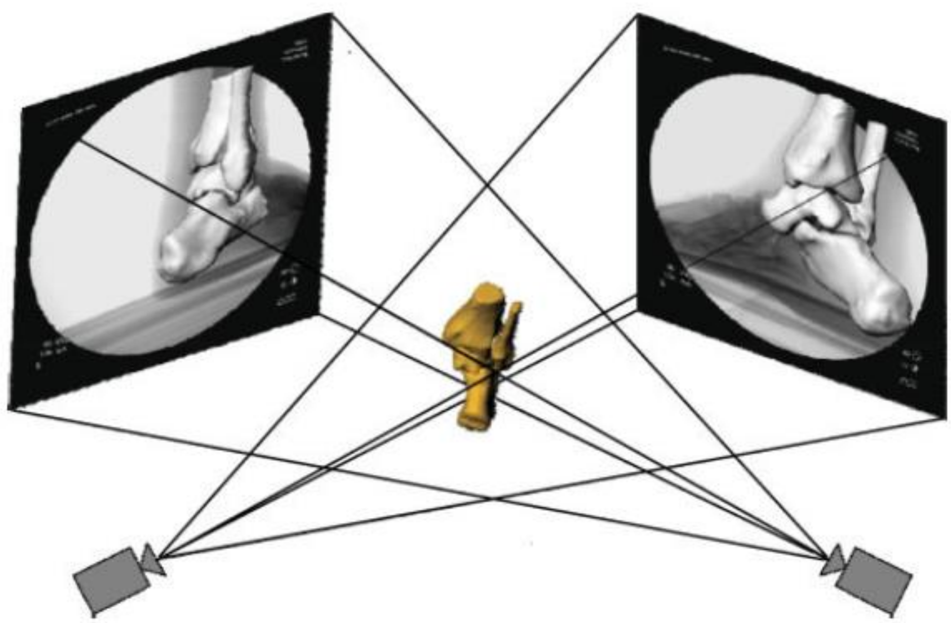

Figure 2.8. Reproduction of in-vivo AJC positions using dual plane fluoroscopy (de Asla et al., 2006).

CHAPTER 3. SIX DEGREES OF FREEDOM KINEMATICS OF THE HEALTHY ANKLE SYNDESMOSIS JOINT

3.1. Introduction

An estimated 2.15 per 1000 persons experiences an ankle injury each year, resulting in over 2 million sprains in the United States alone (Waterman et al., 2010). In an aged-matched comparison, males 15-24 years old showed higher risk of ankle injury when compared to their female counterparts, while women 30 years or older were at most risk (Waterman et al., 2010). Injury to the syndesmosis joint specifically has been diagnosed in up to 15% of all ankle sprain cases, but in the world of athletics, “high ankle sprains” are the most prevalent injury to occur accounting for up to 30% of all athletic injuries (Waterman et al., 2011). Collegiate football players are 14 times more susceptible to severe syndesmotic ankle injury than any other athlete involved in a contact sport (Hunt et al., 2016). Of the ankle injuries due to sporting activity, more than half resulted in severe fracture of the bones or rupture of the surrounding ankle ligaments (Jensen et al., 1998). Waterman et al. (2011) stated that syndesmotic and medial ankle sprains require the most recuperation time and result in life-long dysfunction, while Hermans et al. (2010) said that 40% of people suffering from severe high ankle sprains report joint instability 6 months after the initial injury. Although the incidence of syndesmotic injury to the general population is not overwhelming, its alarmingly high occurrence rate is a concern for better understanding of the joint and its proper treatment.

The distal tibiofibular syndesmosis joint consists of a fibrous interosseous membrane and four stabilizing ligaments that allow for only slight movements of the fibula relative to the tibia. In the case of severe ankle sprains, excessive external rotation and dorsiflexion of the foot can cause tearing of these stabilizing ligaments, distraction of the bones, or even fracture to the fibula. Unfortunately there exists a gap in knowledge of fibular articulation and load bearing, lending to the difficulty in accurately and properly repairing the joint during surgical fixation. In addition, clear and consistent metrics for evaluation of syndesmotic fixation to optimize rehabilitation and patient satisfaction are also lacking.

A comprehensive understanding of the motion occurring at the syndesmosis joint could drastically reduce the risk of misdiagnosing injury, set a gold standard of normal range of motion (ROM) for clinicians to aim to recover during rehabilitation, prevent prolonged time missed from leisure activity or sports competition, and limit life-long complications and discomfort for athletes and young active adults. Additionally, gaining insight on joint biomechanics could define baseline measures for more physiological loading conditions in cadaveric testing of current rigid and dynamic devices or serve as design parameters for new fixation devices.

The overall goal of the work was to provide a descriptive analysis of healthy syndesmosis articulation by identifying six DOF kinematics of the syndesmosis and talocrural joints and defining healthy range of motion (ROM) of the ankle joint. These data may improve diagnosis and treatment severe high ankle sprains.

3.2. Methods

3.2.1. Participants

Six volunteers (Table 3.1) with no prior history of lower limb injury were recruited locally and provided consent, in full accordance with the University of Denver Institutional Review Board, to participate in the study. The average anthropometric data for all participants were 29.3 ± 2.5 years, 174.3 ± 6.9 cm height, 158.1 ± 24.4 lbs body weight, 23.3 ± 3.8 kg/m^2 body mass index (BMI). All subjects fell within a normal healthy BMI range and reported leading active lifestyles of regular moderate-level exercise (Table 3.1). Measurements of foot length, width, and height of various boney landmarks were taken of the dominant foot using a goniometer and according to McPoil et al.'s (2005 & 2013) methodologies. These values were used to describe the longitudinal arch angle (LAA) of each participant for the purpose of classifying foot structure and type: pronated, neutral, or supinated (McPoil and Cornwall, 2005). The average LAA measured was 152.0 ± 9.9 degrees.

Table 3. 1. Participant anthropometric data.

	Females (n = 3)		Males (n = 3)	
	Mean	SD	Mean	SD
Age (years)	30.7	3.1	28.0	1.0
Height (cm)	168.8	4.0	179.8	3.3
Weight (lbs)	129.8	2.4	186.3	23.7
LAA (deg)	149.0	11.3	155.0	9.5
Dominant Leg (Right\Left)	3\0	-	2\1	-

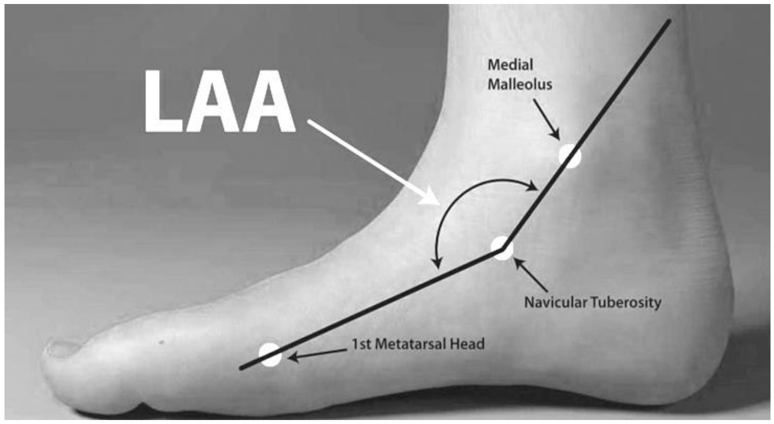

Figure 3. 1. Measurement of longitudinal arch angle (Mcpoil et al., 2013).

3.2.2. Experimental Protocol

At the University of Denver's Human Dynamics Laboratory (HDL), participants were asked to perform four dynamic weight-bearing activities similar to movements seen in collision sports such as football, soccer, or lacrosse. All of these dynamic motions were weight-bearing and performed on a single-leg: heel rise (calf raise), squat, torso twist, and box jump. Additionally, participants posed in a non-weight bearing and weight-bearing neutral stance, maximum plantarflexion, and maximum dorsiflexion. These activities were chosen to stress the syndesmosis similarly to what occurs in competitive sport high ankle sprain injuries and closely correlate to clinical tests used to diagnose syndesmotic instability.

3.2.3. Instrumentation

All volunteers were instrumented with 29 reflective markers along their dominant leg in order to record the 3D spatial motions of the foot, limb, and pelvis segments via 8 Vicon T-Series near-infrared cameras surrounding the lab space (Vicon, Centennial, CO).

A modified oxford-foot model was used to place 14 of these reflective markers solely on the foot (Figure 3.2). Four floor-embedded force plates collected ground reaction force data in sync with the optical motion capture system (Bertec, Columbus, OH).

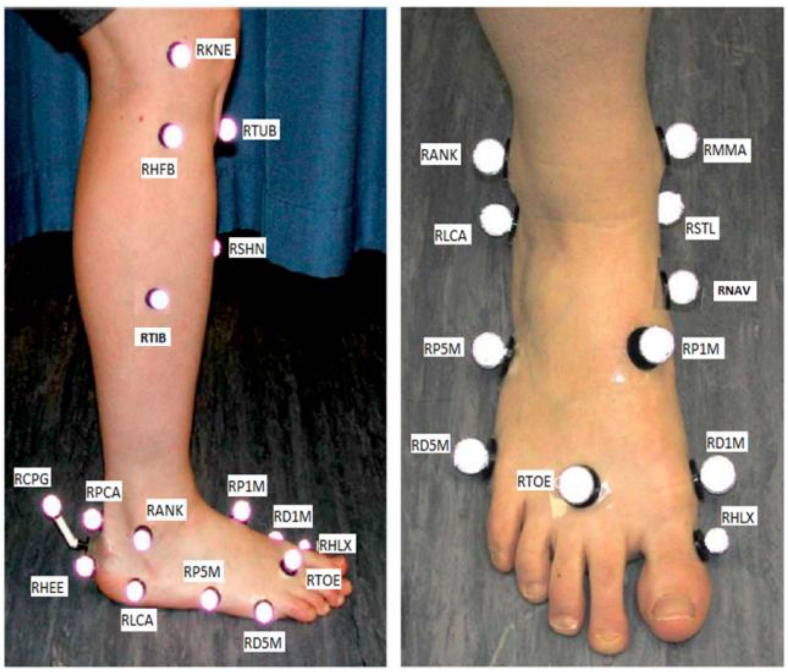

Figure 3. 2. Modified Oxford model for Vicon marker placement (Stebbins et al., 2006).

In addition to 3D motion capture and bi-plane fluoroscopy, 9 electromyography (EMG) surface electrodes were placed over the primary stabilizing, flexor, and extensor muscles of the lower limb in order to measure changes in muscle activation (Figure 3.3).

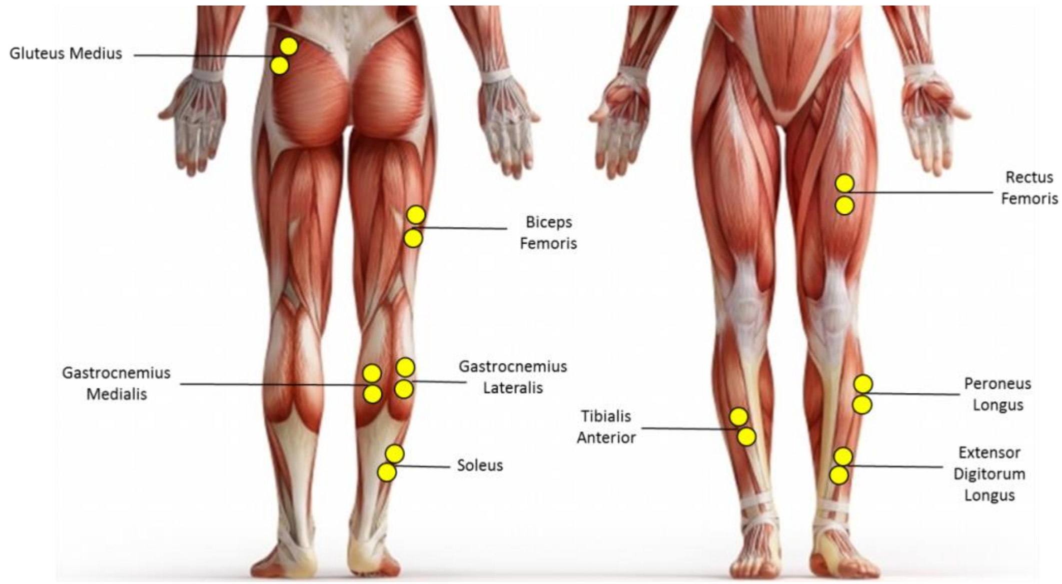

Figure 3. 3. EMG placement on lower limb muscles.

Past work in the Human Dynamics Laboratory at the University of Denver has shown that the use of a dual-plane high-speed stereo radiography (HSSR) enables accurate 3-dimensional measurement of bone motion during dynamic activities to sub-millimeter and sub-degree accuracy (Ivester et al., 2015). Rotational and translational errors associated with the system measurements include 0.4 ± 0.3 degrees and 0.2 ± 0.1mm (Ivester et al., 2015). This image acquisition technique has previously been performed to measure knee kinematics during gait, step-down, and seated knee extension tasks (Kefala et al., 2017). The system consists of two high-definition (1080x1080) high-speed digital cameras and two opposing 16-inch image intensifiers (Figure 3.4). The gantries housing the x-ray emitters and image-intensifiers were positioned 65 degrees relative to one another in order to capture slightly off-sagittal views of the foot. All activities were captured at a frame rate of 50fps excluding the box jump, which was captured at an increased frequency of 100fps. Pulsed radiography settings were fixed at 75kV, 100mA, with a pulse width of 1250μs. In this setting, x-ray was only released at the moment of image capture to significantly reduce unnecessary exposure to radiation (Kefala et al., 2017).

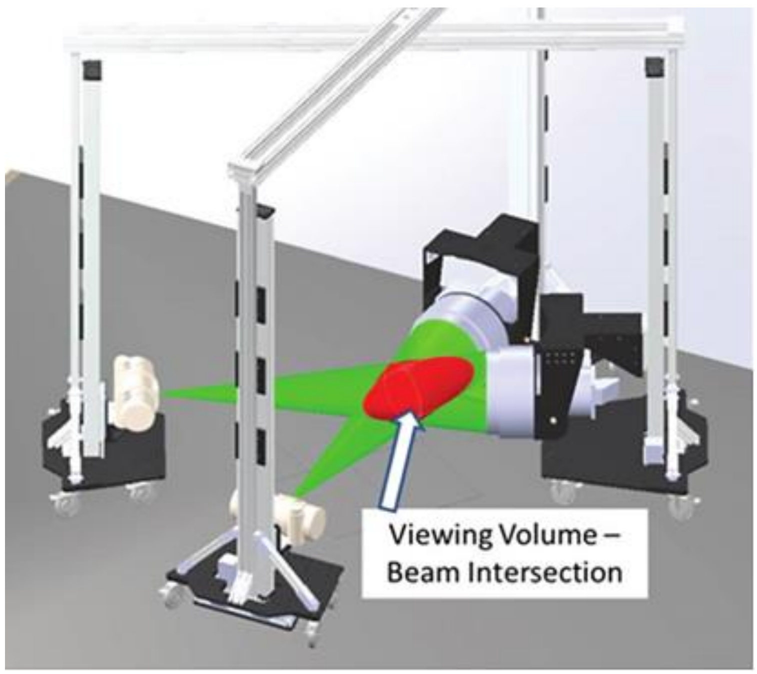

Figure 3. 4. HSSR configuration and capture volume (Ivester et al., 2015).

Undistortion and calibration of the raw fluoroscopy images was done using a custom built radio opaque mesh and calibration cube of known dimensions (Ivester et al., 2015; Kefala et al., 2017). Open-source software was then used to adjust the relative positioning and orientation of the subject's talus, fibula, and tibial bones, reconstructed from CT, to the images using direct linear transformation (DLT) algorithms (XROMM, Brown University, RI). Each volunteer had computed tomography (CT) scans taken from the base of their neutral foot up proximally 10cm from the ankle joint. One millimeter thick CT slices of the bone were used to reconstruct 3-dimensional subject-specific geometries of the tibia, fibula, and talus (ScanIP, Simpleware Inc.). Tracking bone motion was done via a 3D/2D image overlay matching process of the reconstructed bone to the fluoroscopic x-ray images in order to quantify translations and rotations at each pose (Autoscoper, Brown University). Acquiring HSSR imaging in synchrony with whole-body measurements (e.g. 3D motion capture and electromyography) establishes a connection between joint-level and whole-body biomechanics.

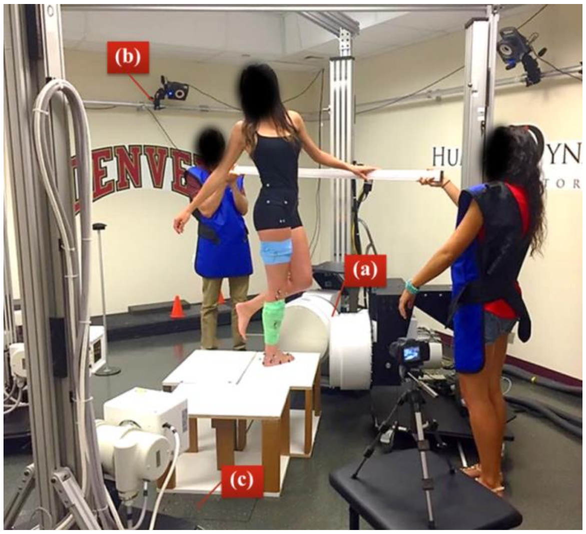

Figure 3. 5. Single-leg torso twist activity showing off-sagittal alignment of the foot with respect to the HSSR (a) image intensifiers. Also pictured: (b) Vicon cameras and (c) floor-embedded force plates.

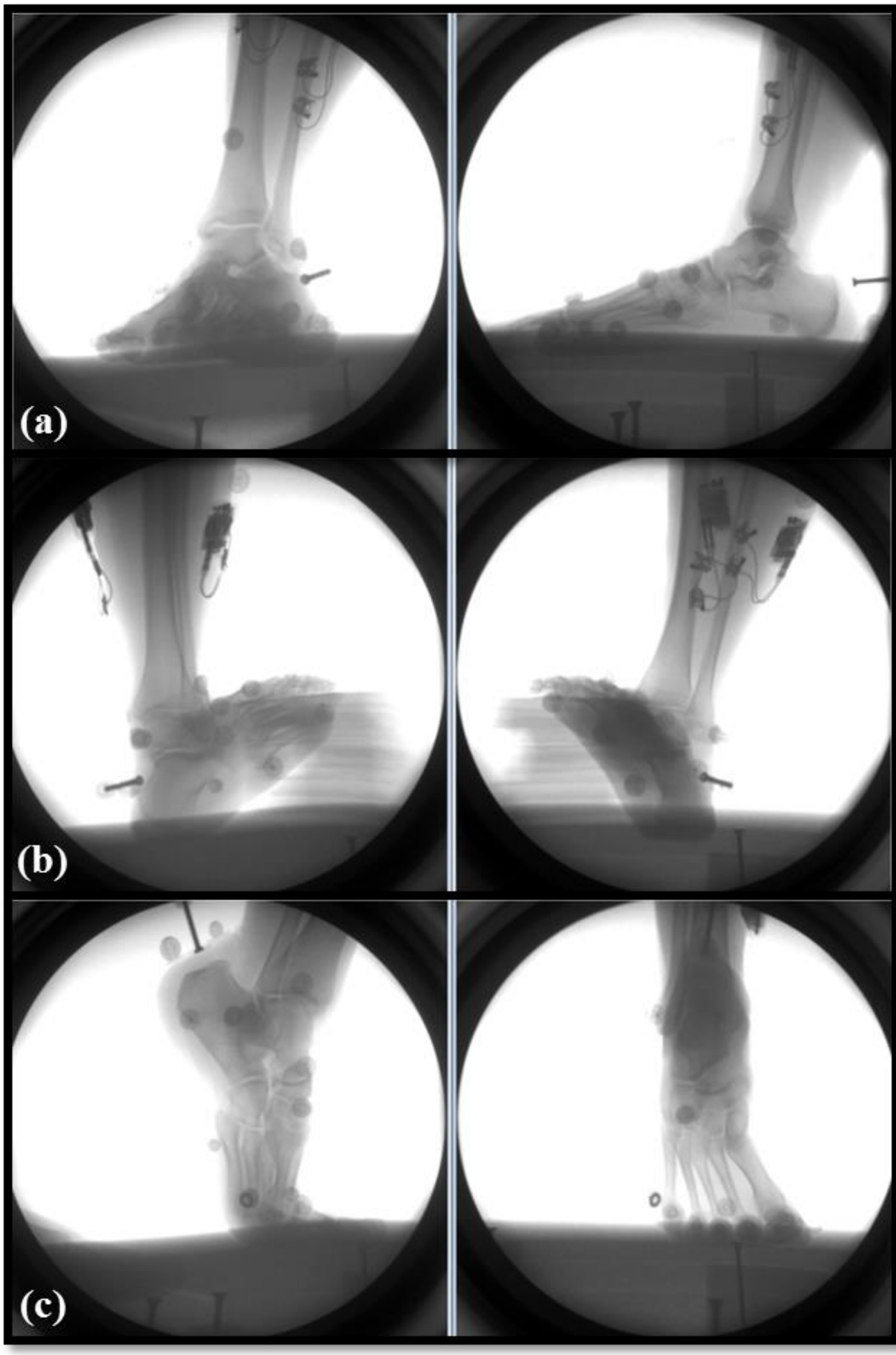

Figure 3. 6. Dual plane high-speed stereo radiography images of a foot in the static weight-bearing poses: (a) neutral, (b) dorsiflexion, (c) plantar flexion.

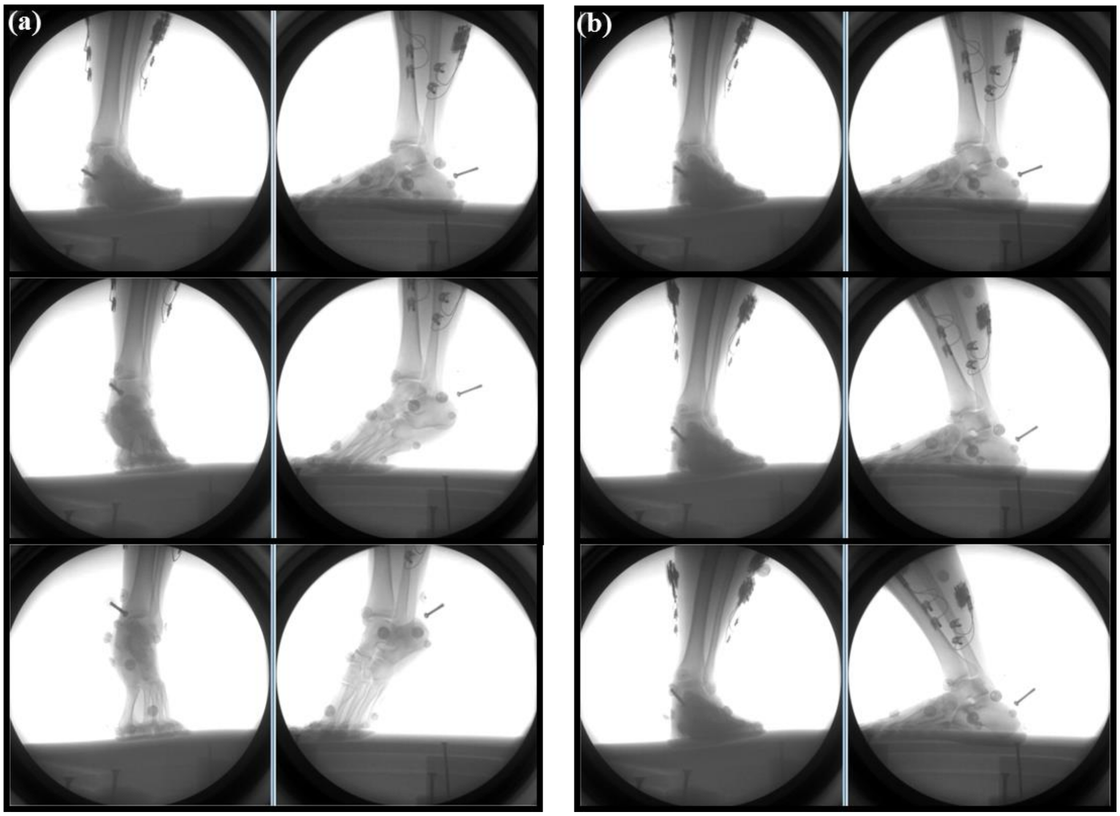

Figure 3. 7. Sequence of HSSR images showing single-leg: (a) heel rise and (b) squat exercises.

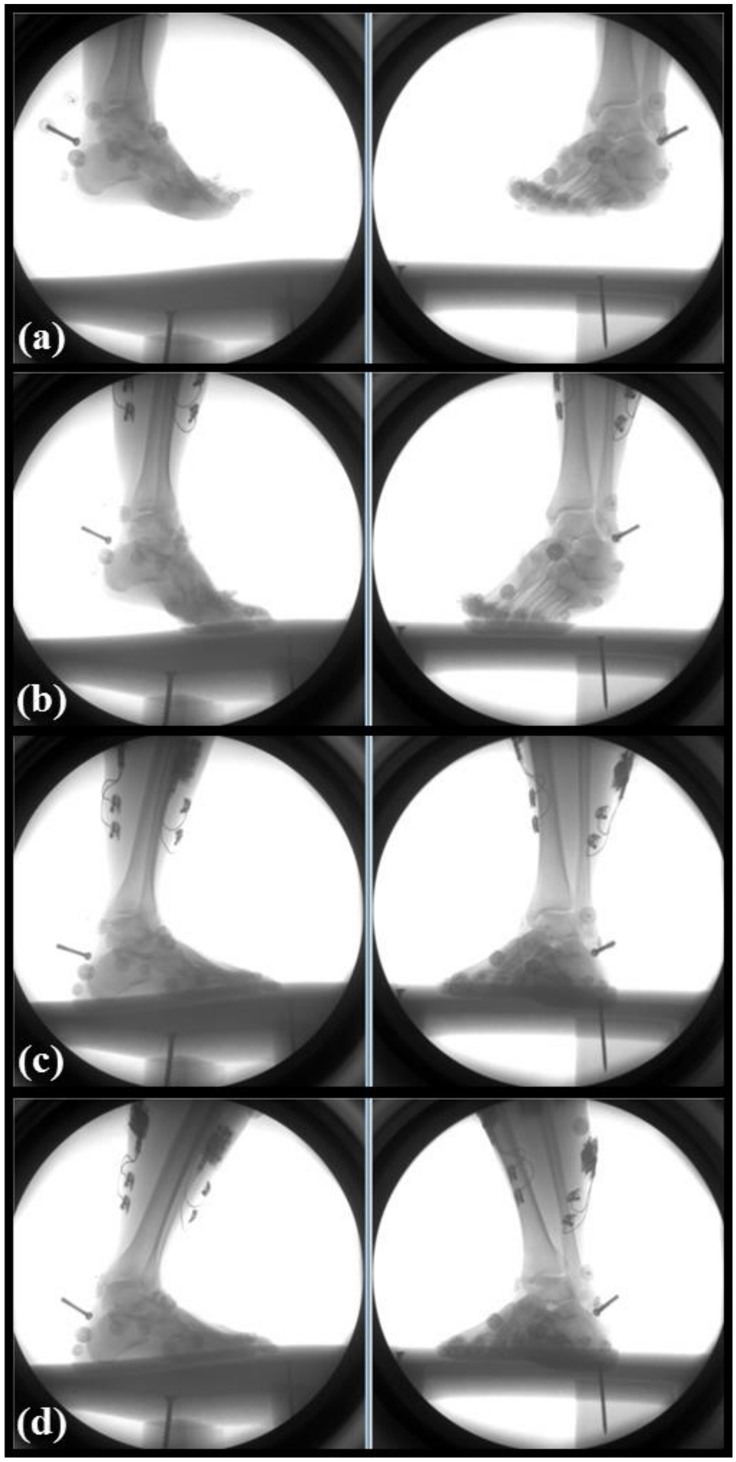

Figure 3. 8. Various phases of the box jump activity: (a) flight, (b) toe-strike, (c) heel strike, (d) stabilization.

3.2.4. Post Processing

Prior to bone tracking and kinematic analysis, local coordinate systems (LCS) built directly from easily identifiable landmarks of the bone were created using modified methods outlined by Grood and Suntay (1983) and the international society of biomechanics (ISB) (2002). All six DOF kinematics of the fibula and talus could be calculated relative to the tibia and normalized to each subjects' non-weight bearing neutral pose. Positive translations for the fibula coincide with lateral (L), anterior (A), and superior (S) directions. Rotations were deemed positive according to the right-hand rule and correlated to forward flexion (FF), inversion (IN), and internal rotation (IR) of the distal fibula. Forward and backward flexions were used to describe sagittal plane rotation of the distal fibula and differentiate from the common nomenclature of dorsiflexion/plantarflexion used to describe whole foot and talocrural joint motions. The same positive coordinate system was assigned to the talus, although dorsiflexion and plantarflexion (DF/PF) were used to describe sagittal plane motion (Figure 3.9). All other annotations for rotation and translation correspond to terminology commonly seen in literature. Appendix A provides an in-depth description of each LCS construction.

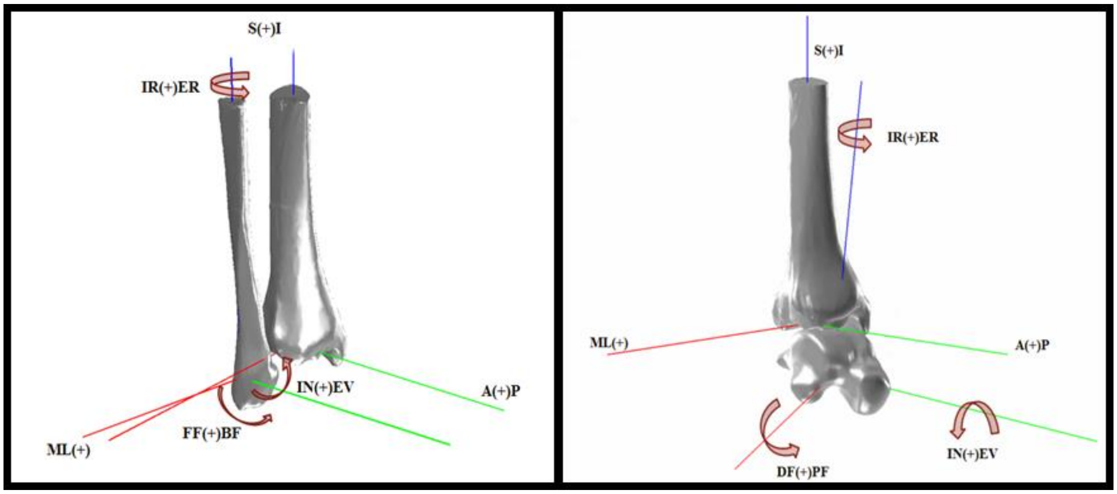

Figure 3. 9. Local coordinate system assignments for the (a) tibia and fibula of the syndesmosis and (b) talus and tibia of the talocrural joint. Medial/Lateral = M/L, anterior/posterior = A/P, superior/inferior = S/I, forward/backward flexion = FF/BF, dorsiflexion/plantarflexion = DF/PF, inversion/eversion = IN/EV, internal/external rotation = IR/ER.

3.2.5. Data Analysis

Three-dimensional translational and rotational motions were expressed relative to the positioning of the bones during a non-weight-bearing neutral pose of the foot and calculated using methods described by Grood and Suntay (1983). The six DOF kinematics and overall range of motion (ROM) within in the joints were dependent variables in this case. Small values for these variables were indicative of minimal excursion between the bones from their initial non-weight bearing neutral position. Articulation of the fibula and talus about the tibia were compared across various time points of the dynamic activities. For heel rise and squat, percent completion from the initial weight-bearing neutral stance (0% task completion) to the point of maximum plantarflexion or dorsiflexion (100% task completion) defined the limits of the activity analyzed. Torso twist was examined at the initial neutral stance, maximum external rotation, second neutral pose, and then maximum internal rotation. The box jump activity was analyzed at the frames in which the foot was in flight and nearly neutral (Pre), instant of initial contact typically seen as a toe strike (TS), heel strike (HS), instant when the maximum ground reaction force (GRF) occurs, then immediately after maximum GRF to represent a "stabilization" period (Post). Kinematics and ROM were expressed as mean ± standard deviation (SD). Statistical analysis showed no gender differences in kinematics or ROM values.

3.3. Results

Maximum ground reaction forces were measured throughout all static and dynamic tasks. Box jump showed the largest values of GRF at the instant of landing (Table 3.2).

Table 3. 2. Mean maximum ground reaction force components measured from the force plates.

Average Max Box Jump GRF (N)		
	Mean	**SD**
F_x	184.3	88.0
F_y	69.4	82.7
F_z	-1330.3	557.0

3.3.1. Tibiofibular & Talocrural ROM

Changes in fibular and talar positioning about the tibia relative to their initial non-weight bearing neutral locations are illustrated in Figure 3.10.

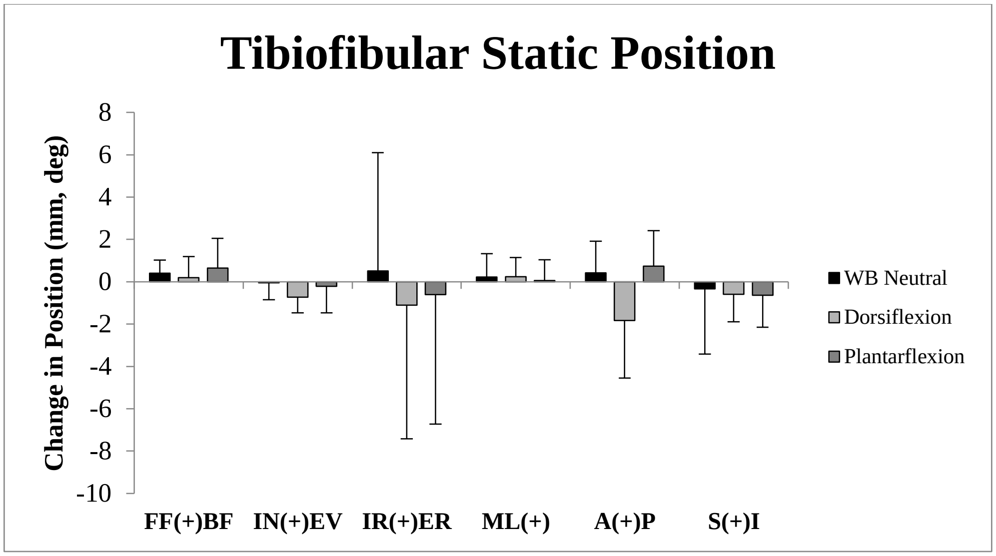

(a)

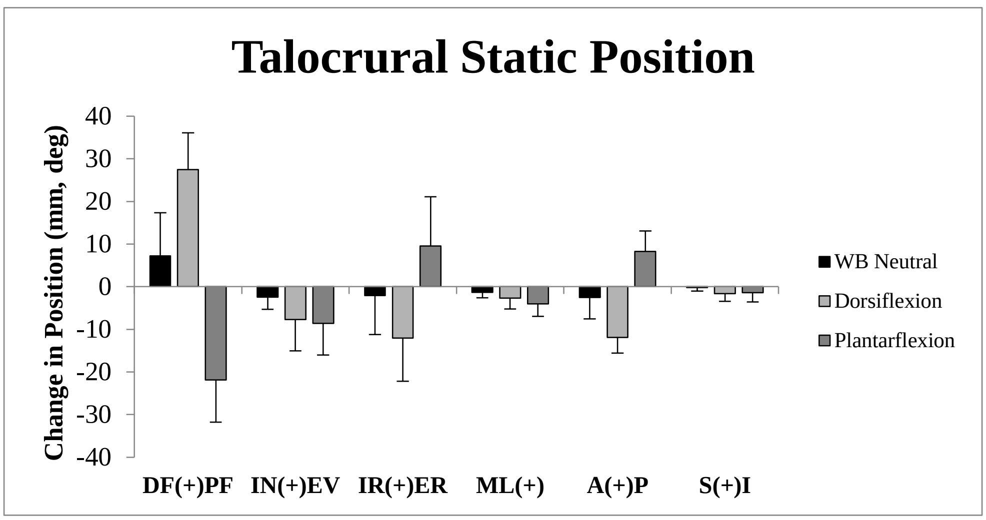

(b)

Figure 3. 10. Mean ± SD changes in weight-bearing static poses when compared to non-weight bearing neutral pose kinematics for (a) syndesmosis and (b) talocrural joints.

Table 3.3. Mean ± SD kinematics from static weight-bearing poses for (a) syndesmosis (b) talocrural joints.

(a)

Tibiofibular Static Pose Kinematics	FF(+)BF		IN(+)EV		IR(+)ER		ML(+)		A(+)P		S(+)I	
	Mean	SD	Mean	SD	Mean	SD	Mean	SD	Mean	SD	Mean	SD
WB Neutral	0.4	0.6	0.0	0.8	0.5	5.6	0.2	1.1	0.4	1.5	-0.3	3.1
Dorsiflexion	0.2	1.0	-0.7	0.7	-1.1	6.3	0.2	0.9	-1.8	2.7	-0.6	1.3
Plantarflexion	0.7	1.4	-0.2	1.3	-0.6	6.1	0.1	1.0	0.7	1.7	-0.6	1.5

(b)

Talocrural Static Pose Kinematics	DF(+)PF		IN(+)EV		IR(+)ER		ML(+)		A(+)P		S(+)I	
	Mean	SD	Mean	SD	Mean	SD	Mean	SD	Mean	SD	Mean	SD
WB Neutral	7.3	10.1	-2.5	2.8	-2.0	9.2	-1.3	1.3	-2.5	5.1	-0.2	0.8
Dorsiflexion	27.5	8.6	-7.7	7.4	-12.1	10.1	-2.7	2.6	-11.9	3.7	-1.6	1.8
Plantarflexion	-21.9	9.9	-8.6	7.4	9.5	11.6	-4.0	3.0	8.3	4.7	-1.4	2.2

There were no significant differences noted between degrees of freedom across static poses for the fibula ($P = 0.432$) or talus ($P = 0.211$). In general, static weight bearing caused minimal motion of the fibula. The greatest movements were seen in the dorsiflexed pose where the fibula externally rotated 1.1 ± 6.3 degrees and translated posteriorly 1.8 ± 2.7 mm. The talus showed notable ranges of motion in DF/PF, IR/ER, and A/P degrees of freedom. During dorsiflexion, the talus flexed 27.5 ± 8.6 degrees, externally rotated 12.1 ± 10.1 degrees, and shifted posteriorly 11.9 ± 3.7 mm. While plantarflexed, the talus exhibited 21.9 ± 9.9 degrees of extension, 9.5 ± 11.6 degrees of internal rotation, and 8.3 ± 4.7 mm of anterior translation.

The mean tibiofibular kinematics for each dynamic task are reported in Figure 3.11.

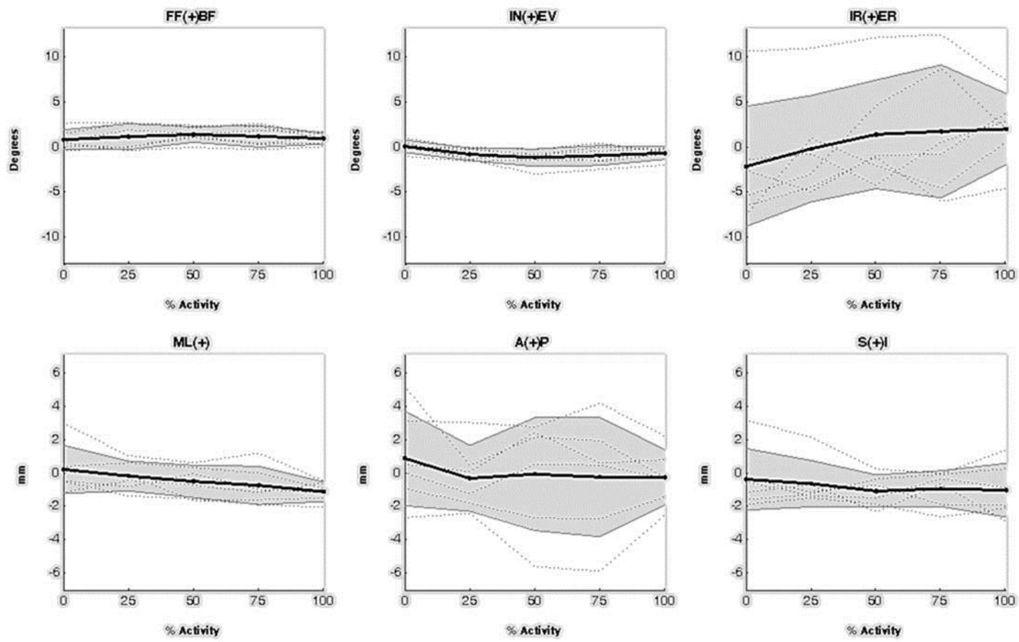
FF(+)BF
IN(+)EV
IR(+)ER
ML(+)
A(+)P
S(+)I
Degrees
mm
% Activity
(a)

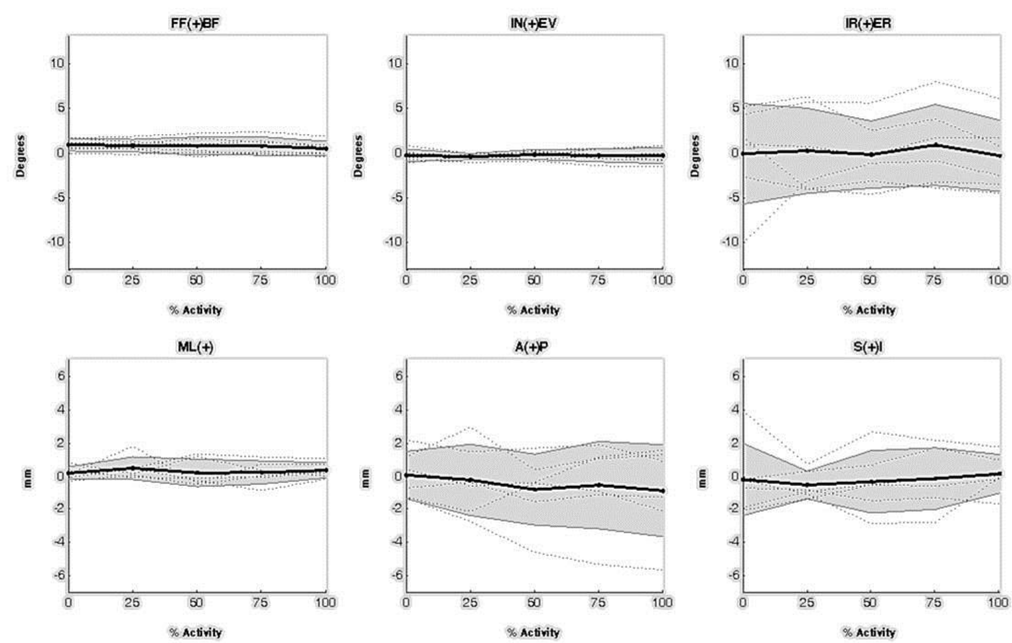
FF(+)BF
IN(+)EV
IR(+)ER
ML(+)
A(+)P
S(+)I
Degrees
mm
% Activity
(b)

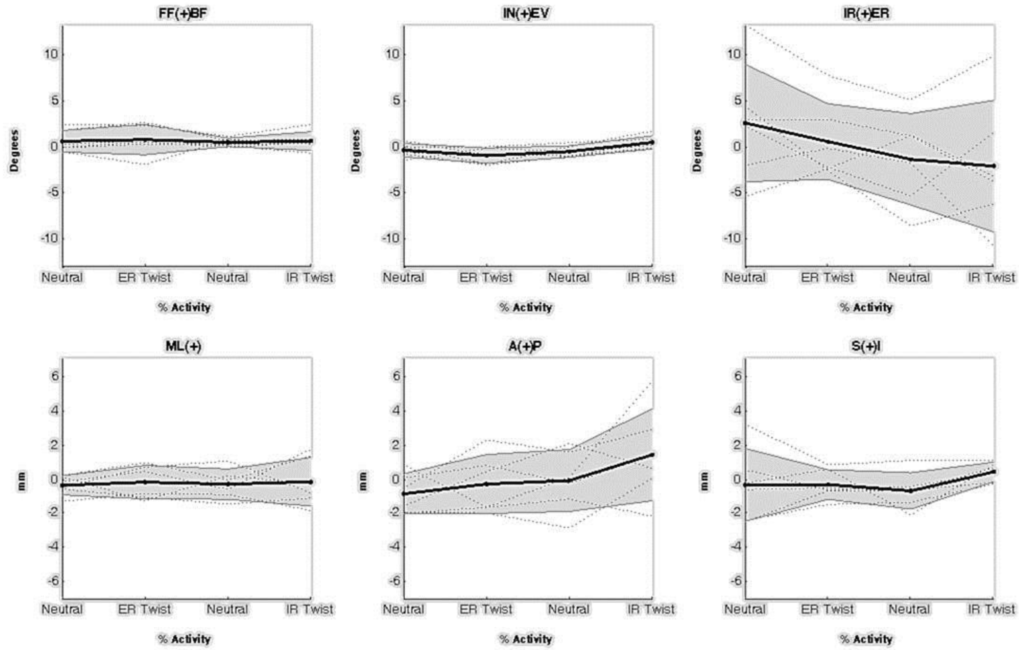

(c)

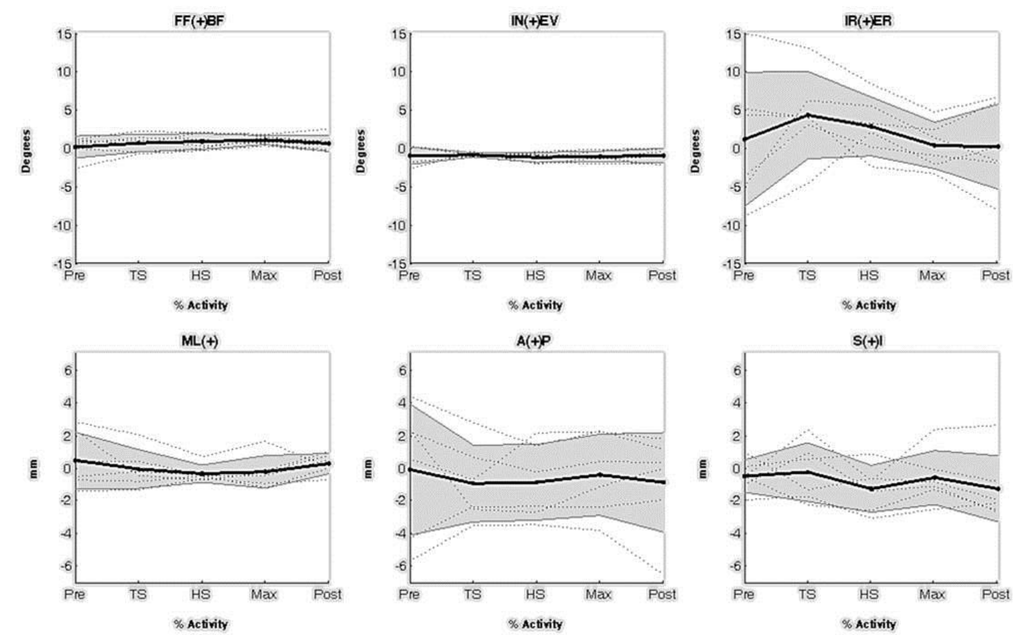

(d)

Figure 3. 11. Mean ± SD six DOF kinematics of the distal tibiofibular joint (mean = solid black line, individual subjects = grey dashed lines, SD = shaded region). All performed as single-leg weight-bearing activities: (a) heel rise, (b) squat, (c) torso twist, and (d) box

jump and referenced to a non-weight bearing neutral pose. Phases of box jump analyzed: Pre = flight, TS = toe-strike, HS = heel-strike, Max = maximum GRF, Post = stabilization.

During calf raise, the fibula initially rested externally rotated (2.2 ± 6.6 degrees) while the foot was in neutral stance, then ended internally rotated (1.9 ± 3.9 degrees) at maximum plantarflexion. A slight medial, posterior, and inferior excursion was also observed as the foot progressed through heel-rise. Surprisingly, deep squatting did not show a distinct opposite pattern in IR/ER when compared to heel-rise and only a minimal posterior translation was recorded at maximum dorsiflexion (0.9 ± 2.8 mm). The results of torso twist indicated a clear anterior shift of the fibula from neutral to the maximum internally rotated point of the upper body (1.4 ± 2.7 mm). Maximal internal rotation of the upper body also left the fibula externally rotated (2.1 ± 7.1 degrees) and superior (0.4 ± 0.6 mm) from when the body was positioned neutrally. External rotation of the torso did not result in correspondingly large rotational motions, although the fibula was slightly internally rotated (0.5 ± 4.1 degrees) and posterior (0.3 ± 0.9 mm). The box jump activity provided an interesting span of results since the full task essentially encompassed non-weight-bearing neutral, plantarflexion, dorsiflexion, and high loading scenarios. In the initial phase of the box jump during flight, the fibula was 1.1 ± 8.7 degrees internally rotated, 0.9 ± 4.0 mm posterior, and 0.5 ± 1.7 mm lateral. Toe-strike indicated additional internal rotation (4.3 ± 5.7 degrees) of the fibula, as well as posterior (0.9 ± 2.3 mm) and medial (0.5 ± 1.7 mm) translations. Heel-strike marked a drastic external rotation of the fibula and continued through stabilization where it ended oriented only 0.2 ± 5.5 degrees internally rotated with respect to the tibia. At the moment when maximum ground reaction force (GRF) occurred, the fibula was jolted anterior and superiorly approximately 0.5 and 0.7mm, respectively. The instant after maximum GRF, considered the stabilization phase (Post), the fibula maximally externally rotated, and translated laterally, posteriorly, and inferiorly. Heel-strike also marked the point in which the fibula shifted from medial to lateral translation.

The average six DOF kinematics of the talus with respect to the tibia are shown in Figure 3.12.

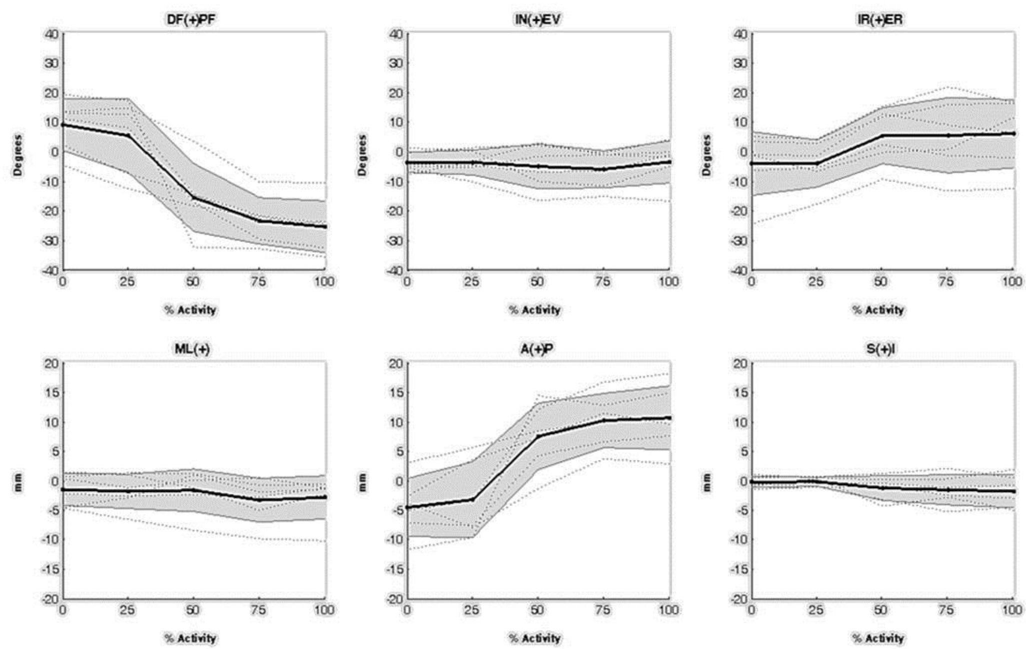

(a)

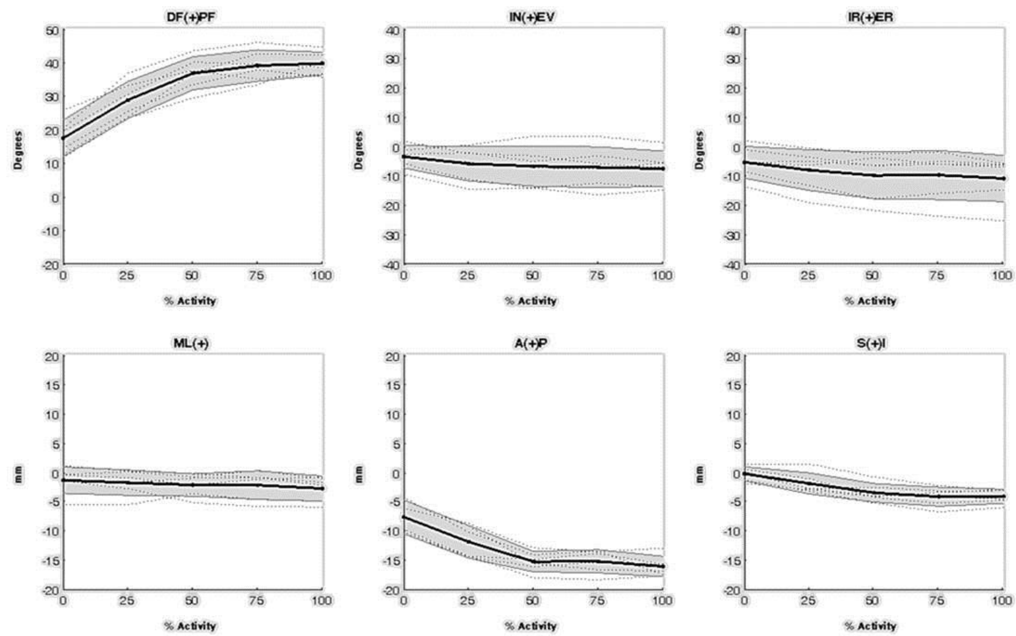
DF(+)PF
IN(+)EV
IR(+)ER
ML(+)
A(+)P
S(+)I
Degrees
mm
% Activity

(b)

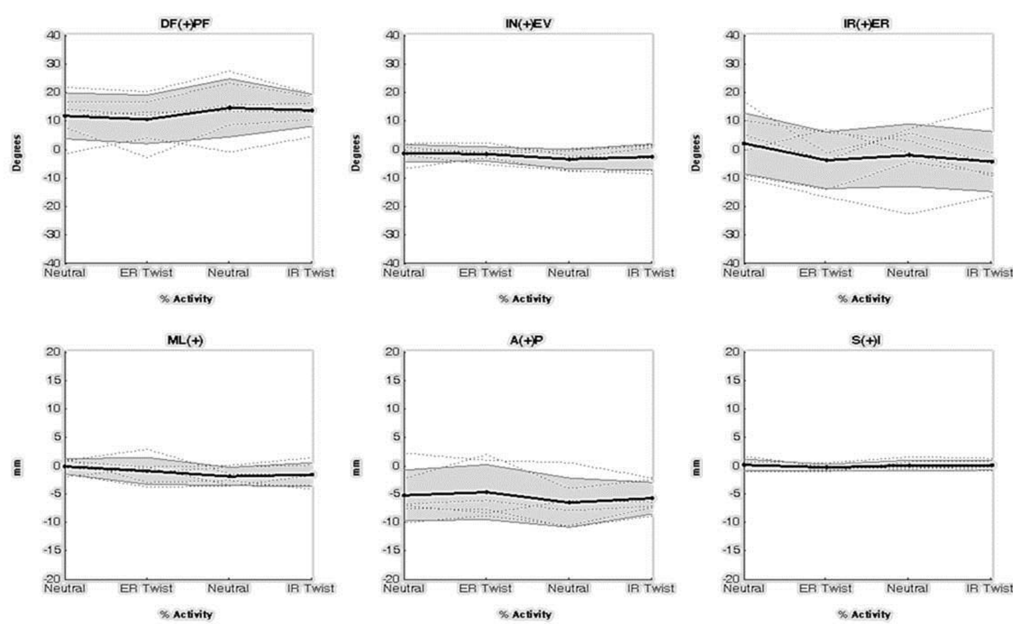
DF(+)PF
IN(+)EV
IR(+)ER
ML(+)
A(+)P
S(+)I
Degrees
mm
Neutral
ER Twist
Neutral
IR Twist
% Activity

(c)

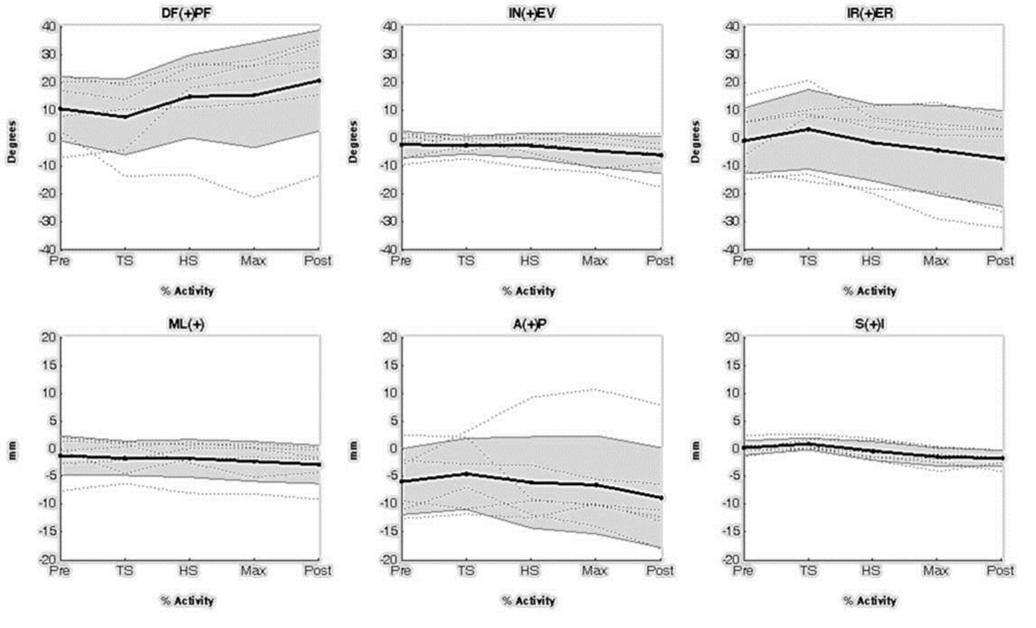

(d)

Figure 3. 12. Mean ± SD six DOF kinematics of the talocrural joint (mean = solid black line, individual subjects = grey dashed lines, SD = shaded region). All performed as single-leg weight-bearing activities: (a) heel rise, (b) squat, (c) torso twist, and (d) box jump and referenced to a non-weight bearing neutral pose. Phases of box jump analyzed: Pre = flight, TS = toe-strike, HS = heel-strike, Max = maximum GRF, Post = stabilization.

Heel-rise caused distinct plantarflexion, internal rotation, and anterior translation of the talus as the task progressed. An opposing trend was then seen during single-leg squat: dorsiflexion, external rotation, and posterior translation. Twisting of the torso did not demonstrate significant or distinct talar motion when compared to the other dynamic activities. As was the case for the fibula, the box jump maneuver illustrated unique patterns for talar articulation. Clear plantarflexion, internal rotation, and anterior movements were observed from flight to toe-strike phases. Heel-strike through stabilization displayed a rapid opposition in motion to dorsiflexion, external rotation, and posterior translation.

3.3.2. Range of Motion

Total ranges of motion in the syndesmosis and talocrural joints were defined for each dynamic task (Figures 3.13 & 3.14). For this study, range of motion was calculated as the difference between maximum and minimum kinematic values reported for a given activity. ROM expresses the absolute upper and lower limits of rotational and translation changes measured from the non-weight bearing neutral, as well as general positioning of the bone relative to the tibia.

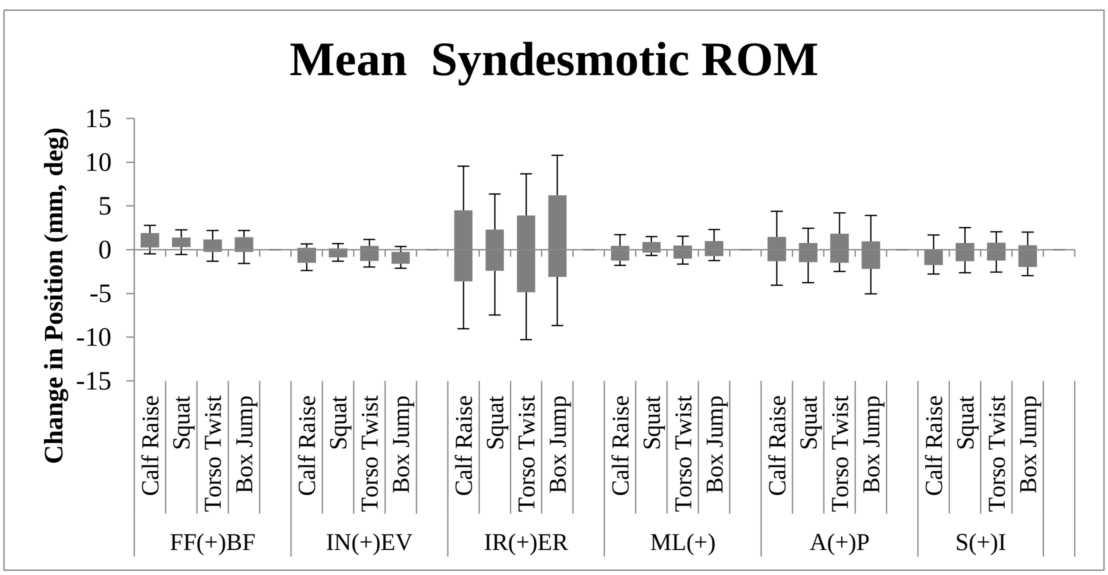

Figure 3. 13. Mean ± SD syndesmosis joint ROM for heel rise, squat, torso twist, and box jump tasks.

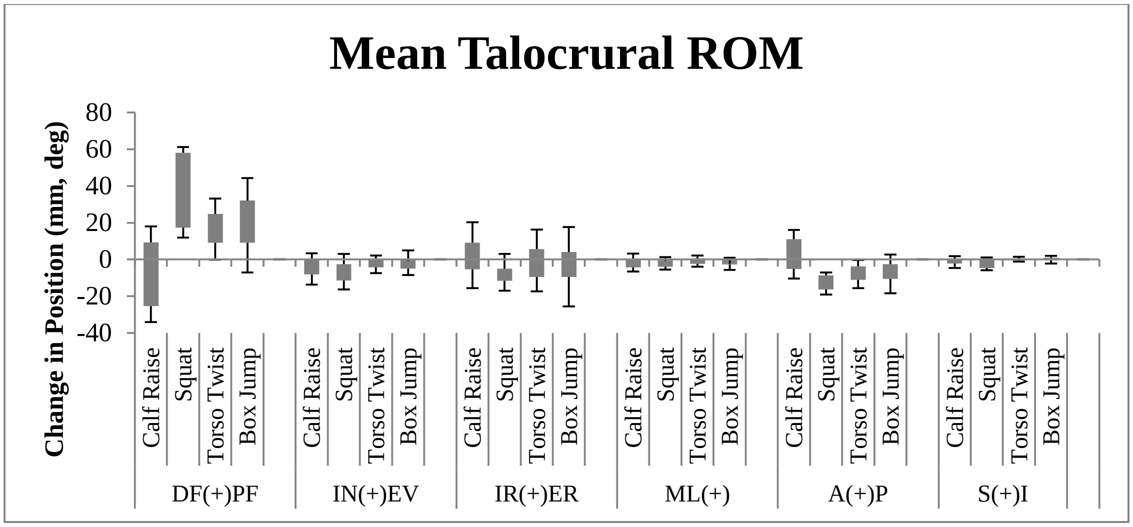

Figure 3. 14. Mean ± SD talocrural joint ROM for heel rise, squat, torso twist, and box jump tasks.

Table 3. 4. Mean ROM for all dynamic activities for (a) syndesmosis (b) talocrural joints.

(a)

Dynamic Syndesmotic ROM	FFBF		INEV		IRER		ML		AP		SI	
	Mean	SD	Mean	SD	Mean	SD	Mean	SD	Mean	SD	Mean	SD
Calf Raise	1.3	0.3	1.7	1.0	8.1	3.3	1.7	0.9	2.8	1.4	1.9	0.8
Squat	0.8	0.2	1.0	0.2	4.7	2.8	1.2	0.6	2.2	1.2	2.1	0.8
Torso Twist	1.4	0.9	1.7	1.0	8.8	2.5	1.5	0.5	3.3	2.2	2.0	0.7
Box Jump	1.7	0.7	1.4	0.5	9.3	3.5	1.7	1.0	3.2	1.0	2.5	0.9

(b)

Dynamic Talocrural ROM	DFPF		INEV		IRER		ML		AP		SI	
	Mean	SD	Mean	SD	Mean	SD	Mean	SD	Mean	SD	Mean	SD
Calf Raise	34.7	12.9	8.2	3.8	14.5	3.4	3.8	2.3	16.3	7.1	2.7	1.8
Squat	23.3	6.6	6.2	2.9	6.5	3.8	2.3	1.3	8.7	3.3	4.2	1.3
Torso Twist	6.6	3.9	4.3	1.7	15.0	3.4	3.0	1.6	3.5	1.5	1.2	0.8
Box Jump	17.8	9.8	7.1	3.6	13.3	4.9	3.3	1.9	8.0	5.7	2.9	1.3

For the syndesmosis joint, squatting imposed the least amount of overall excursion in the bone causing 0.8 ± 0.2 degrees, 1.0 ± 0.2 degrees, 4.7 ± 2.8 degrees in FF/BF, IN/EV, and IR/ER orientations, respectively. Total translational motions were 1.2

± 0.6 mm, 2.2 ± 1.2 mm, 2.1 ± 0.8 mm along the M/L, A/P, and S/I planes. Total motions for the calf raise showed 1.3 ± 0.3 degrees, 1.7 ± 1.0 degrees, 8.1 ± 3.3 degrees in FF/BF, IN/EV, and IR/ER as well as 1.7 ± 0.9 mm, 2.8 ± 1.4 mm, 1.9 ± 0.8 mm in M/L, A/P, and S/I directions, respectively. Torso twist and box jump activities caused the most change in IR/ER with 8.8 ± 2.5 degrees and 9.3 ± 3.5 degrees, as well as the greatest ranges in A/P showing 3.3 ± 2.2 mm and 3.2 ± 1.0 mm. The box jump activity also displayed the largest ranges in motion overall in FF/BF (1.7 ± 0.7 degrees) and S/I (2.5 ± 0.9 mm).

As expected, the ROM values measured for the talocrural joint were far greater than those for the syndesmosis. Maximum FF/BF were measured for calf raise (34.7 ± 12.9 degrees), while torso twist showed a mere 6.6 ± 3.9 degree change. Torso twist did however exhibit the most ranges in IR/ER (15.0 ± 3.4 degrees) and squat the least (6.5 ± 3.8 degrees). Calf raise and box jump had slightly less values in IR/ER than torso twist. Anterior-posterior ROM were highest for the calf raise exercise (16.3 ± 7.1 mm) and minimal during torso twist (3.5 ± 1.5 mm). Generally there were minimal variation and similar magnitudes of ROM in IN/EV, M/L, and S/I across all activities.

3.4. Discussion

Six DOF kinematic analyses of the syndesmosis and talocrural joints showed vast differences in overall bone articulation and highlighted the very small yet highly dynamic motions of the fibula during rapid weight-bearing maneuvers.

Generally, the kinematics of the fibula measured stereo radiography coincided with motions previously collected through cadaveric or other in-vivo testing methods. The fibula showed a constant forward flexed and everted orientation with respect to the tibia across all activities. This is indicative of its natural and congruent positioning within the incisura of the tibia to maintain stability at the joint. Static neutral standing caused minimal changes in motion in comparison to the dynamic tasks. In a neutral stance, the ankle experiences minimal shear stresses and the ligaments stabilizing the syndesmosis are minimally tensioned, thus explaining the lack of bone motion measured. When evaluating across all static weight-bearing poses, maximum dorsiflexion induced the greatest amount of excursion, which was in external rotation and posterior translation directions. This is consistent with the defined mechanism of injury for the syndesmosis joint. Dynamic exercises caused the greatest amount of motion in IR/ER, A/P, and S/I degrees of freedom especially during torso twist and box jump. This is in agreeance with Wang et al.'s, (2015) findings. Shear stresses on the distal joint that cause bone distraction are typically the result of quick twisting in the upper body while the foot remains planted. The effects of this were particularly apparent with internal rotation of the torso because an external rotating moment was applied to the foot causing the distal bones to externally rotate as well as translate anterior-superiorly.

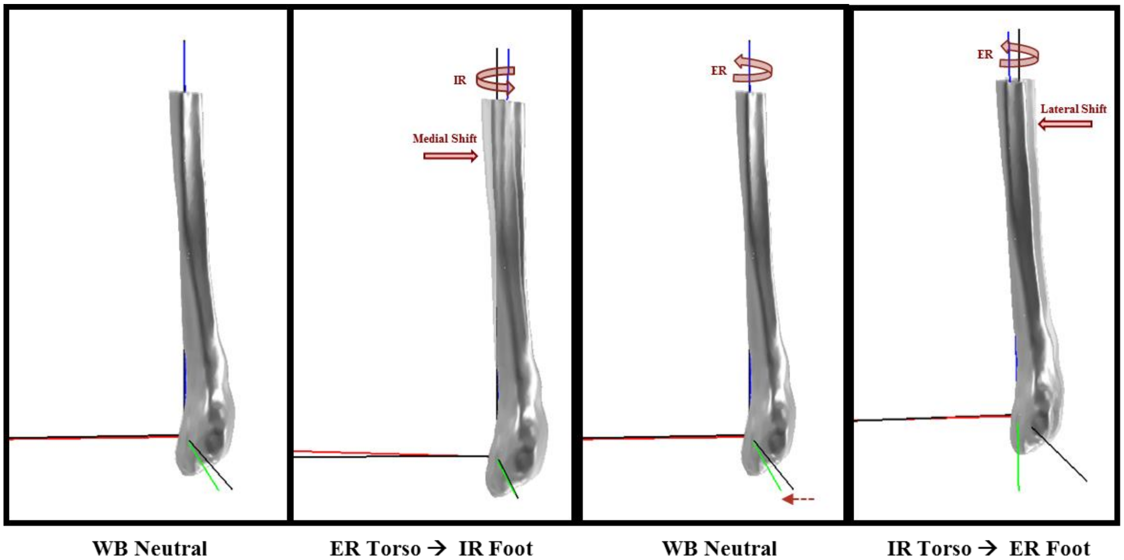

Figure 3. 15. Visual representation of fibular motion during torso twist. The transparent fibula with the black axis represents the fixed non-weighting neutral position. The solid bone with red (M/L), green (A/P), blue (S/I) axis represents the new spatial location of the fibula relative to the non-weight bearing neutral pose.

The box jump activity showed distinct kinematic patterns in fibular articulation as the foot progressed from flight phase to toe-strike (internal rotation, posterior and medial translations), then a rapid opposition in motions upon heel-strike to stabilization. The moment in which the maximum ground reaction force (GRF) occurs, marks an anterior and superior jolt of the fibula. The instance after GRF was considered a stabilization phase in which the fibula reaches maximum external rotation, and translates lateral, posterior, and inferior. During box jump, the ankle was subjected to forces up to 2.6 times body weight which is grossly larger than what has been used in any cadaveric testing and could explain this “jolting” reaction of the bone. Heel-strike also marks the point in which the fibula transitions from shifting medially to laterally. The values presented in this study are similar in magnitude to Wang et al.'s, (2015) dual-plane fluoroscopy measurements, although our calculations for IR/ER are higher. This discrepancy could be due to the high-demand tasks examined that would exert higher forces on the joint as compared to slow walking which was measured by Wang et al., (2015).

The tibiotalar kinematics provided a complimentary insight into the more distal responses in bone motion to these high-impact activities. Clear kinematic patterns of plantarflexion, internal rotation, and anterior translation were seen during heel-rise, while the reverse occurred with squatting. This supports past research indicating that talocrural joint is primarily responsible for plantar/dorsiflexion of the hind foot (Figures 3.16 and 3.17).

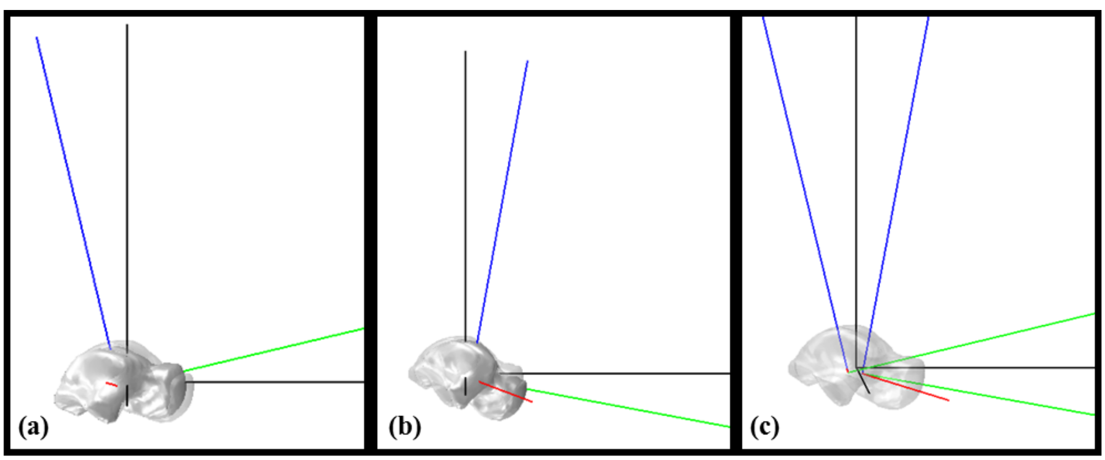

Figure 3. 16. Visual representation of talar motion during heel rise: (a) neutral weight bearing (0% activity), (b) maximum plantarflexion (100% activity), (c) 0% and 100% activity position comparison. The transparent bone with the black axis represents the fixed non-weighting neutral position. The solid bone with red (M/L), green (A/P), blue

(S/I) axis represents the new spatial location relative to its non-weight bearing neutral pose.

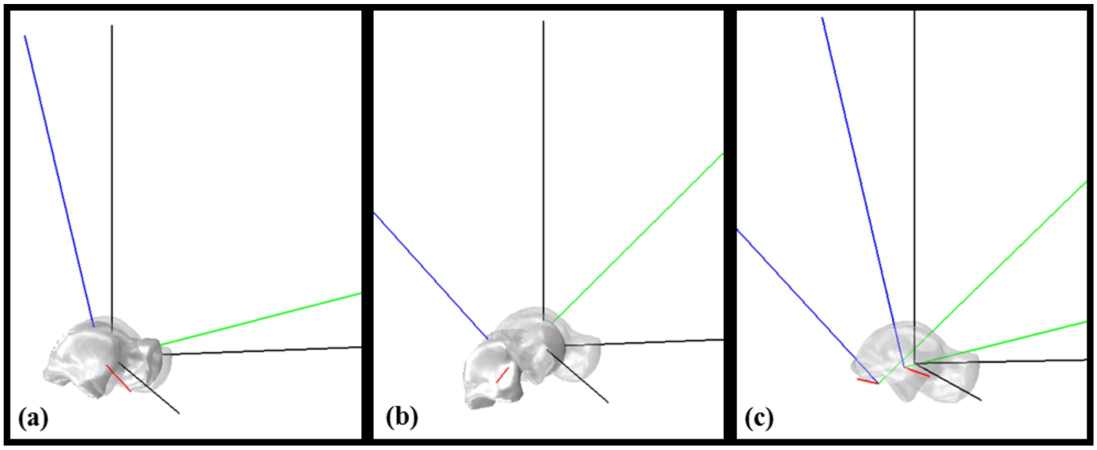

Figure 3. 17. Visual representation of talar motion during single-leg squat: (a) neutral weight bearing (0% activity), (b) maximum dorsiflexion (100% activity), (c) 0% and 100% activity position comparison. The transparent bone with the black axis represents the fixed non-weighting neutral position. The solid bone with red (M/L), green (A/P), blue (S/I) axis represents the new spatial location relative to its non-weight bearing neutral pose.

The lack of articulation during the torso twist indicates that the talus acts more of a sturdy base of support for the tibia and fibula to directly articulate on. The box jump maneuver also illustrated clear unique patterns of talar articulation from flight to toe-strike phases, then a rapid reversal in motion from heel-strike and through stabilization. All activities showed minimal magnitudes or changes in IN/EV kinematics which were indicative of the subtalar joint providing a majority of this movement for the hind foot.

ROM could be used as a metric to illustrate joint laxity along each anatomical plane. These measures could potentially optimize medical device design by clearly pin pointing specific degrees of freedom in which large and problematic motions occur within the joint that may require more robust constraining. Additional measures were defined in this study to be considered as potential tools for quantifying joint laxity: distal fibula path length and 3D excursion volume (Figures 3.18 and 3.19). A trajectory of the most distal prominence on the fibula was traced as its spatial positioning changed each dynamic task, while the sum of the distance travelled by that point defined its total path length. The 3D excursion volume combined all subject point trajectories into a single point cloud to illustrate total possible space spanned by the distal bone. Point tracing provides a map and quantifiable measures for the 3D micro motions of a specific point of interest on the bone. Clinically, this could be used to track the movement of the metallic buttons or screws implanted for syndesmotic repair.

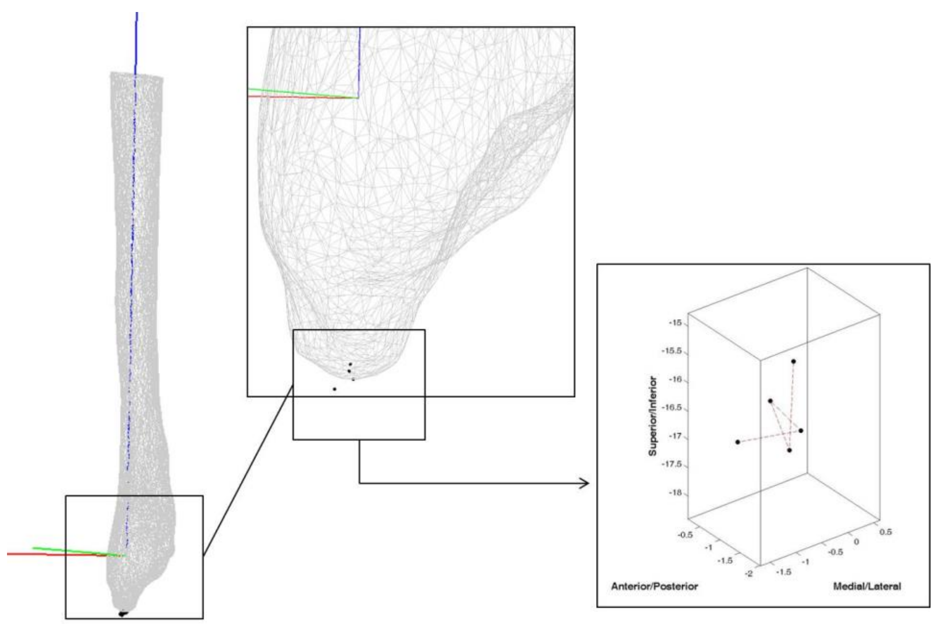

Figure 3. 18. Point tracing of the most distal prominence on the fibula and calculated path length from the traced trajectory (spatial units are in mm).

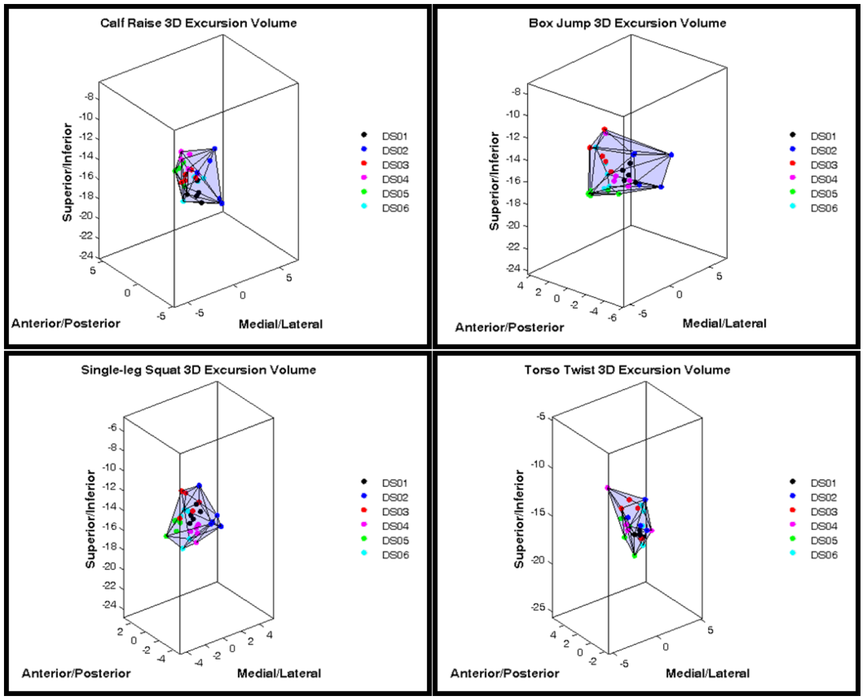

Figure 3. 19. Comparison of excursion point cloud volume for the distal fibula across dynamic activities (DS01-DS06 represent all subjects).

3.4.1. Limitations

Certain limitations should be noted for the study. First, the sample size (n = 6) could be considered relatively small compared to other studies with published kinematic data. A larger sample size could have provided statistical significance in some measures reported, although given time and cost constraints as well as the high accuracy of the HSSR system and similar anthropometric data among the subject cohort, it seemed unnecessary to expand the healthy participant population. Additionally, internal and external rotation proved to be the most variable measure. In order to minimize standard deviations, tracking was performed by a single person to limit inter-tracker variability. The activities reported, such as box jump and torso twisting, have never been measured using fluoroscopy. Not having previous data sets to compare the results of these activities to heed another limitation to the study, although illustrates the innovation this work contributes to healthy baseline data sets.

3.4.2. Conclusions

Currently, syndesmosis fixation devices are designed to primarily prevent lateral distraction of the fibula. The data presented in this work indicates a potential paradigm shift in how implantable devices are designed and that medial-lateral dislocation may be a secondary effect to larger alternate motions within the joint such as IR/ER, A/P, and S/I. Additionally, notable variation in individual joint angles and ROM across subjects was observed and speculated to be the result of distinctive bone geometry and muscle activation. Therefore, pairing in-vivo kinematics with EMG data to drive subject-specific muscle simulations in open-source software such as OpenSim could better describe individual joint kinetics, stability mechanisms such as muscular co-contraction, and the biomechanical effects of these implantable medical devices.

CHAPTER 4. MEDIAL AND LATERAL CLEAR SPACE OF THE ANKLE JOINT

4.1. Introduction

In the world of athletics the incidence of lower limb injuries, specifically to the ankle and foot, has been growing substantially among collegiate and professional athletes resulting in increased time away from practice and competition. In a study performed by Hunt et al. (2016) evaluating the incidence of foot/ankle injuries across 37 collegiate sports, it was found that female athletes sustained injury at a substantially higher rate of 53% compared to an injury rate of 47% for male athletes. This suggests that there may be important anatomical, physiological, and functional differences between female and male athletes that could contribute to higher biomechanical risk factors for ankle injuries. Additionally, lower limb injuries resulting in missed time were far more common in sports such women's soccer, women's cross-country, women's gymnastics, and men's cross-country where repetitive jumping or running is present (Hunt et al., 2016).

Injury to the syndesmotic joint specifically is more commonly referred to as a "high ankle sprain", and is the most prevalent ankle injury to occur among the athletic population. Damage to this fibrous joint accounts for up to 30% of all foot/ankle injuries reported during sporting activities (Waterman et al., 2011). Typically, harm to the syndesmosis occurs in sports such as football, soccer, lacrosse, and hockey where it is common for an athlete to experience rapid and extreme dorsiflexion-external rotations of the foot. This mechanism of injury is often seen when a player plants their foot in preparation for a cutting maneuver then collides with another player causing them to fall forward, as well as in ice skating or skiing when an athlete catches their toe edge and their body continues with forward momentum. Many have claimed that in these particular sports the incidence of injury rises drastically of upwards to 75% (Nussbaum et al., 2001; Wright et al., 2004). Another study concluded that collegiate football players are 14 times more susceptible to severe syndesmotic ankle injury than any other athlete involved in a contact sport (Hunt et al., 2016).

Severe syndesmotic sprains have been noted by clinicians as the most difficult ankle injury to accurately diagnose and treat, require the most recuperation time, and often results in life-long dysfunction (Waterman et al., 2011). Hermans et al. (2010) found that 40% of people suffering from severe high ankle sprains report instability 6 months after their initial injury. Additionally, of all ankle injuries reported during a sporting activity, more than half result in severe fracture of the bones or complete rupture of the surrounding ligaments (Jensen et al., 1998). When diagnosing syndesmotic injury, clinicians may ask patients to perform maneuvers such as a toe-rise, walking, or a series of single-leg hops to assess functional disability. Provocative tests such as the squeeze, external rotation, Cotton, fibular translation, or cross-leg are also commonly used to evaluate pain and integrity of the syndesmosis (Hunt et al., 2015). However, none of these tests clearly indicate the need for surgical fixation, which only becomes apparent in the case of class III injuries where frank diastasis of the bones is easily diagnosed via x-ray, magnetic resonance imaging (MRI), or computed tomography (CT) (Williams et al., 2014). Radiographic measurements of a tibiofibular (lateral) clear space >6mm or a tibiotalar (medial) clear space >4mm are indicative of severe injury and need for surgical fixation (Hunt et al., 2015). The clinical measure of medial clear space is defined as the distance between the medial talar dome and lateral face of the tibial malleolus. Lateral clear space measures the gap within the syndesmosis from the lateral posterior incisura of the tibia to the medial border of the fibula taken 1 cm proximal to the joint line. Radiographs are taken in mortise and A/P views. Stress films indicating diastasis of greater than 2mm when compared to the un-injured limb provide additional clues for inherent syndesmotic instability requiring internal fixation (Rammelt et al., 2008). For competitive athletes, misdiagnosis or improper treatment of high ankle sprains could result in unnecessary surgery for less severe class II injuries, malreduction of the bones during surgical fixation, prolonged time missed from competition, or life-long complications and discomfort. The alarmingly high occurrence rate of syndesmotic injury among young athletes and its inherent risk for chronic disability raises a cause for concern to better understand the injury and improve treatment methodologies.

Healthy six degrees of freedom (DOF) kinematics for the syndesmosis and talocrural joints were previously established and used to define normal ROM of the fibula and talus relative to the tibia during static weight-bearing and high-impact dynamic activities (Chapter 3). This baseline data allowed for further analysis of the medial and lateral clear space widening that occurs during these high-stress and sport-like maneuvers. Defining limits for healthy joint distraction could potentially improve diagnostic measures of syndesmotic injury and shed light on alternative approaches to treatment.

4.2. Methods

Chapter 3 of this document describes in detail how high-speed stereo radiography (HSSR) was used to capture in-vivo motion of the distal tibia, fibula, and talus with sub-millimeter and sub-degree accuracy. Participant information, experimental protocol, and all instrumentation used previously in chapter 3 remained the same.

Calculations of the medial and lateral clear space distances were done via a custom MATLAB code. First, subject-specific bone geometries were converted into a point cloud which then had tracking data applied to drive the spatial change of the bone throughout the activity. The tibial point cloud was sectioned (Figure 4.1) such that only the medial malleolus and some of the distal plafond were used for calculating tibiotalar clear space, whereas the full distal tibia point cloud was used for lateral clear space calculations. Fifty centimeters of the distal fibula point cloud was extracted in order to focus clear space calculations solely on the syndesmotic portion of the bone. No sectioning of the talus was necessary since the medial malleolus had already been separated. Minimum distances were then calculated from one object (fibula or talus) point cloud to the nearest neighbor's point cloud defining the second object (tibia). This brute-force method returned gap distance values between the tibia-fibula and tibia-talar faces for every point-point combination in the bone cloud geometry. Sectioning of the bone not only defined the distinct medial and lateral clear space windows to be measured, but also drastically decreased computational time. A nearest neighbor path was drawn between the bones to illustrate the exact location of the minimum gap distance (Figure 4.2). A contour plot displaying all clear space distances <5mm were mapped along the fibula and talus geometries to visually illustrate changes in anatomical spacing between the bones (Figure 4.2).

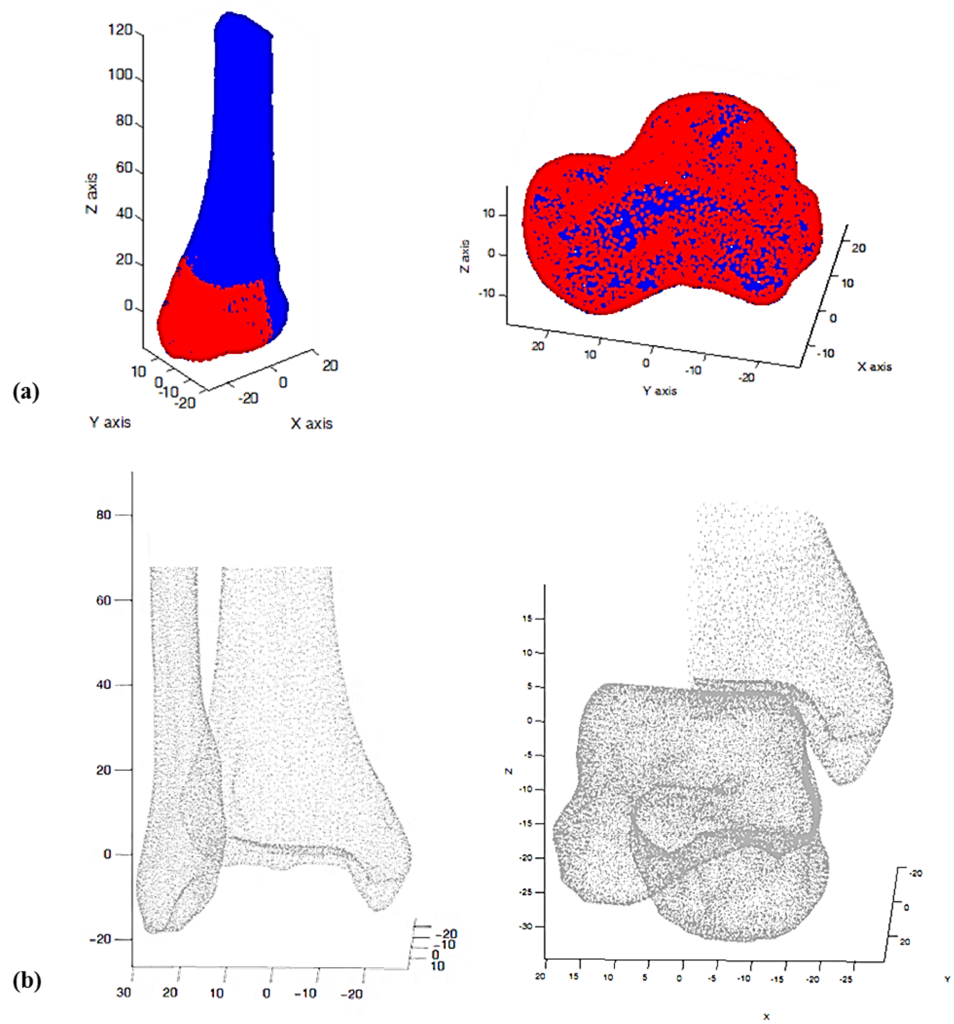

Figure 4. 1. (a) Bone sectioning and (b) point cloud extraction for lateral and medial clear space measurements. Blue points indicate original bone, while red points are the sectioned bone to be used for the point cloud.

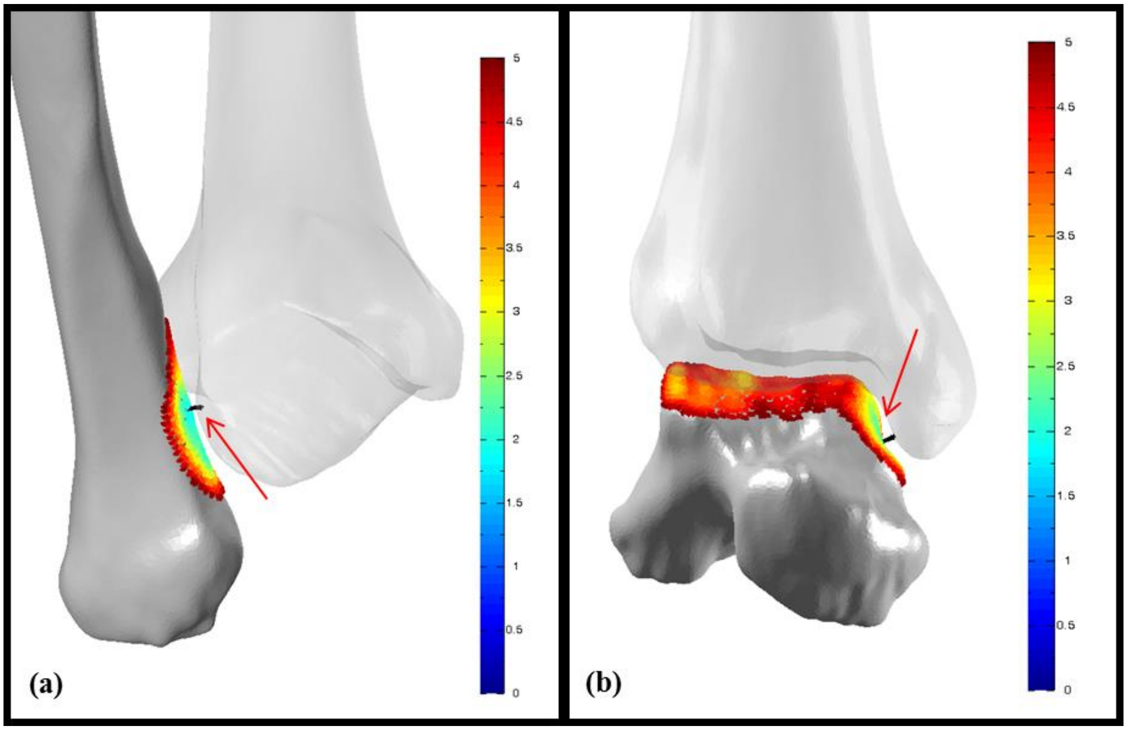

Figure 4. 2. Anatomical contour plot of bone spacing and identification of minimum (a) lateral and (b) medial clear spaces, as indicated by the black line connecting the bones.

4.2.1. Data Analysis

All data were expressed in terms relative to the positioning of the bones during a non-weight bearing neutral pose of the foot. Small values in clear space indicate a minimal gap distance between the bones. The scaling for the contour plots range from 0-5 mm of clear space distances. Since these are healthy subjects, it was anticipated that values would not exceed 5mm that would otherwise indicate severe injury. Dark blue on the contour represents the absolute minimum separation (0mm) between the bones, whereas red illustrates the upper limit of bone separation (5mm). Articulation of the fibula and talus about the tibia was compared across consistent time points in the dynamic task. For heel rise and squat, percent completion from initial weight-bearing neutral stance (0% task completion) to the point of maximum plantarflexion or dorsiflexion (100% task completion) defined the limits of the activity analyzed. Torso twist was examined at the initial neutral stance, maximum external rotation, second neutral pose, and then maximum internal rotation. The box jump activity was analyzed at the frames in which the foot was in flight and nearly neutral, initial instant of contact (typically a toe strike), heel strike, the instant of maximum ground reaction force (GRF), and then immediately after max GRF to represent a "stabilization" period. Differences in mean clear space throughout the dynamic activities were examined using one-way ANOVA and Tukey's HSD post-hoc. Linear regression was done to compare the effect percent task completion on joint clear space distances for heel rise and squatting tasks. The level of significance was set to $\alpha = 0.05$. No significant differences were found between genders.

4.3. Results

4.3.1. Lateral Clear Space

Syndesmotic gap distance measurements of the statics poses illustrated distinct effects of weight-bearing and foot positioning on fibular distraction from the tibia.

Table 4. 1. Mean lateral clear space distances for poses.

Lateral Syndesmosis Clear Space (mm)		
	Mean	**SD**
Non-WB	1.4	0.5
WB	1.7	0.6
Dorsiflexion	1.8	1.2
Plantarflexion	0.7	0.5

Joint distraction in the neutral stance increased 0.3mm with weight-bearing. Dorsiflexion displayed the greatest amount of syndesmotic gap space (1.8 ± 1.2 mm), whereas plantarflexion compressed the joint to absolute its minimum gap distance (0.7 ± 0.5 mm).

Changes in mean lateral clear spaces between the tibia and fibula are presented below for all dynamic activities (Figure 4.3).

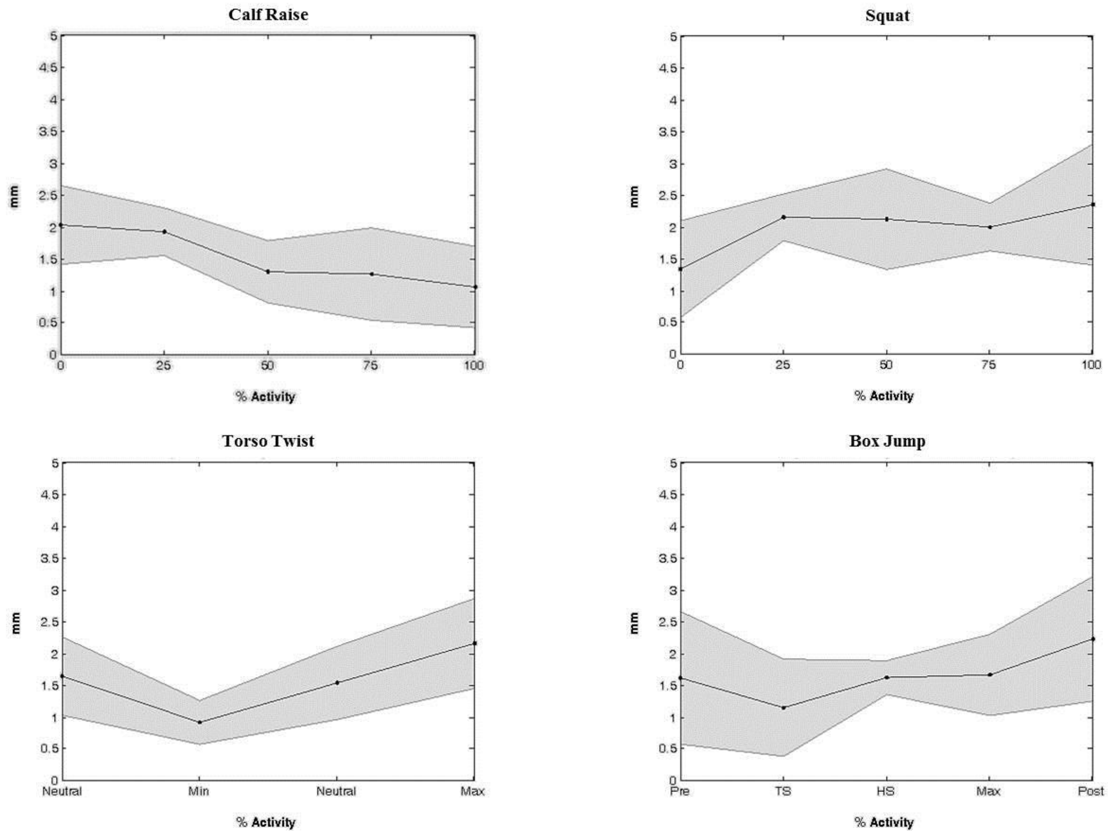

Figure 4. 3. Mean ± SD lateral clear space of the syndesmosis joint for calf raise, squat, torso twist and box jump. Phases of box jump: Pre = flight, TS = toe-strike, HS = heel-strike, Max = maximum GRF, Post = stabilization.

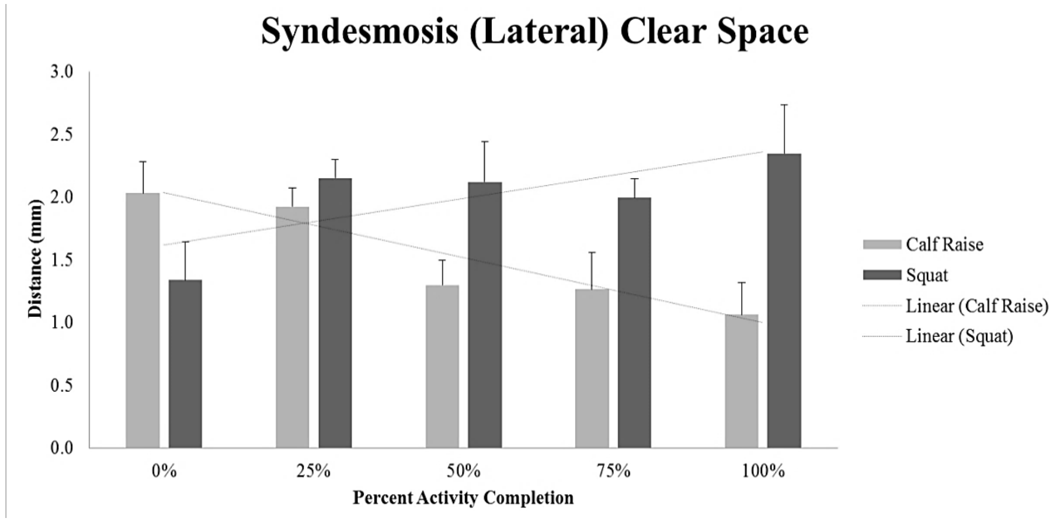

Figure 4. 4. Direct comparison of minimum syndesmotic gap distance vs percent task completed for single-leg calf raise (heel rise) and squat. Analysis shows significant linear regression for calf raise (P=0.001) and squat (P=0.045).

Table 4. 2. Mean lateral clear space distances for throughout heel-rise.

Lateral Syndesmosis Clear Space (mm)		
Percent Completion	**Mean**	**SD**
0%	2.0	0.6
25%	1.9	0.4
50%	1.3	0.5
75%	1.3	0.7
100%	1.1	0.6

Table 4. 3. **Mean lateral clear space distances for throughout squat.**

Lateral Syndesmosis Clear Space (mm)		
Percent Completion	**Mean**	**SD**
0%	1.3	0.8
25%	2.2	0.4
50%	2.1	0.8
75%	2.0	0.4
100%	2.3	0.9

Calf raise and squat indicated significant and opposing linear regressions for mean clear space values vs percent activity completion. From neutral stance (0% completion) to maximum plantarflexion (100% completion) of the calf raise, there was a significant decrease (P=0.001) in clear space distance of 2.0 ± 0.6 mm to 1.1 ± 0.6 mm. Single-leg squat showed a significant increase (P=0.045) in syndesmotic gap space from neutral (1.3 ± 0.8 mm) to maximum dorsiflexion (2.3 ± 0.9 mm).

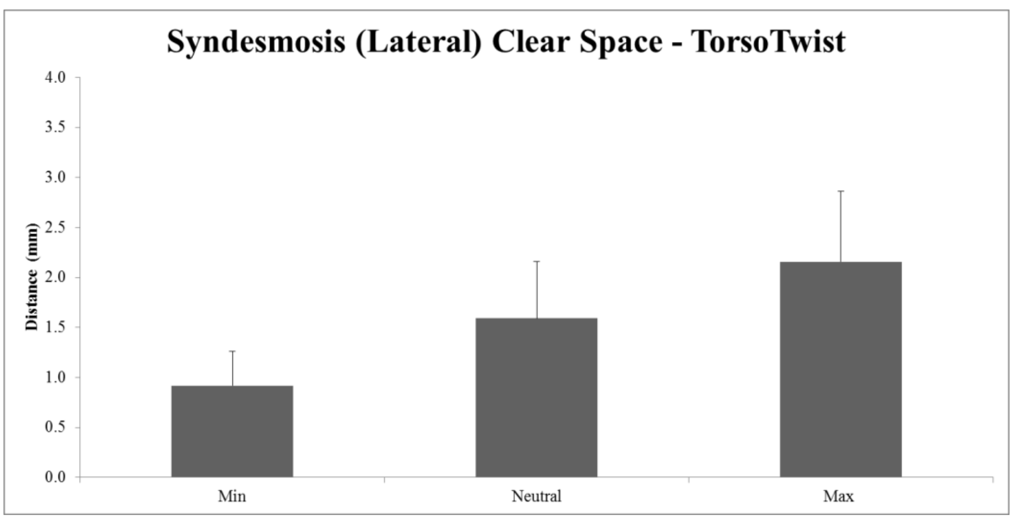

Figure 4. 5. Mean minimum and maximum clear space distances from external or internal twisting of the torso. Analysis shows a significant difference between min and max values (P=0.012).

Table 4. 4. Mean lateral clear space distances for extreme torso twist, neutral, and twisting to the opposite extreme.

Lateral Syndesmosis Clear Space (mm)		
Twist Pose	**Mean**	**SD**
Min	0.9	0.3
Neutral	1.6	0.6
Max	2.2	0.7

At either direction of torso rotation, absolute minimum (0.9 ± 0.3 mm) or maximum (2.2 ± 0.7 mm) clear space distances were observed (Figure 4.5). A comparison between the mean maximum and minimum gap distances showed significance (P = 0.012). The neutral stance during this activity averaged 1.6 ± 0.6 mm in tibiofibular separation.

Lateral clear space measurements throughout box jump correlated nicely to flexion/extension motions of the foot known to cause either distraction or compression of the joint (Figure 4.6).

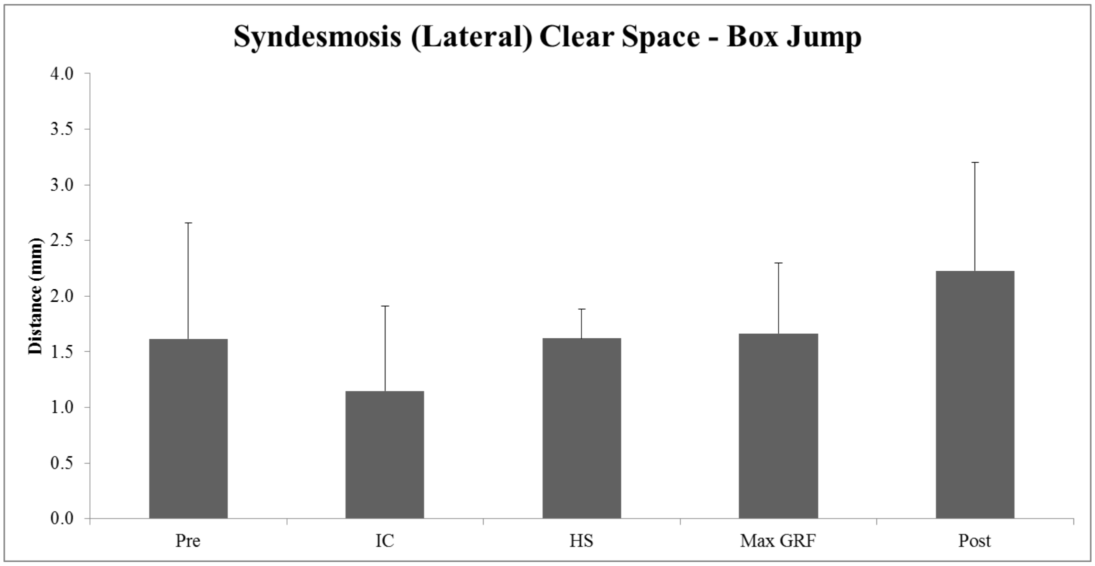

Figure 4. 6. Mean lateral clear space distances throughout box jump activity (P = 0.254).

Table 4. 5. Mean lateral clear space distances for various phases of box jump.

Lateral Syndesmosis Clear Space (mm)		
Box Jump Phase	**Mean**	**SD**
Pre	1.6	1.0
IC	1.1	0.8
HS	1.6	0.3
Max GRF	1.7	0.6
Post	2.2	1.0

Previously it was shown that plantarflexion of the foot is associated with medial translation of the fibula, thus causing a decrease in syndesmotic clear space. This was observed when the foot began in a near neutral position during flight phase (Pre) then plantarflexed in preparation for initial contact with the surface to mark the toe-strike phase. Upon landing when heel-strike occurs, the ankle rapidly dorsiflexed and instant distraction of the joint was seen. The additional loading from GRF's did not cause further distraction, although the stabilization phase that followed showed the greatest amount of clear space widening between the tibia and fibula. This maximum distraction between the bones was likely due to deeper squatting of the volunteer in order to balance. Increased dorsiflexion at the ankle pushed the fibula farther away from the tibia. These values measured were not significantly different between phases of the box jump (P=0.254).

4.3.2. Medial Clear Space

Gap distances between the tibial malleolus and talar dome for each of the statics poses were far less telling than the tibia-fibula measurements.

Table 4. 6. Mean medial clear space distances for static poses.

Medial Tibiotalar Clear Space (mm)		
	Mean	**SD**
Non-WB	2.1	1.2
WB	1.8	1.3
Dorsiflexion	1.8	1.5
Plantarflexion	2.1	1.3

Joint distraction in the neutral stance decreased 0.3mm with weight-bearing, indicating compression of the talus to support loading. Dorsiflexion did not show a change in clear space (1.8 ± 1.5 mm) from weight-bearing, and plantarflexion caused slight distraction of the joint (2.1 ± 1.3 mm). Again, there were no significant differences between these measurements.

Changes in mean medial clear spaces between the malleolus of the tibia and talar dome are shown below for all dynamic activities (Figure 4.7).

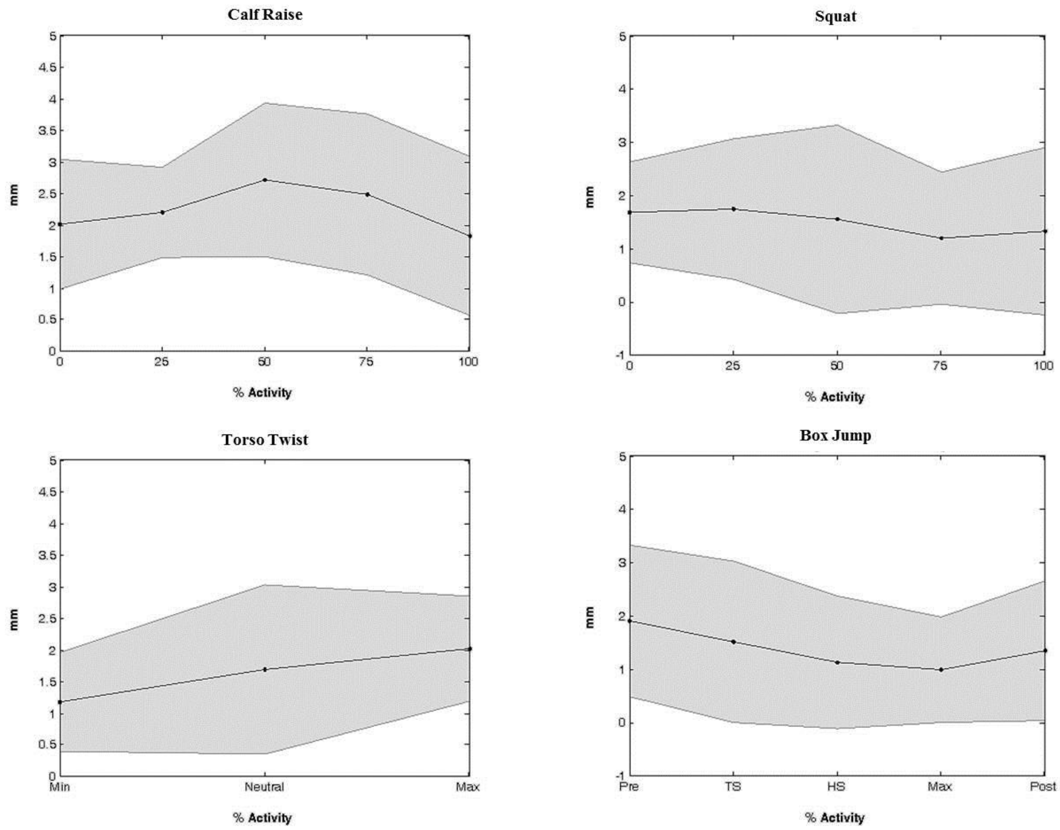

Figure 4. 7. Mean ± SD medial clear space of the talocrural joint for calf raise, squat, torso twist, and box jump. Phases of box jump: Pre = flight, TS = toe-strike, HS = heel-strike, Max = maximum GRF, Post = stabilization.

Table 4. 7. Mean medial clear space distances for throughout heel-rise.

Medial Tibiotalar Clear Space (mm)		
Percent Completion	**Mean**	**SD**
0%	2.0	1.0
25%	2.2	0.7
50%	2.7	1.2
75%	2.5	1.3
100%	1.8	1.3

Table 4. 8. Mean medial clear space distances for throughout squat.

Medial Tibiotalar Clear Space (mm)		
Percent Completion	Mean	SD
0%	1.7	0.9
25%	1.7	1.3
50%	1.5	1.8
75%	1.2	1.2
100%	1.3	1.6

Minimum medial clear spacing is seen at maximum heel-rise (1.8 ± 1.25 mm), although there was no distinctive trend in clear space distraction as the activity progresses. Single-leg squatting showed a general pattern of decreasing clear space from neutral standing to maximum dorsiflexion. The minimum tibiotalar gap distance occurred at the deepest point in the squat (1.3 ± 1.6 mm). The overall change in medial clear space distance was 0.4 mm. There were no significant differences between percent of activity completion.

Table 4. 9. Mean medial clear space distances for extreme torso twist, neutral, and twisting to the opposite extreme.

Medial Tibiotalar Clear Space (mm)		
Twist Pose	Mean	SD
Min	1.2	0.8
Neutral	1.7	1.3
Max	2.0	0.8

Similar to the behavior of the fibula, extreme torso twisting caused both maximum and minimum joint displacements. However, the difference in these joint space values between both twisting directions and neutral stance were not significant (P = 0.405). An overall change of 0.8 mm in medial clear space widening was measured throughout the task.

Tibiotalar clear space throughout the box jump showed a general decreasing trend in which the absolute minimum occurred at maximum GRF. The large force produced from the foot impacting the ground could have caused the talus to be wedged even deeper into the ankle resulting in further compression of the joint space.

Table 4. 10. Mean medial clear space distances for various phases of box jump.

Medial Tibiotalar Clear Space (mm)		
Box Jump Phase	**Mean**	**SD**
Pre	1.9	1.4
IC	1.5	1.5
HS	1.1	1.2
Max GRF	1.0	1.0
Post	1.3	1.3

Overall, joint gap spaces did not exceed 2.3 ± 0.9 mm and 2.7 ± 1.2 mm for the syndesmosis and talocrural joints. These values fall well within the normal range of lateral and medial clear spacing for a healthy ankle joint as identified by clinicians via x-ray image measurements. The absolute minimum values calculated for the syndesmosis and talocrural joints were 0.9 ± 0.3 mm and 1.0 ± 1.0 mm respectively (Table 4.11).

4.4. Discussion

Previous analysis of six DOF kinematics for the syndesmosis and talocrural joints (Chapter 3) showed vast differences in overall bone articulation, and highlighted the very small yet very dynamic motions of the fibula during rapid weight-bearing maneuvers. Generally, the static poses caused minimal bone motion when compared to dynamic tasks. This can be explained by the lack of shear stresses present at the joint that are otherwise seen during fast awkward twisting motions of the body.

From chapter 3 it was concluded that maximum dorsiflexion induced the greatest amount of fibular excursion among all static poses, with external rotation and posterior translation being the predominant motions. This is consistent with the defined mechanism of injury for the syndesmosis joint. The dynamic exercises on the other hand, displayed the greatest amount of movement in IR/ER, A/P, and S/I degrees of freedom, which was especially notable during torso twist and box jump. The data presented in chapter 3 indicated a potential paradigm shift on how lateral dislocation of the fibula may be a secondary movement in response to other motions predominantly occurring in the joint that could lead to syndesmotic rupture. This claim seems to be further supported by the findings in this chapter on lateral and medial clear space widening.

Although kinematic behaviors between the syndesmosis and talocrural joints varied greatly, the overall distraction within each were relatively the same; both having exhibited consistent gap width measurements and minimal changes in bone dislocation (Table 4.11). The small values of clear space widening illustrate the invaluable stability that the surrounding ligaments provide by limiting excessive separation of the bones and maintaining the integrity of the ankle joint.

Table 4. 11. Absolute maximum and minimum clear space distances of all dynamic activities for syndesmosis and talocrural joints.

Lateral Syndesmosis Clear Space (mm)				
	Min		Max	
	Mean	SD	Mean	SD
Calf Raise	1.1	0.6	2.0	0.6
Squat	1.3	0.8	2.3	0.9
Torso Twist	0.9	0.3	2.2	0.7
Box Jump	1.1	0.8	2.2	1.0

Medial Tibiotalar Clear Space (mm)				
	Min		Max	
	Mean	SD	Mean	SD
Calf Raise	1.8	1.3	2.7	1.2
Squat	1.2	1.2	1.7	1.3
Torso Twist	1.2	0.8	2.0	0.8
Box Jump	1.0	1.0	1.9	1.4

Syndesmotic gap distance measurements of the static poses provided a clear snapshot into expected fibular dislocation due to foot positioning: distraction from non-weight-bearing to weight-bearing neutral, maximum widening while dorsiflexed and minimum gap distance in plantarflexion. Calf raise and squat illustrated significant and opposing linear regression with mean clear space and advancement through the activity. Syndesmotic gap spaces significantly decreased with increasing plantarflexion, whereas gap distances significantly increased as dorsiflexion increased.

Traditionally it has been thought that internal rotation of the torso placed an externally rotating moment on the planted foot, and thus resulted in fibular dislocation from the tibia. In this study however, it was observed that both maximum internal or external rotation of the torso caused either absolute maximum or minimum distractions of the joint. For some subjects, IR of the torso created maximum dislocations while others experienced maximum dislocations with ER of the torso. This could be an effect of each subjects' individual biomechanical response to balance, where some may have inadvertently supinated or pronated their foot during twisting, rather than keeping it flatly planted. Doing so would surely change the biomechanical response at the joint. In either case, it is clear that maximally twisting the torso while single-leg weight bearing can impose awkward moments and stressed on the ankle in a manner that can be considered a major mechanism of injury to the syndesmosis.

Lateral clear space measurements throughout the box jump activity clearly illustrated joint compression from flight phase (Pre) to toe-strike (TS) as the foot plantarflexes, and immediate joint separation with continuous dorsiflexion during the last three phases of landing and balancing was also observed. The stabilization phase showed the greatest amount of foot dorsiflexion and thus the largest clear space widening between the tibia and fibula.

Medial clear space distances between the tibia and the talus did not show as significant of differences in comparison to the fibula, but still provided valuable insight on distal joint motion. Static weight-bearing imposed minimal and non-significant changes in joint distractions. Minimal and indistinct trends were seen in medial clear space changes for heel-rise or squat. Similar to the behavior of the fibula, extreme torso twisting caused both maximum and minimum joint displacements of the talus. However, the difference in these joint space values between both twisting directions and the neutral stance was not significant. It was established previously that forces up to 2.6 times body weight were experienced during box jump landing. Tibiotalar clear spaces reached an all-time minimum at the point of maximum GRF, most likely due to the talus being wedged further into the proximal ankle joint causing compression.

4.4.1. Limitations

Certain limitations were inherent in this study. As mentioned before, the sample size (n = 6) could be considered relatively small compared to other studies with published kinematic data. Although given time and cost constraints as well as the high accuracy of the HSSR system and closeness in anthropometric data among the subject cohort, it seemed unnecessary to expand the healthy participant population. Internal and external rotations proved to be the most variable measure in the kinematic data. Errors associated with the kinematic data would unavoidably carry over into the calculations of medial-lateral clear space. To minimize these standard deviations, tracking was performed by a single person to limit inter-tracker variability and tracking files were routinely tuned if gap distance values seemed physiologically unrealistic.

4.4.2. Conclusions

This work has defined normal limits of medial and lateral clear space widening to describe healthy bone distractions within the ankle joint complex. The consistent gap width measurements and minimal changes in bone dislocations suggest that lateral separation of the bones during high-stress and high-impact activities may be an after effect to other larger excursions occurring within the joint. If this is indeed the case, then a shift in treating and rehabilitating syndesmotic injuries should focus on protecting IR/ER, A/P, and S/I movements of the fibula, not solely M/L translation. Currently, surgical fixation focuses on preventing lateral distraction of the fibula and given the results of this study, this does not seem to be the primary degree of freedom needing constraint. Additionally, locating the point at which the minimum and maximum gap distance occurs between the bones, then tracing its migration throughout a dynamic task could provide insight into how damaging joint separation progresses (Figure 4.12). Combining these clinical measures with in-vivo kinematic and EMG data could better describe individual joint kinetics, stability techniques such as muscular co-contraction, mechanisms of injury, and biomechanical effects of implantable device design.

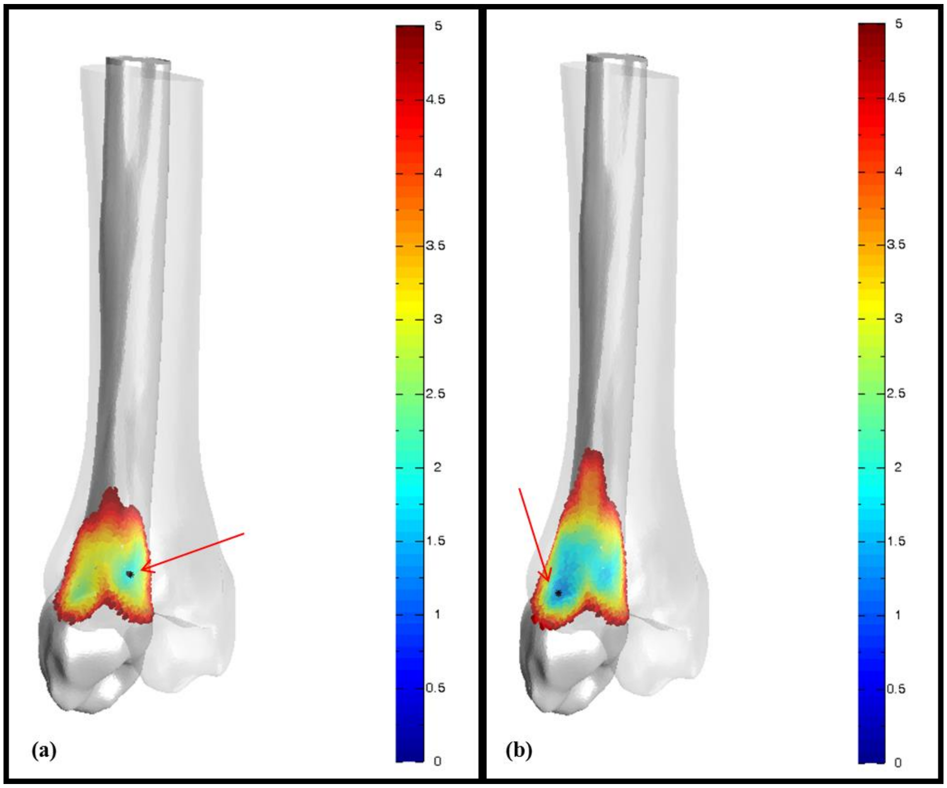

Figure 4. 8. Migration of absolute minimum distance point during calf raise (a) neutral stance and (b) maximum plantarflexion.

CHAPTER 5. CONCLUSIONS AND FUTURE RECOMMENDATIONS

The objective of this research was to develop a baseline understanding of healthy syndesmotic articulation and define normal limits of joint distraction during stressful dynamic activities. A general lack of understanding for the unique role that the fibula plays during high-impact tasks in overall ankle strength, stability, and mobility contributes to the difficulty and inaccuracy of properly treating syndesmotic injuries. The data presented establishes a definition for healthy range of motion (ROM) in the syndesmosis and talocrural joints as well as bringing to light the need for alternative approaches in treatment of severe high ankle sprain injuries.

5.1. Six Degree of Freedom Kinematics and Range of Motion

In-vivo six DOF kinematics were measured for the syndesmosis and talocrural joints using dual-plane high-speed stereoradiography in order to define healthy range of motion (ROM) of the ankle joint. Kinematic analyses showed vast differences in overall ROM between the two joints. The very small yet highly dynamic micro motions of the fibula highlighted the elastic behavior of syndesmosis crucial for enduring rapid high-impact loading such as those seen in collision sports. The dynamic activities tested caused the greatest amount of motions in IR/ER, A/P, and S/I degrees of freedom, especially with torso twist and box jump. The effects of shear stress on the distal joint known to cause bone distraction are typically the result of quick twisting in the upper body while the foot remains planted. This reaction was particularly apparent with internal rotation of the torso causing an external rotating moment to the foot and distal bones. Static neutral standing caused minimal change in motion in comparison to the dynamic tasks, although static dorsiflexion did induce the greatest amount of bone excursion with external rotation and posterior translation being the predominate movements observed. This is consistent with the accepted mechanism of injury for the syndesmosis joint.

The tibiotalar joint showed clear kinematic patterns of plantarflexion, internal rotation, and anterior translation during heel-rise, while the reverse motions occurred upon squatting. This suggests that the talocrural joint is primarily responsible for plantar/dorsiflexion of the hind foot. There was also a distinct lack of motion during the torso twist indicating that the talus serves more as a sturdy base of support for the tibia and fibula to directly articulate on. All activities showed minimal magnitudes and changes in IN/EV kinematics which are indicative of the subtalar joint primarily providing these movements for the hind foot.

5.2. Lateral and Medial Clear Space

Limits of medial and lateral clear space widening between the fibula, talus, and tibia were measured to describe healthy bone distraction within the ankle joint complex.

It was found that total distractions within each joint were relatively small and equal in magnitude. The small values of clear space widening illustrate the instrumental stability provided by the surrounding ligaments to limit excessive separation of the bones and maintain the integrity of the ankle joint.

Syndesmotic gap space significantly decreased with increasing plantarflexion, whereas gap distance significantly increased as dorsiflexion increased. Both maximum internal and external rotation of the torso caused maximum distraction of the syndesmosis which could be an effect of individual biomechanical responses to maintain balance, such as slight supination or pronation the foot. Ultimately, it was made clear that twisting the upper body while single-leg standing can impose awkward moments and stresses on the ankle in a manner to evoke injury to the syndesmosis.

Tibiotalar distances showed minimal and non-significant changes for almost all activities, except for twisting and box jump. Similar to the behavior of the fibula, extreme torso twisting caused maximum displacement of the talus. Tibiotalar clear space reached an all-time minimum at the point of maximum GRF during box jump landing, which is most likely due to the talus being wedged further into the proximal joint causing compression.

5.3. Future Work

Future experimental work could include comparison of injured and post-injury repair athletes in order to examine differences in functional ROM relative to the healthy baseline data set presented in this work. Cadaveric testing of various fixation methods using the ground reaction forces measured from the embedded force plates could provide more realistic loading conditions to better represent stresses athletes experience during competition. Examination of foot type potentially having an influence on kinematics, and possibly an impact on risk to syndesmosis injury would be another valuable study. Comparison between alternative rehabilitation regimes in restoring functional and anatomical ROM could be beneficial for trainers and physical therapists.

ROM measurements could be used as metrics to illustrate joint laxity along each anatomical plane. This measure could help optimize medical device design by clearly pin pointing specific degrees of freedom in which large and problematic motions occur within the joint and that may require more robust constraints. Additional measures defined in this study to be considered as tools for quantifying joint laxity include distal fibula path length and 3D excursion volume. These metrics provide a map and quantifiable measures for the 3D micro motions of specific points of interest on the bone. Clinically, this could be used to track the movement of the metallic buttons or screws implanted for syndesmotic repair. Furthermore, locating the point at which the minimum and maximum gap distance occurs between the bones, then tracing its migration throughout a dynamic task could provide insight into how damaging joint distraction progresses. Combining these metrics with in-vivo kinematic and EMG data could better describe individual joint kinetics, stability techniques such as muscular co-contraction, mechanisms of joint injury, and the biomechanical effects of implantable device design.

These data presented indicate a potential paradigm shift in how syndesmosis motion is viewed and how injuries are treated. The design of implantable devices should potentially focus on larger motions that occur within the joint (IR/ER, A/P, and S/I) in addition to medial-lateral dislocations of the bone.

LIST OF REFERENCES

Bartonicek, J., 2003. Anatomy of the tibiofibular syndesmosis and its clinical relevance. Surg. Radiol. Anat. 25, 379–386.

Bauer, M., Jonsson, K., Nilsson, B., 1985. Thirty-year follow-up of ankle fractures. Acta Orthop. Scand. 56, 103–106.

Beumer, A., Valstar, E.R., Garling, E.H., Niesing, R., Ranstam, J., Lofvenberg, R., Swierstra, B.A., 2003. Kinematics of the distal tibiofibular syndesmosis: Radiostereometry in 11 normal ankles. Acta Orthop. Scand. 74, 337–343.

Clanton, T.O., Williams, B.T., Backus, J.D., Dornan, G.J., Liechti, D.J., Whitlow, S.R., Saroki, A.J., Turnbull, T.L., Laprade, R.F., 2017. Biomechanical Analysis of the Individual Ligament Contributions to Syndesmotic Stability.

Close, J.R., 1956. Some applications of the functional anatomy of the ankle joint. J. Bone Joint Surg. Am. 38–A, 761–781.

de Asla, R., Wan, L., Rubach, H., Li, G., 2006. Six DOF In Vivo Kinematics of the Ankle Joint Complex: Application of a Combined Dual-Orthogonal Fluoroscopic and Magnetic Resonance Imaging Technique. J. Orthop. Res. 1019–1027.

Goh, J.C., Mech, A.M., Lee, E.H., Ang, E.J., Bayon, P., Pho, R.W., 1992. Biomechanical study on the load-bearing characteristics of the fibula and the effects of fibular resection. Clin. Orthop. Relat. Res. 223–228.

Grood, E.S., Suntay, W.J., 1983. Grood and Suntay 1983.pdf. J. Biomech. Eng.

Hansen, M., Le, L., Wertheimer, S., Meyer, E., Haut, R., 2006. Syndesmosis Fixation : Analysis of Shear Stress via Axial Load on 3 . 5-mm and 4 . 5- mm Quadricortical Syndesmotic Screws 45, 65–69.

Hermans, J.J., Beumer, A., De Jong, T.A.W., Kleinrensink, G.J., 2010. Anatomy of the distal tibiofibular syndesmosis in adults: A pictorial essay with a multimodality approach. Surg Radiol Anat. 217, 633–645.

Huber, T., Schmoelz, W., Bo, A., 2012. Foot and Ankle Surgery Motion of the fibula relative to the tibia and its alterations with syndesmosis screws : A cadaver study 18, 203–209.

Hughes, J.L., Weber, H., Willenegger, H., Kuner, E.H., 1979. Evaluation of ankle fractures: non-operative and operative treatment. Clin. Orthop. Relat. Res. 111–119.

Hunt, K.J., Goeb, Y., Behn, A.W., Criswell, B., Chou, L., 2015a. Ankle Joint Contact

Loads and Displacement With Progressive Syndesmotic Injury.

Hunt, K.J., Hurwit, D., Robell, K., Gatewood, C., Botser, I.B., Matheson, G., 2016. Incidence and Epidemiology of Foot and Ankle Injuries in Elite Collegiate Athletes. Am. J. Sports Med. 1–8.

Hunt, K.J., Phinistkul, P., Pirolo, J., Amendola, A., 2015b. High Ankle Sprains and Syndesmotic Injuries in Athletes 23, 661–673.

Ivester, J.C., Cyr, A.J., Harris, M.D., Kulis, M.J., Rullkoetter, P.J., Shelburne, K.B., 2015. A Reconfigurable High-Speed Stereo-Radiography System for Sub-Millimeter Measurement of In Vivo Joint Kinematics. J. Med. Device. 9, 41009.

Jensen, S.L., Andresen, B.K., Mencke, S., Nielsen, P.T., 1998. Epidemiology of ankle fractures. A prospective population-based study of 212 cases in Aalborg, Denmark. Acta Orthop Sc. 69, 48–50.

Kefala, V., Cyr, A.J., Harris, M.D., Hume, D.R., Davidson, B.S., Kim, R.H., Shelburne, K.B., 2017. Assessment of Knee Kinematics in Older Adults Using High-Speed Stereo Radiography. Med Sci Sports Exerc. *In Press*.

McPoil, T.G., Cornwall, M.W., 2005. Use of the longitudinal arch angle to predict dynamic foot posture in walking. J. Am. Podiatr. Med. Assoc. 95, 114–20.

Mcpoil, T.G., Cornwall, M.W., Abeler, M.G., Devereaux, K.J., Flood, L.J., Merriman, S.E., Sullivan, S., Van Der Laan, M.J., Villadiego, T. a, Wilson, K., 2013. Clinical Research on Foot & Ankle The Optimal Method to Assess the Vertical Mobility of the Midfoot: Navicular Drop versus Dorsal Arch Height Difference? Clin Res Foot Ankle 1, 1–7.

Metzler, A. V., Johnson, D.L., 2013. Dynamically Unstable Syndesmosis Injuries. Orthopedics 36, 209–211.

Michelsen, J.D., Ahn, U.M., Helgemo, S.L., 1996. Motion of the ankle in a simulated supination-external rotation fracture model. J. Bone Joint Surg. Am. 78, 1024–31.

Mukhopadhyay, S., Metcalfe, A., Guha, A.R., Mohanty, K., Hemmadi, S., Lyons, K., O’Doherty, D., 2011. Malreduction of syndesmosis - Are we considering the anatomical variation? Injury 42, 1073–1076.

Naqvi, G.A., Cunningham, P., Rcsi, F.F.R., Lynch, B., Galvin, R., Awan, N., Frcsi, T., 2009. Fixation of Ankle Syndesmotic Injuries Comparison of Tight Rope Fixation and Syndesmotic Screw Fixation for Accuracy of Syndesmotic Reduction 2828–2835.

Norkus, S.A., Floyd, R.T., 2001. The Anatomy and Mechanisms of Syndesmotic Ankle Sprains. J. Athl. Train. 36, 68–73.

Nussbaum, E.D., Hosea, T.M., Sieler, S.D., Incremona, B.R., Kessler, D.E., 2001. Prospective Evaluation of Syndesmotic Ankle Sprains Without Diastasis * 29, 31–35.

Ogilvie-Harris, M.B., Reed, S.C., Hedman, T.P., 1994. Disruption of the Ankle Syndesmosis: Biomechanical Study of the Ligamentous Restraints. J. od Arthrosc. Relat. Surg. 10, 558–560.

Peter, R.E., Harrinton, R.M., Henley, M.B., Tencer, A.F., 1994. Biomechanical Effects of Internal Fixation of the Distal Tibiofibular Syndesmotic Joint: Comparison of Two Fixation Techniques.

Press, C.M., Gupta, A., Hutchinson, M.R., 2009. Management of Syndesmosis Injuries in the Elite Athlete. Curr. Sports Med. Rep. 8, 228–233.

Rammelt, S., Zwipp, H., Grass, R., 2008. Injuries to the Distal Tibiofibular Syndesmosis: an Evidence-Based Approach to Acute and Chronic Lesions. Foot Ankle Clin. 13, 611–633.

Ramsey, P.L., Hamilton, W., 1976. Changes in tibiotalar area of contact caused by lateral talar shift. J. Bone & Jt. Surg. 58, 356 LP-357.

Roach, K.E., Way, W., Rm, A., Wang, B., Way, W., Kapron, A.L., Fiorentino, N.M., Foreman, K.B., 2016. In-vivo Kinematics of the Tibiotalar and Subtalar Joints in Asymptomatic Subjects : A High-speed Dual Fluoroscopy Study.

Schepers, T., Van Lieshout, E.M.M., de Vries, M.R., Van der Elst, M., 2011. Complications of syndesmotic screw removal. Foot ankle Int. / Am. Orthop. Foot Ankle Soc. [and] Swiss Foot Ankle Soc. 32, 1040–1044.

Sora, C., Sora, M., Strobl, B., Staykov, D., 2004. Evaluation of the ankle syndesmosis : A plastination slices study Evaluation of the Ankle Syndesmosis : A Plastination Slices Study.

Stebbins, J., Harrington, M., Thompson, N., Zavatsky, A., Theologis, T., 2006. Repeatability of a model for measuring multi-segment foot kinematics in children. Gait Posture 23, 401–410.

Thompson, M.C., Gesink, D.S., 2000. Biomechanical Comparison of Syndesmosis Fixation with 3 . 5- and 4 . 5-mil- limeter Stainless Steel Screws 736–741.

Thormeyer, J.R., Leonard, J.P., Hutchinson, M., 2012. Syndesmotic Injuries in Athletes, Dr. Kennet. ed, An International Perspective on Topics in Sports Medicine. InTech.

Thornes, B., Shannon, F., Guiney, A.-M., Hession, P., Masterson, E., 2005. Suture-Button Syndesmosis Fixation. Clin. Orthop. Relat. Res. NA;, 207–212.

Thornes, B., Walsh, A., Hislop, M., Murray, P., O'Brien, M., 2003. Suture-endobutton fixation of ankle tibio-fibular diastasis: a cadaver study. Foot ankle Int. 24, 142–6.

Wang, C., Yang, J., Wang, S., Ma, X., Wang, X., Huang, J., Zhang, C., Chen, L., Xu, J., Geng, X., Wang, K., 2015. Three-dimensional motions of distal syndesmosis during walking. J. Orthop. Surg. Res. 10, 166.

Waterman, B.R., Belmont Jr., P.J., Cameron, K.L., Svoboda, S.J., Alitz, C.J., Owens, B.D., 2011. Risk Factors for Syndesmotic and Medial Ankle Sprain Role of Sex , Sport , and Level of Competition. Am. J. Sports Med. 39, 992–998.

Waterman, B.R., Owens, B.D., Davey, S., Zacchilli, M.A., Belmont Jr., P.J., 2010. The Epidemiology of Ankle Sprains in the United States. J. Bone Jt. Surg. 92, 2279.

Williams, B.T., Ahrberg, A.B., Goldsmith, M.T., Campbell, K.J., Shirley, L., Wijdicks, C.A., Laprade, R.F., Clanton, T.O., 2014. Ankle Syndesmosis A Qualitative and Quantitative Anatomic Analysis. Am. J. Sports Med. 43, 42–44.

Wright, R.W., Barile, R.J., Surprenant, D.A., Matava, M.J., 2004. Ankle Syndesmosis Sprains in National Hockey League Players. Am. J. Sports Med. 32, 1941–1945.

Wuest, T.K., 1997. Injuries to the Distal Lower Extremity Syndesmosis.

Xenos, J.S., Hopkinson, W.J., Mulligan, M.E., Olson, E.J., 1995. Xenos.pdf.

Yildirim, H., Mavi, A., Ph, D., Orhan, B., 2003. Evaluation of the Fibular Incisura of the Tibia with Magnetic 387–391.

APPENDIX A. ANATOMICAL COORDINATE SYSTEMS

The local coordinate systems assigned to the tibia, fibula, and talus were built by forming orthogonal planes between easily located anatomical landmarks of the bones. Historically the lower limb has been modeled with the tibia and fibula as a single rigid body, where the individual articulation of the fibula is not considered. For this study, a modified Grood & Suntay (1983) method was used to construct the distal tibial coordinate system since the proximal shaft was not included in the CT scan. The same methodology used to construct the tibial coordinate system was translated to the fibula to build similar coordinates. The talar coordinate system was also constructed by selecting easily identifiable landmarks and modifying past research methods.

Tibial Coordinate System

1. Use the reference geometry tool to select a center node on the proximal surface of the tibial shaft and an opposing node approximately on the center of the tibial plafond. This line should generally run through the center of shaft and is considered the “mechanical axis”.

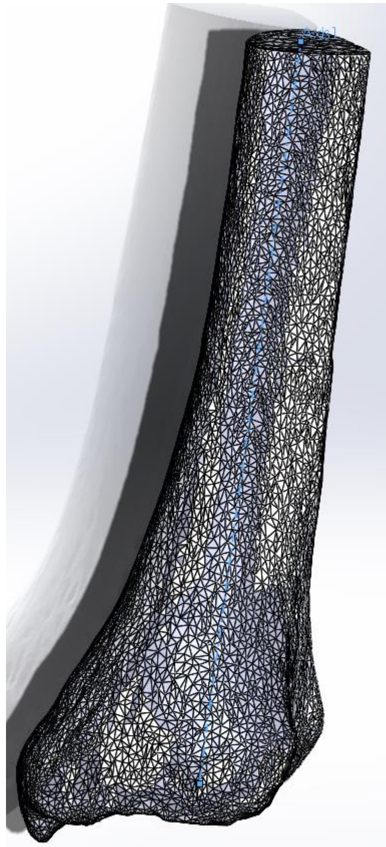

2. Select the most distal node on the medial malleolus and create a reference plane (Plane 1) that intersects this point and is perpendicular to the mechanical axis.

3. Select a node that marks the most superior prominence of the medial malleolus. Create a plane (Plane 2) intersecting this point that is parallel to Plane 1.

4. Using Plane 1 & Plane 2, create a Mid Plane (Plane 3).

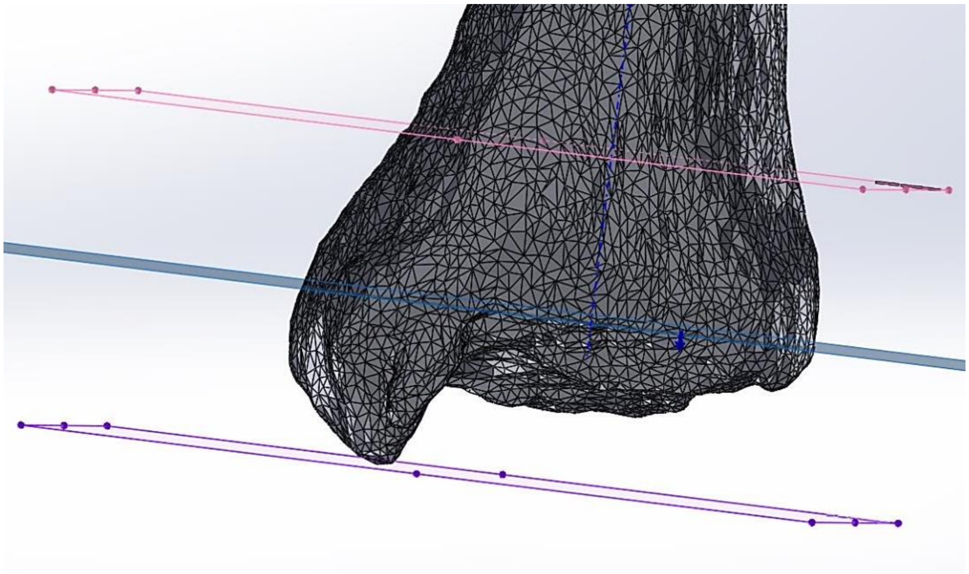

5. Select the most anterior node on the medial malleolus to create a plane (Plane 4) that is perpendicular to Plane 3.

6. Create Plane 5 which is parallel to Plane 4 and intersects the mechanical axis.

7. Locate the most medial point of the malleolus to create a plane (Plane 6) that is perpendicular to Plane 5 and Plane 3.

8. Use Plane 6 to build a parallel plane (Plane 7) that intersects the mechanical axis.

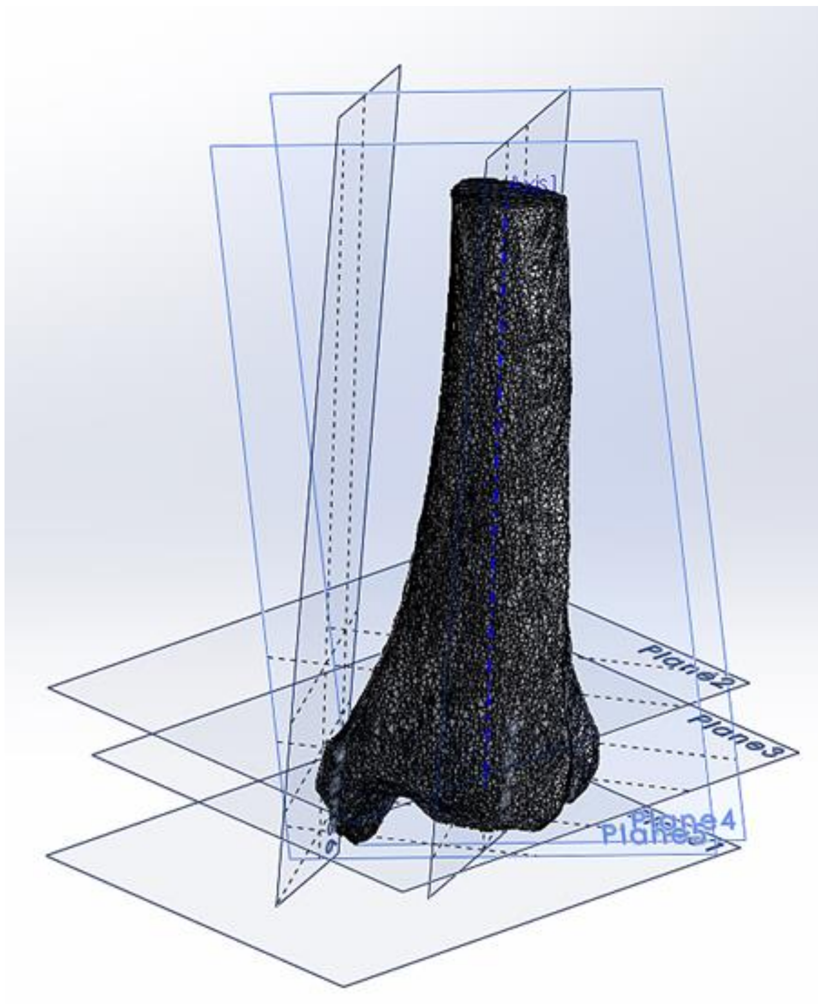

9. Planes 3, 5, and 7 define your transverse, frontal, and sagittal planes. The intersection of all three planes is the origin of your local coordinate system.

10. Section the bone at Plane 3 to clearly expose this intersection of planes.

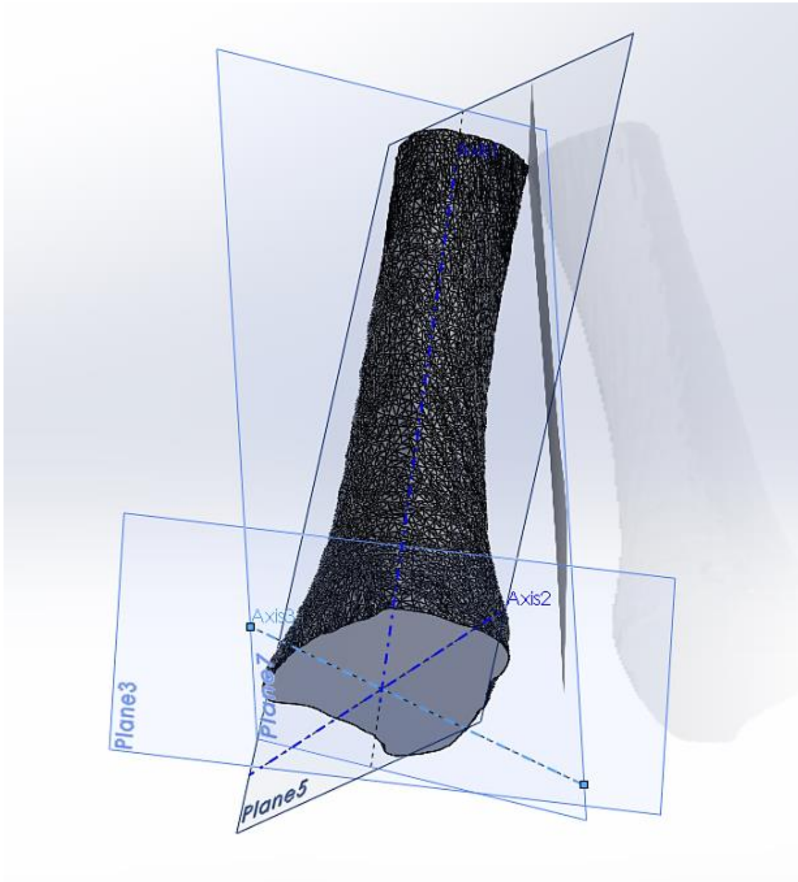

11. Overlay axis in M/L, A/P, and S/I directions by selecting the planes as reference.

12. Assign a reference coordinate system at the origin aligning x-y-z of the LCS with lateral, anterior, and superior directions.

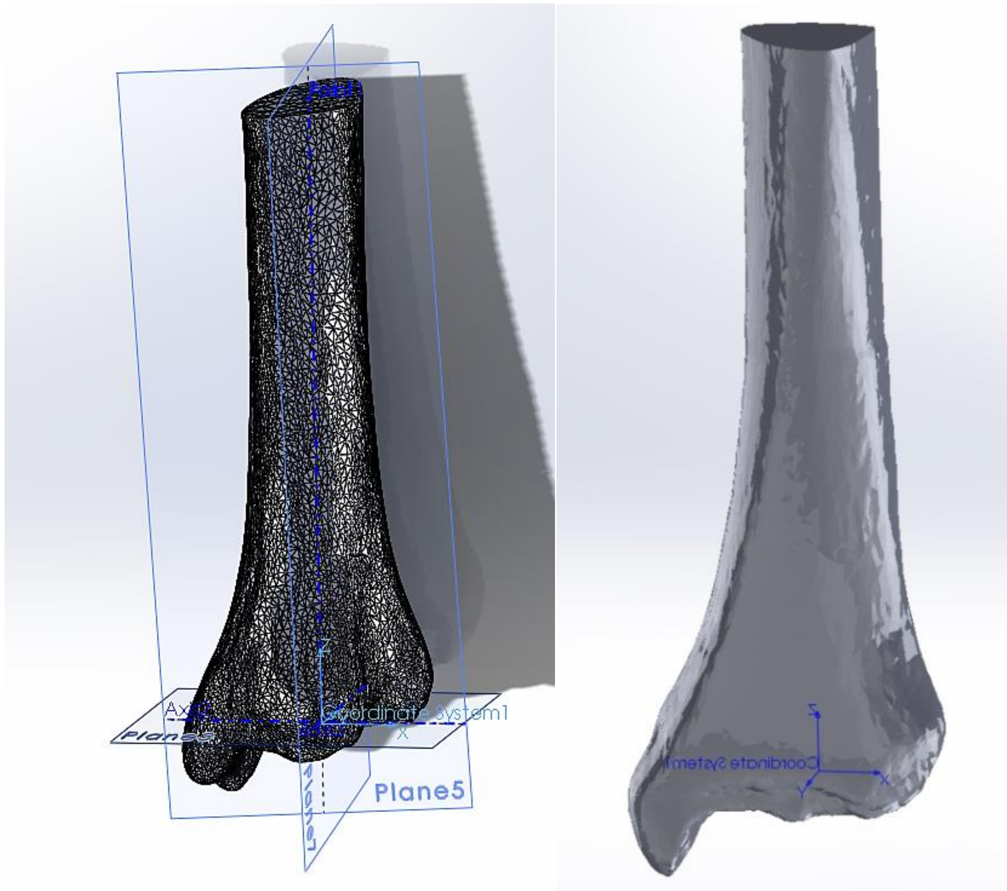
Coordinate System1
X
Plane5

Fibular Coordinate System

1. Use the reference geometry tool to select a center node on the proximal surface of the fibular shaft and an opposing node approximately on the center of the most distal malleolus. This line should generally run along the length of the shaft and slightly lateral from the center. This is the “mechanical axis”.

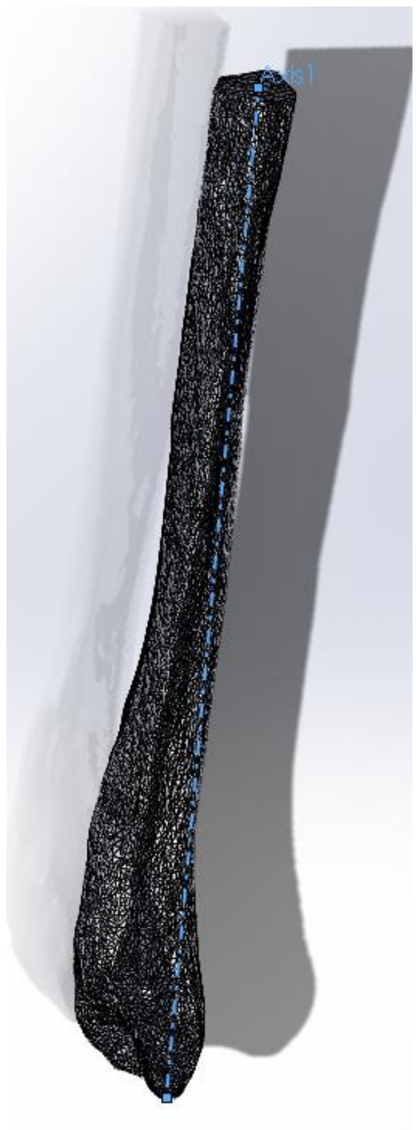

2. Select the most distal node on the malleolus and create a reference plane (Plane 1) that intersects this point and is perpendicular to the mechanical axis.

3. Select a node that marks the most superior prominence of the malleolus. Create a plane (Plane 2) intersecting this point that is parallel to Plane 1.

4. Using Plane 1 & Plane 2, create a Mid Plane (Plane 3).

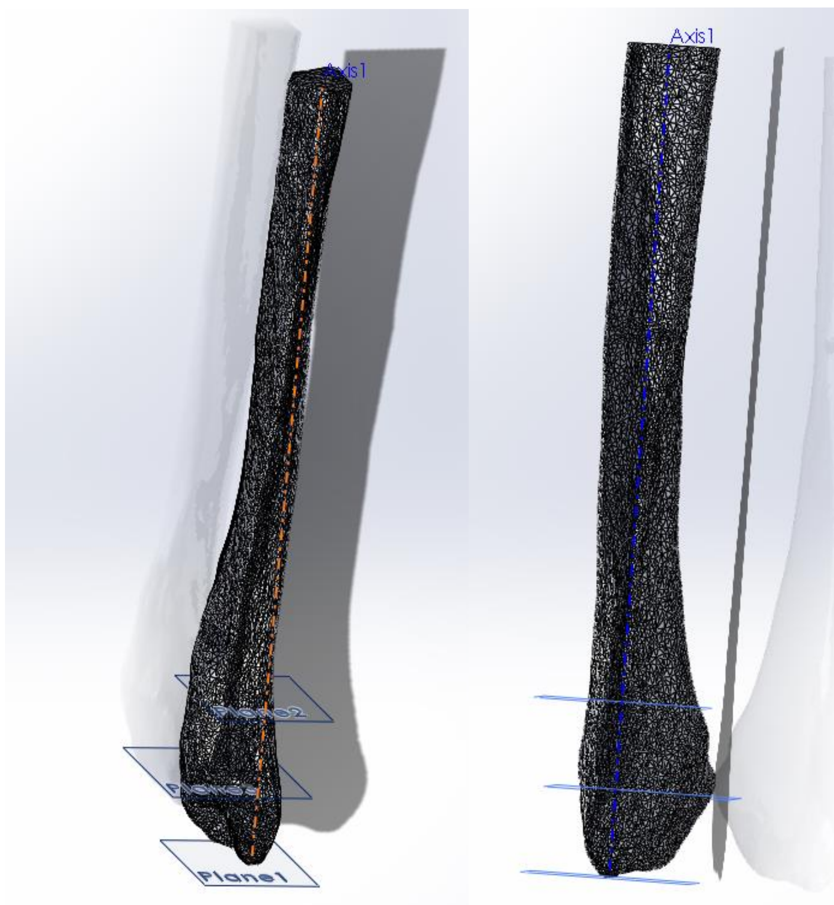

5. Select the most anterior node on the medial malleolus to create a plane (Plane 4) that is perpendicular to Plane 3.

6. Create Plane 5 which is parallel to Plane 4 and intersects the mechanical axis.

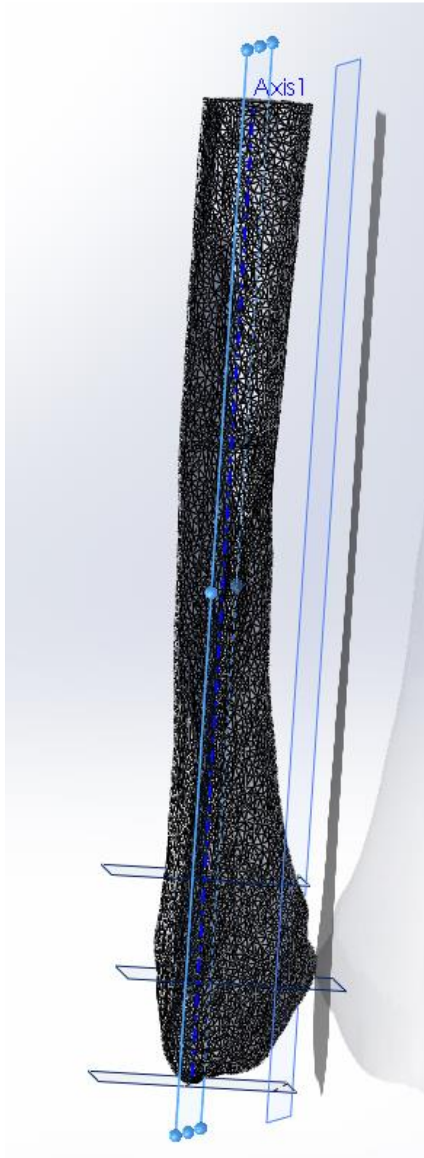

7. Locate the most lateral point of the malleolus to create a plane (Plane 6) that is perpendicular to Plane 5 and Plane 3.

8. Use Plane 6 to build a parallel plane (Plane 7) that intersects the mechanical axis.

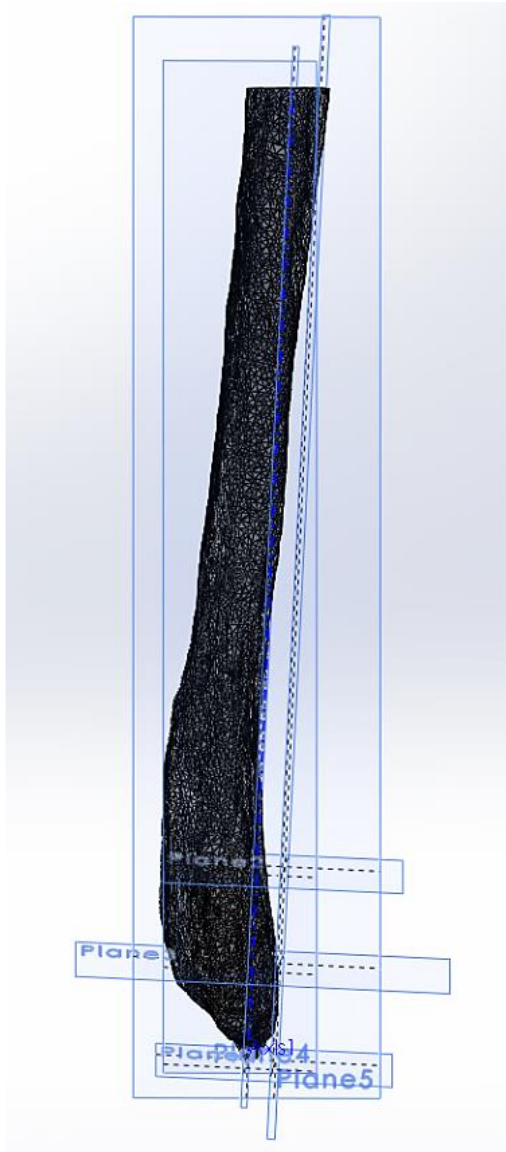

9. Planes 3, 5, and 7 define your transverse, frontal, and sagittal planes. The intersection of all three planes is the origin of your local coordinate system.

10. Section the bone at Plane 3 to clearly expose this intersection of planes.

11. Overlay axis in M/L, A/P, and S/I directions by selecting the planes as reference.

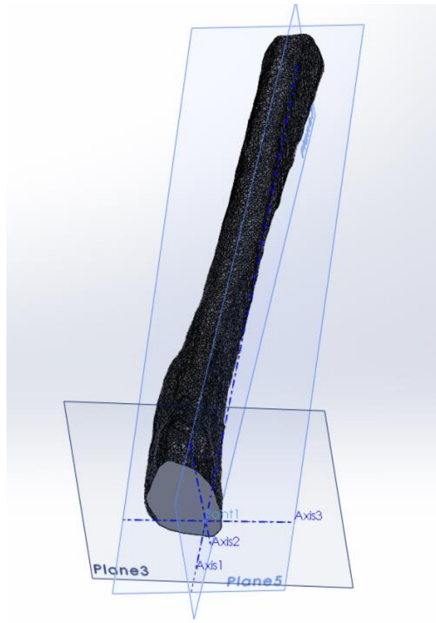

12. Assign a reference coordinate system at the origin aligning x-y-z of the LCS with lateral, anterior, and superior directions.

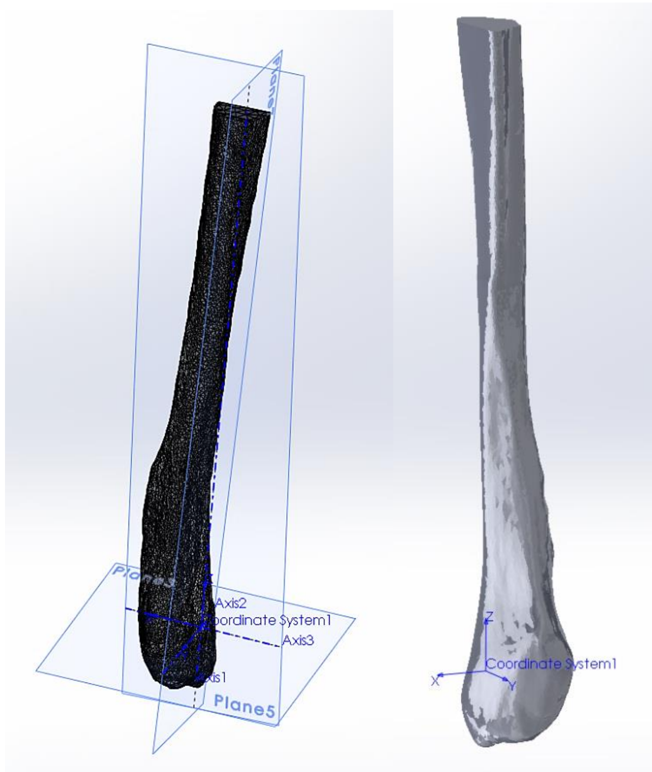

Talar Coordinate System

1. Use the reference geometry tool to select a center node on the most anterior surface of the talar head and an opposing node approximately on the center of the most posterior process.

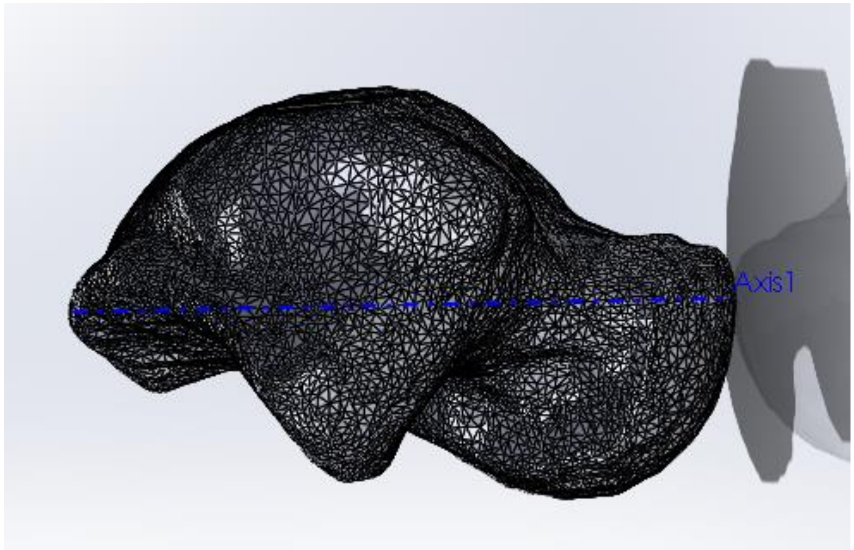

2. Select that same node on the posterior process and create a reference plane (Plane 1) that intersects this point and is perpendicular to the mechanical axis.

3. Select the most anterior node on the talar head and create a plane (Plane 2) intersecting this point that is parallel to Plane 1.

4. Using Plane 1 & Plane 2, create a Mid Plane (Plane 3).

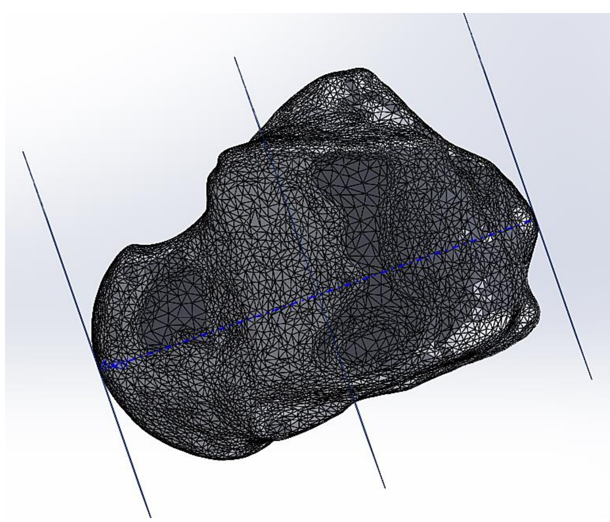

5. Form a new axis (Axis 2) that spans the most superior and center nodes of the medial and lateral talar dome.

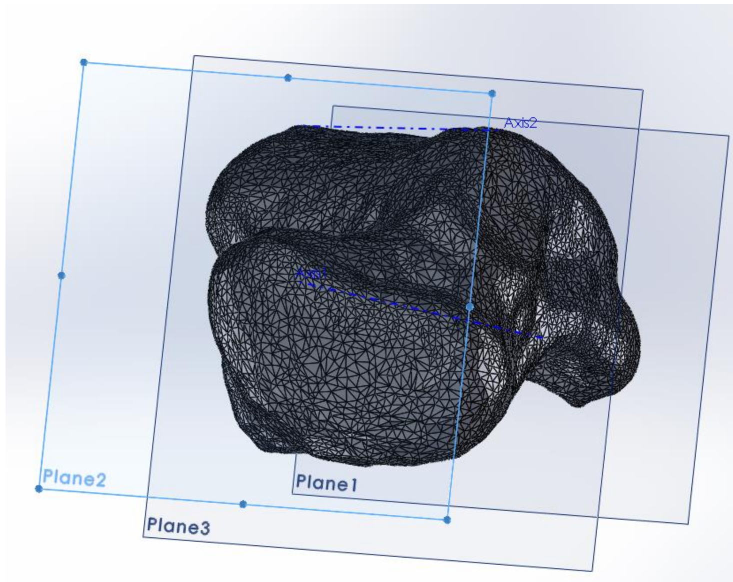

6. Create a plane (Plane 4) that intersects Axis 2 and is perpendicular to Plane 3.

7. Locate the most posterior and center point of the talar head to create a plane (Plane 5) that is parallel to Plane 4.

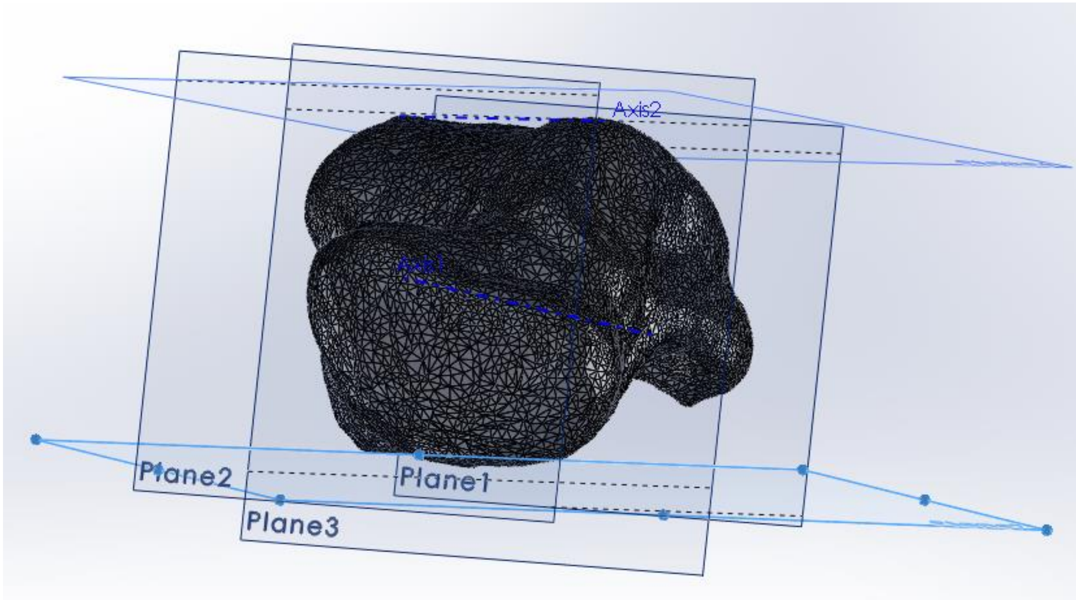

8. Using Plane 4 & Plane 5, create a Mid Plane (Plane 6).

9. Locate the most lateral point near the center of the talar dome. Create a plane (Plane 7) that intersects this point and is perpendicular to Plane 6 and Plane 3.

10. Form Plane 8 that intersects Axis 1 and is parallel to Plane 7.

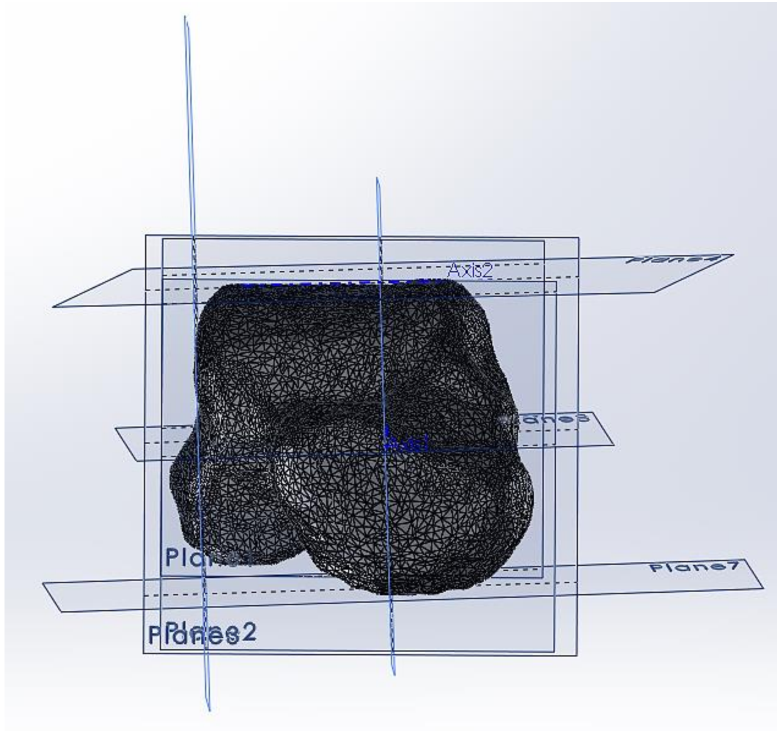

11. Planes 3, 6, and 8 define your transverse, frontal, and sagittal planes. The intersection of all three planes is the origin of your local coordinate system.

10. Section the bone at Plane 6 to clearly expose this intersection of planes.

11. Overlay axis in M/L, A/P, and S/I directions by selecting the planes as reference.

12. Assign a reference coordinate system at the origin aligning x-y-z of the LCS with lateral, anterior, and superior directions.

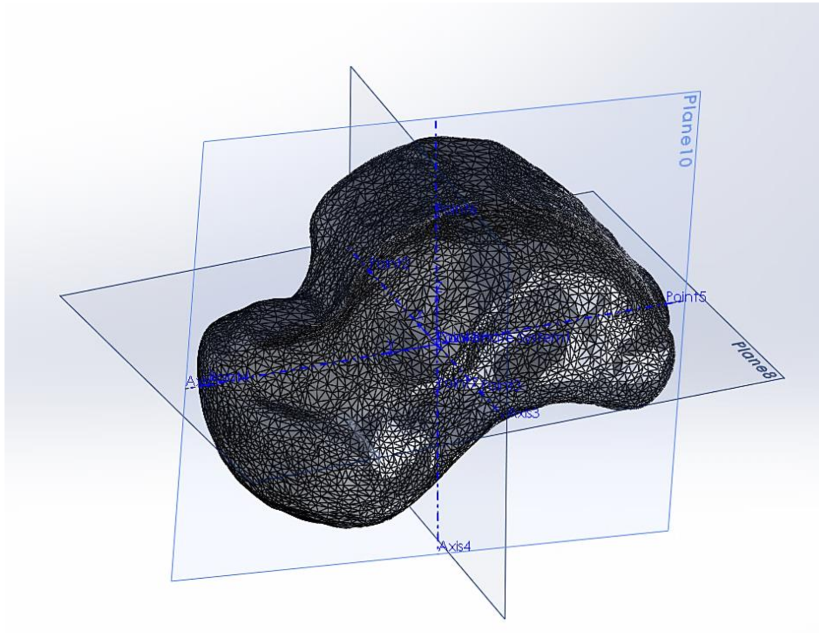
Plane10
Point5
Plane8
Axis3
Axis4

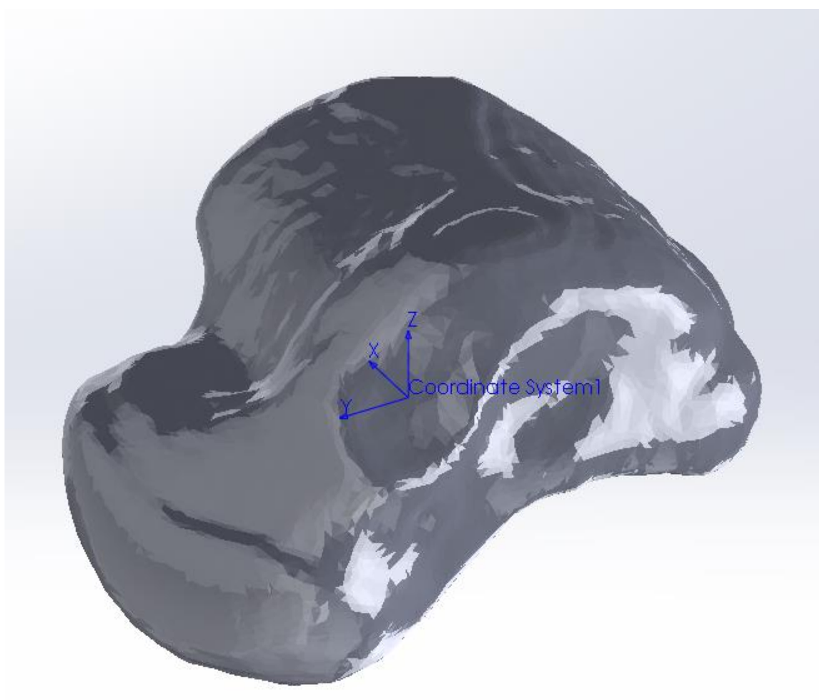
Z
X
Y
Coordinate System1

Table B1. Modified Oxford model for reflective marker placement

Abbrev.	Anatomical Landmark	Abbrev.	Anatomical Landmark	Diam.
[RMMA]	Medial Malleolus	[LMMA]	Medial Malleolus	*6mm
[RANK]	Lateral Malleolus	[LANK]	Lateral Malleolus	*6mm
[RSTL]	Sustentaculum Tali	[LSTL]	Sustentaculum Tali	14mm
[RLCA]	Lateral Calcaneus	[LLCA]	Lateral Calcaneus	14mm
[RHEE]	Inferior Calcaneus	[LHEE]	Inferior Calcaneus	14mm
[RPCA]	Superior Calcaneus (in line with HEE marker)	[LPCA]	Superior Calcaneus (in line with HEE marker)	14mm
[RCPG]	Wand Marker-Mid Calcaneus	[LCPG]	Wand Marker-Mid Calcaneus	
[RP1M]	Dorsal: medial aspect of base of 1st metatarsal	[LP1M]	Dorsal: medial aspect of base of 1st metatarsal	14mm
[RP5M]	Base of 5th metatarsal	[LP5M]	Base of 5th metatarsal	*14mm
[RD1M]	Medial Aspect: head of 1st metatarsal head	[LD1M]	Medial Aspect: head of 1st metatarsal head	*6mm
[RD5M]	Lateral Aspect-head of 5th metatarsal	[LD5M]	Lateral Aspect-head of 5th metatarsal	*14mm
[RHLX]	Medial Aspect: proximal phalanx of Hallux	[LHLX]	Medial Aspect: proximal phalanx of Hallux	14mm
[RTOE]	Dorsal Aspect-between 2nd and 3rd metatarsal heads	[LTOE]	Dorsal Aspect-between 2nd and 3rd metatarsal heads	*14mm
[RNAV]	Navicular Tuberosity	[LNAV]	Navicular Tuberosity	*6mm

[RTROC]	Trochanter	[LTROC]	Trochanter
[RTHGH]	Thigh Shank	[LTHGH]	Thigh Shank

[RQUAD]	Quad Tendon
[RMedKNE]	Medial Femoral Condyle
[RLatKNE]	Lateral Femoral Condyle
[RTUB]	Tibial Tuberosity
[RHFB]	Head of Fibula
[RSHN]	Anterior Shin (in line with RTUB "anatomical ankle joint center")
[RTIB]	Lateral Shank

[LQUAD]	Quad Tendon
[LMedKNE]	Medial Femoral Condyle
[LLatKNE]	Lateral Femoral Condyle
[LTUB]	Tibial Tuberosity
[LHFB]	Head of Fibula
[LSHN]	Anterior Shin (in line with RTUB "anatomical ankle joint center")
[LTIB]	Lateral Shank

[RPSIS]	Right Sacral Dimple
[LPSIS]	Left Sacral Dimple
[LILCR]	Left Iliac Crest
[RILCR]	Right Iliac Crest
[LASIS]	Left ASIS
[RASIS]	Right ASIS

Table B2. Electromyography (EMG) surface electrodes applied to the lower limb

Function	
Gluteus Medius (GLUT)	Stability of hip / Internal rotation of thigh
Biceps Femoris (BF)	Flexion and lateral rotation of knee / Extension and lateral rotation of hip
Rectus Femoris (RF)	Knee extension / Hip flexion
Peroneus Longus/Brevis (PER)	Plantarflexion / Eversion of ankle
Tibialis Anterior (TA)	Dorsiflexion of ankle / Inversion of foot
Medial Gastrocnemius (MG)	Flexion of ankle / Flexion of knee
Lateral Gastrocnemius (LG)	Flexion of ankle / Flexion of knee
Soleus (SOL)	Plantarflexion of the ankle
Extensor Digitorum Longus (EDL)	Dorsiflexion / Eversion of foot Extension of toes

APPENDIX C. POST PROCESSING WORK FLOW

Fluoroscopy File Preparation

1. Using Cineviewer software, save the .cine fluoroscopy files from both Camera A and Camera A as .tiff stacks (detailed documentation can be found on the DU Center for Orthopeadic Biomechanics Server: R:\Research Common\HDL\Personal Folders\Hogg\Thesis Appendix Documentation\Convert cine file to sequential tiffs.pdf)

2. Use XROMM Undistorter Software to undistort images according to the standardized mesh (detailed documentation by Kefala et al. (2017))

3. Using the XROMM Calibration software, calibrate the undistorted images to the fluoroscopy volume space by using the imaged calibration cube and known 3D spatial locations of the beads on cube (detailed documentation by Kefala et al. (2017))

Subject Specific Bone Model Preparation

1. Check the quality of the CT file using any DICOM viewing software (Radiant) to ensure a neutral positioning of the foot and a continuous image sequence of bone slices

2. Use ScanIP to segmentation the bones of interest (detailed documentation found on the DU Center for Orthopeadic Biomechanics Server: R:\Research Common\HDL\Personal Folders\Hogg\Thesis Appendix Documentation\ScanIP _Bone_Segmentation.pdf)

3. Utilize MeshLab software to re-mesh bone into a binary .stl file such that it can be imported into Solidworks:

1. Open Meshlab. File -> Import Mesh. Open the femur STL. If asked to Unify Duplicated Vertices, check the box and click “OK”.
2. If the bone appears black (otherwise go to (C)): Filters -> Normals, Curvatures and Orientation -> Invert Faces Orientation. Check “Force Flip” only, click Apply, then Close.
3. Filters -> Remeshing, Simplification and Reconstruction -> Quadratic Edge Collapse Decimation. Enter 19999 for “Target number of faces”, Quality threshold to 1. Leave defaults otherwise. Check the following (in addition): Preserve Boundary of the mesh, Preserve Normal, Planar Simplification. Click Apply, Click Close.
4. File -> Export Mesh As. Don’t change the name, just overwrite the original. Change Files of type: to *.stl. Click Save. Keep defaults and click OK.

4. Solidworks is used to build the LCS of each bone described in Appendix A

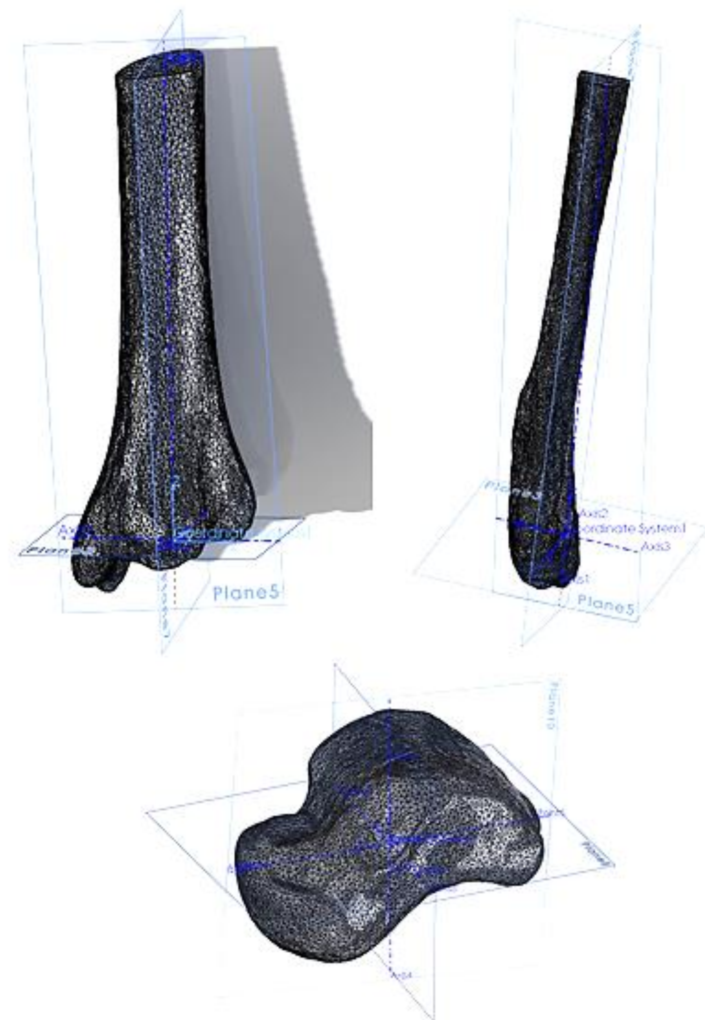

5. A custom written Matlab code re-writes the bone .stl file with the LCS and origin assigned

6. 3D Slicer can then be used to convert the LCS oriented bone into a .tiff stack without buffering to be imported into the tracking software (detailed documentation found on the DU Center for Orthopeadic Biomechanics Server: R:\Research Common\HDL\Personal Folders\Hogg\Thesis Appendix Documentation\3D Slicer_Convert STL to sliced images.docx).

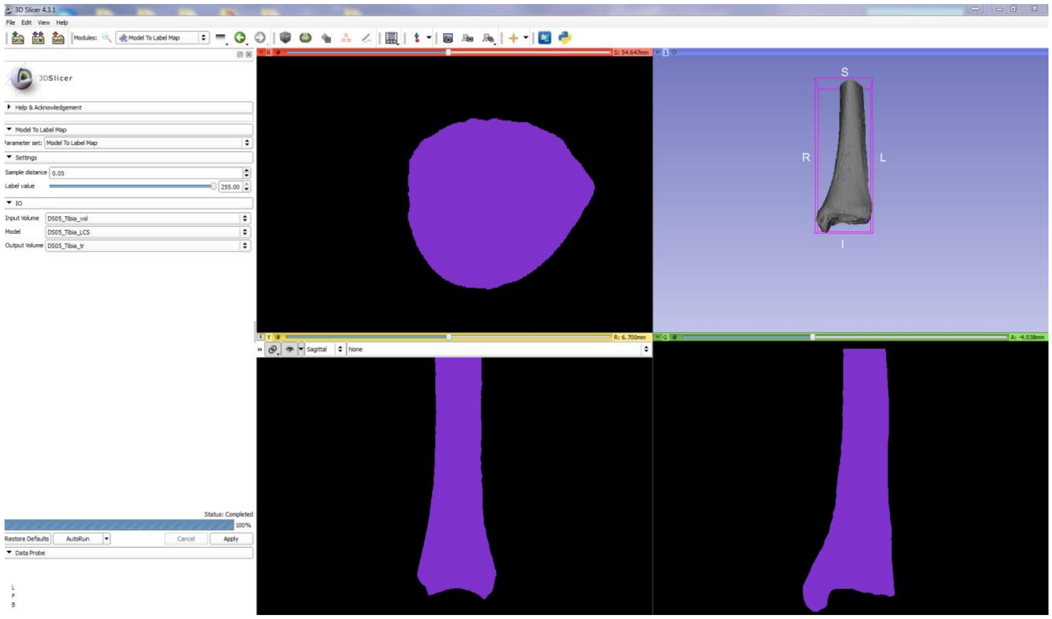

7. Use XROMM Autoscoper software to image match the subject-specific bone rendering to fluoroscopy images. Adjust the filtering in the program as needed (detailed documentation found on the DU Center for Orthopeadic Biomechanics Server).

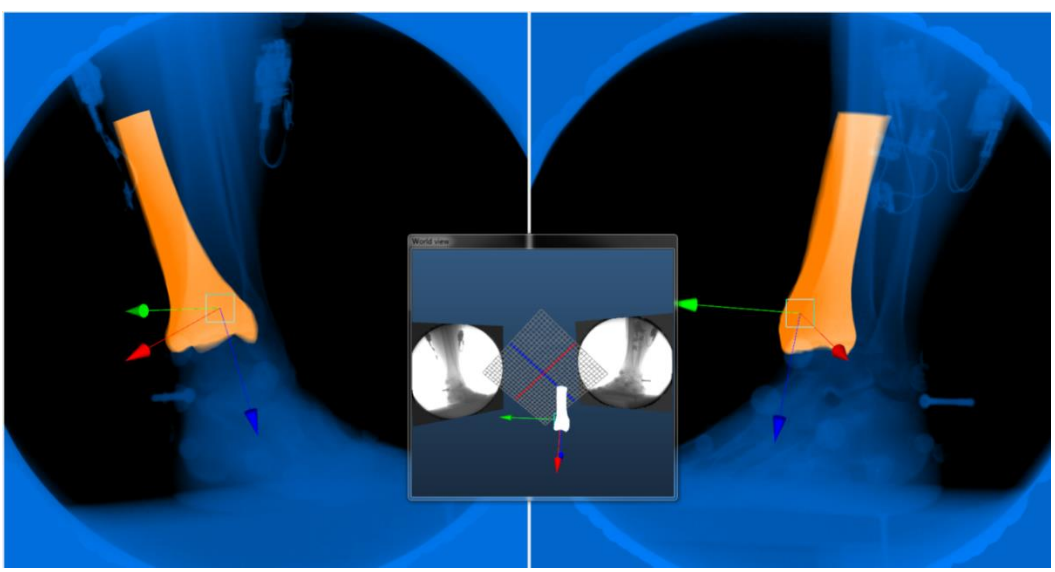

8. The .trc files are then used as inputs for the custom written Matlab code to define the spatial orientation of the bone at each specified frame in the activity.